DEVELOPMENT OF HUMAN STEM CELL-BASED MODEL FOR DEVELOPMENTAL TOXICITY TESTING

XING JIANGWA

(BME, SHANGHAI JIAO TONG UNIVERSITY, CHINA)

A THESIS SUBMITTED

FOR THE DEGREE OF DOCTOR OF PHILOSOPHY

MECHANOBIOLOGY INSTITUTE

NATIONAL UNIVERSITY OF SINGAPORE

2015

DECLARATION

I hereby declare that this thesis is my original work and it has been written by me in its entirety. I have duly acknowledged all the sources of information which have been used in the thesis.

This thesis has also not been submitted for any degree in any university previously.

Xing Jiangwa

20 January 2015

Acknowledgements

First of all, I would like to extend my great gratitude and sincere appreciation to my PhD supervisor Prof. Hanry Yu for his enduring mentorship and support. His training for not only being a good researcher but also being a good team leader and member was extremely helpful for me. His passion for translational research inspires me along the way. Great thanks are extended to Dr. Yi-Chin Toh, who was a former lab member as Research Scientist in IBN and now working as Assistant Professor in NUS. She has been a great mentor, helpful colleague and kindest friend to me along my PhD study. My project wouldn't move forward smoothly without her valuable advice and contributions. I really enjoy working and having various discussions with her about science and life. I am very grateful for my Thesis Advisory Committee (TAC) members, Prof. Yusuke Toyama, and Prof. Sungsu Park as well. They have raised critical questions for my project and provided me many useful suggestions both for my project and for my personal development as a PhD candidate.

Next I would like to thank my great lab members for their generous support. Great thanks should be extended to my senior Dr. Shuoyu Xu, who helped me a lot in image processing. I'm grateful to other team project members I have been happily working with, Dr. Farah Tasnim, Dr. Huan Li, Ms. Yinghua Qu and Dr. Junjun Fan. I have learned how to work in a team and utilize everyone's specialties to best contribute to the projects. I would like to thank Ms. Wai Han Lau, Dr. Shu Ying Lee and Mr. Weian Zhang for

their help in microscopy. Great thanks are extended to Ms. Wenhao Tong, Ms. Qiwen Peng and Ms. Jie Yan, who used to seat in the same office with me. We were all Sagittarius PhD candidates of similar age, and shared quite a lot sweet and bitter memories together. The courage and support we gave to each other means a lot to my PhD life.

Sincere appreciation should also be given to my parents, who have shown great understanding and support to my PhD study here in Singapore. I'm also quite grateful to Prof. Chwee Teck Lim, Prof. Shivashankar G V, Dr. Man Chun Leong and Dr. Shefali Talwar for their guidance during my lab rotation four years ago, who actually introduced me to cell-related biological research and taught me practical techniques I could use throughout these four years. I would like to thank IBN and BMRC for their generous financial supports for research and MBI for my scholarship. Last but not least, I would like to thank Prof. Yanan Du for his scientific inputs during my PhD qualification exam, and thank all the thesis examiners for their precious time in evaluating this thesis.

Table of Contents

Summary

Spatially and temporally organized cell differentiation and tissue morphogenesis characterize the whole embryo development process, and unintended exposure to teratogenic compounds can lead to various birth defects. However, current animal-based models for developmental toxicity testing is limited by time, cost and high inter-species variability, while human pluripotent stem cell (hPSC) models are only focusing on recapitulating cell differentiation with neither spatial control nor morphogenic movements.

In this dissertation, a human-relevant *in vitro* model, which recapitulated two cellular events characteristic of embryogenesis, was developed to identify potentially teratogenic compounds. Firstly mesoendoderm differentiation was only induced to the periphery of micropatterned hPSC (μP-hPSC) colonies, where there were higher integrin-mediated adhesions compared with colony interior. Spatially polarized integrin adhesions in a cohesive hPSC colony compete to recruit Rho-ROCK activated myosin II away from E-cadherin mediated cell-cell junctions to promote differentiation at that locality, resulting in a heterogeneous cell population. When further inducing the mesoendoderm differentiation from 1 day to 3 days, tissue morphogenesis could be recapitulated, which was mainly collective cell migration *in vitro*. Cells at the colony periphery actually underwent epithelial-mesenchymal transition (EMT) and directed collective cell migration to form an annular mesoendoderm pattern which was similar as *in vivo*. When treated with known teratogens, the

two cellular processes (cell differentiation and collective cell migration) were disrupted and the morphology of the mesoendoderm pattern was altered. Image processing and statistical algorithms were developed to quantify and classify the compounds' teratogenic potential. The μP-hPSC model not only could capture the dose-dependent effects of teratogenicity but also could correctly classify species-specific drug (Thalidomide) and false negative drug (D-penicillamine) in the conventional mouse embryonic stem cell test. This model offers a scalable screening platform to mitigate the risks of teratogen exposures in human.

List of Publications

Jiangwa Xing, Yi-Chin Toh, Shuoyu Xu, Hanry Yu. A method for human teratogen detection by geometrically confined cell differentiation and migration. Scientific Reports. 2015. (Accepted)

Yi-Chin Toh, **Jiangwa Xing**, Hanry Yu. Modulation of integrin and E-cadherin-mediated adhesions to spatially control heterogeneity in human pluripotent stem cell differentiation. Biomaterials 50 (2015): 87-97.

Patent

H. Yu, Y.C. Toh, **J. Xing,** "Method and system for *in vitro* developmental toxicity testing", Singapore Patent granted on Sep. 30 2013: PCT/SG2013/000426

List of Figures

List of Tables

List of Symbols and Abbreviation

3D	three-dimentional
AD	anterior-posterior
aHDF	adult human dermal fibroblast
AJ	adherens junction
ANOVA	analysis of variance
BMD	benchmark dose
BMP	bone morphogenetic protein
CHEST	chicken embryo toxicity screening test
C_{max}	peak plasma *in vivo* concentration
DC	disruption concentration
DMSO	dimethyl sulfoxide
DVE	distal visceral endoderm
EB	embryoid body
EcadFc	E-cadherin Fc
ECM	extracellular matrix
ECVAM	The European Centre for the Validation of Alternative Methods
EMT	epithelial mesenchymal transition
ERK	extracellular signal-regulated kinases
ESAC	ECVAM Scientific Advisory Committee
FACS	fluorescence-activated cell sorting

FBS	fetal bovine serum
FETAX	frog embryo teratogenesis assay
FGF	fibroblast growth factor
FZD	Frizzled
GD	gastation day
hESC	human embryonic stem cell
hPSC	human pluripotent stem cell
hPST	human pluripotent stem cell test
IC_{50}	the half maximal inhibitory concentration
ID_{50}	50% of inhibition of differentiation concentration
iPSC	induced pluripotent stem cell
LC_{25}	25% lethality rate
LC-HRMS	liquid chromatography high resolution mass spectrometry
LIF	leukemia inhibitory factor
LOAEL	lowest observable adverse effect level
MAPK	mitogen-activated protein kinases
mESC	mouse embryonic stem cell
mEST	mouse embryonic stem cell test
MM	micromass
MSC	mesenchymal stem cell
NOAEL	no observable adverse effect level
o/c	ornithine/cystine

P/A	perimeter-to-area
PD	proximal-distal
PDMS	polydimethylsiloxane
PEE	proximal epiblast enhancer
ppMLC	phosphorylated myosin light chain
RA	retinoic acid
ROI	region of interest
ROS	reactive oxygen species
T	brachyury
TGF	transforming growth factor
VPA	valproic acid
VYS	visceral yolk sac
WEC	whole embryo culture
μP-hPSC	micropatterned human pluripotent stem cell

1. Introduction

Developmental toxicology is the study of effects of toxic chemicals and physical agents on the developing offspring [1]. In presence of xenobiotics such as certain pharmaceutical drugs and pesticides, deviant embryo development may happen due to their developmental toxicity such as death, malformation, growth retardation, and functional deficiency. Up to now, many drug screening methods have been developed to evaluate the developmental toxicity of various xenobiotics, including both *in vivo* and *in vitro* platforms. Animal-based *in vivo* tests used to be the only generally accepted methods for developmental toxicity testing. However, they are also known to be the most animal-consuming and expensive tests across all the animal-based tests on any chemicals. For each individual test, 560 animals are needed on average for developmental toxicity screening and 3,200 animals are needed for two-generation reproductive toxicity studies, which cost €54,600 and €328,000 respectively [2]. In addition, these *in vivo* tests are based on the fundamental assumption that animal models can predict human response in developmental toxicity testing and risk assessment. However, studies have shown that there is no more than 60% correlation between different laboratory mammalian species in developmental toxicity responses [3, 4], indicating a high inter-species variation.

In order to reduce animal use in developmental toxicity testing, different *in vitro* methods have been developed for decades. These methods mainly

include the frog embryo teratogenesis assay (FETAX) on xenopus [5], the chicken embryo toxicity screening test (CHEST) [6], the micromass (MM) assay using mouse embryonic mesenchymal cells [7], the mammalian whole embryo culture (WEC) assay using mouse [8] or rat, the zebrafish embryo-larva developmental toxicity assay [9], and the mouse embryonic stem cell test (mEST) [10]. However, to date, none of these methods has been fully proven to give reproducible results sufficiently similar to the results of *in vivo* tests and human data. In addition, another major limitation is that still animal cells or embryos are applied in these platforms, meaning that the inter-species variation problem cannot be avoided.

Since the successful isolation and continuous *in vitro* culture of human embryonic stem cells (hPSCs) in 1998 [11], several groups have been trying to establish hPSC-based *in vitro* models to conquer the inter-species variation problem and produce more human-relevant data [12-17]. Although different downstream evaluation methods were applied, almost all of these models were developed in a temporally-controlled differentiation context using either directed differentiation (i.e., neural or cardiac differentiation etc.) or random differentiation [12, 14-17]. However, in human development, tissue morphogenesis, which involves cell migration, cell shape changes, selective cell growth and apoptosis [18, 19], is equally important and interrelated with regulated cell differentiation in correctly forming different developmental structural motifs at different phases of development [20, 21]. Therefore, a

hPSC-based model which can capture not only differentiation but also the morphogenesis aspect of development might produce more *in vivo*-related drug testing responses and higher predictivity in developmental toxicity screening.

The primary objective of this dissertation is to establish such a hPSC-based model encompassing both spatial patterned differentiation and morphogenetic movements, and apply it for developmental toxicity screening. A complete review of all the background information is presented in Chapter 2. Chapter 3 presents the three specific aims of this dissertation, mainly to study, characterize and apply this *in vitro* hPSC-based model for developmental toxicity screening. Chapter 4-6 mainly introduce the research designs and findings of each of the three aims. Chapter 7 concludes the dissertation and makes recommendations for further relevant studies.

2. Background and Significance

This chapter introduces the background information of the studies presented in this dissertation. In order to detect the developmental toxicity potential of compounds *in vitro*, a model which could recapitulate real embryo development events is most preferable. To achieve that, a basic understanding of human embryo development is necessary. Section 2.1 summarizes the characteristics of and the main factors regulating the embryo development, which provides the general guideline for developing *in vitro* development systems for either mechanism studies or compound screening. Section 2.2 explains the features and significance of developmental toxicity testing, and gives a summary of current *in vivo* animal models. Section 2.3 and Section 2.4 introduce main existing *in vitro* animal-based models and hPSC-based models for developmental toxicity screening respectively.

2.1 Embryogenesis

This section will first give a general idea of mammalian embryogenesis, and then will cover the two main factors regulating normal embryo development, which are biochemical signalling and mechanical transduction.

2.1.1 Mammalian embryogenesis

Basic events in embryogenesis are believed to be highly conserved across species, even for species as disparate as fruit flies, frogs, mice and humans.

Basketter says that " this degree of conservation mainly applies to the most fundamental processes in embryogenesis, such as establishment of the general body plan, pattern formation, cellular induction, and regulation of differentiation via signalling pathways" [3]. In mammals, embryogenesis refers mainly to early stages of prenatal development, while fetal development describes later stages. The whole embryogenesis process mainly includes fertilization, cleavage and morula, formation of the blastula, gastrulation and organogenesis. Among all these stages, gastrulation is believed to be the most important step of development in forming the body plan. It's the process of gastrula formation, during which the single-layered blastula is reorganized into a three-germ-layered structure including endoderm, mesoderm and ectoderm. The three germ layers will eventually give rise to all the tissues and organs of a mammal through organogenesis. The endoderm will form the digestive, respiratory and urinary organs, the ectoderm will give rise to epidermis and the nervous system, and the mesoderm will form all other tissues and organs such as connective tissue and the organs that belong to the motor and circulatory system.

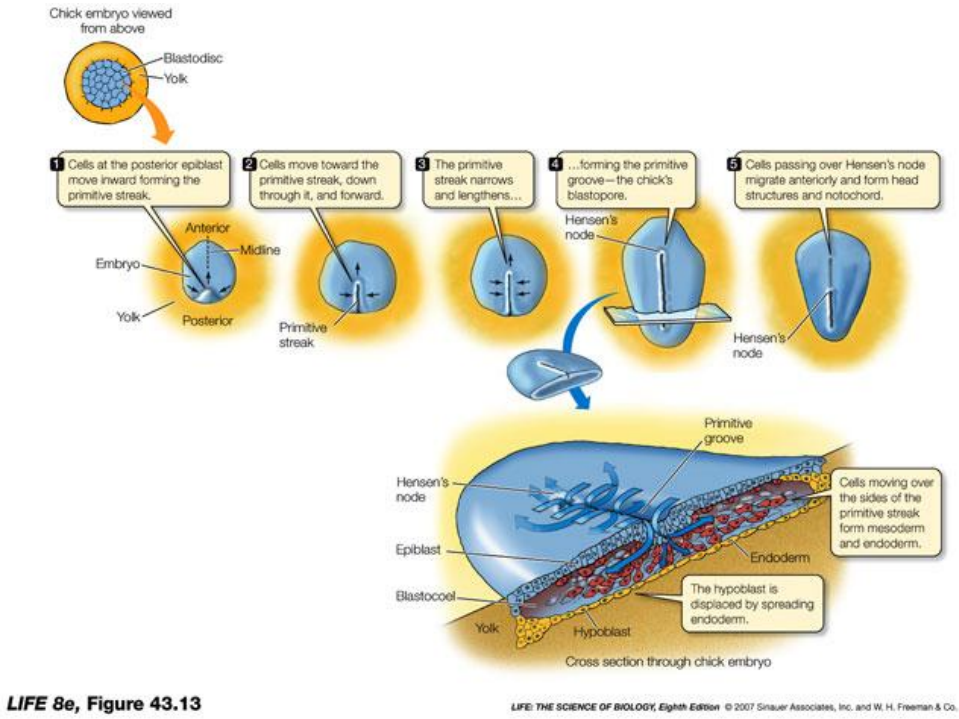

Figure 2.1.1 Gastrulation in a chick embryo. (Adapted from [22])

Gastrulation starts when the primitive streak forms on the posterior side of the embryo. After that, epiblast cells which ingress through the primitive streak form definitive endoderm and mesoderm, whereas the anterior cells of the epiblast will differentiate into ectodermal lineages (Fig. 2.1.1) [23]. The correct gastrula formation, together with other stages of embryogenesis, needs not only the correct cell fate control, but also the correct self-organized spatial control within the embryo. In fact, another key event characterizing embryogenesis, other than cell differentiation, is tissue morphogenesis. Tissue morphogenesis involves cell migration, cell shape changes, selective cell growth and apoptosis [18, 19]. It interrelates with and is equally important as

regulated cell differentiation to correctly form different developmental structural motifs at different phases of development at their desired position [20, 21]. During gastrulation, main morphogenetic movements include invagination, ingression, involution, intercalation and directed migration, all of which are conserved across species (Fig. 2.1.2) [24]. Invagination, ingression and involution are three movements responsible for internalization. Invagination is a process of groove formation in a tissue sheet via cell shape changes such as apical constriction, which occurs during primitive streak formation. Ingression follows invagination, when cells in the groove will undergo epithelial mesenchymal transition (EMT) to become motile mesoendoderm cells and move freely beneath the surface layer. Involution is a movement of cell sheet rolling, normally over an edge or itself. Similar as ingression, cells at the leading edge can undergo EMT and move on the overlying tissue sheet. Intercalation entails radial cell intercalation and mediolateral cell intercalation, which results in either thinning and surface expansion of tissue (the former), or simultaneous convergence and extension of tissue (the latter).

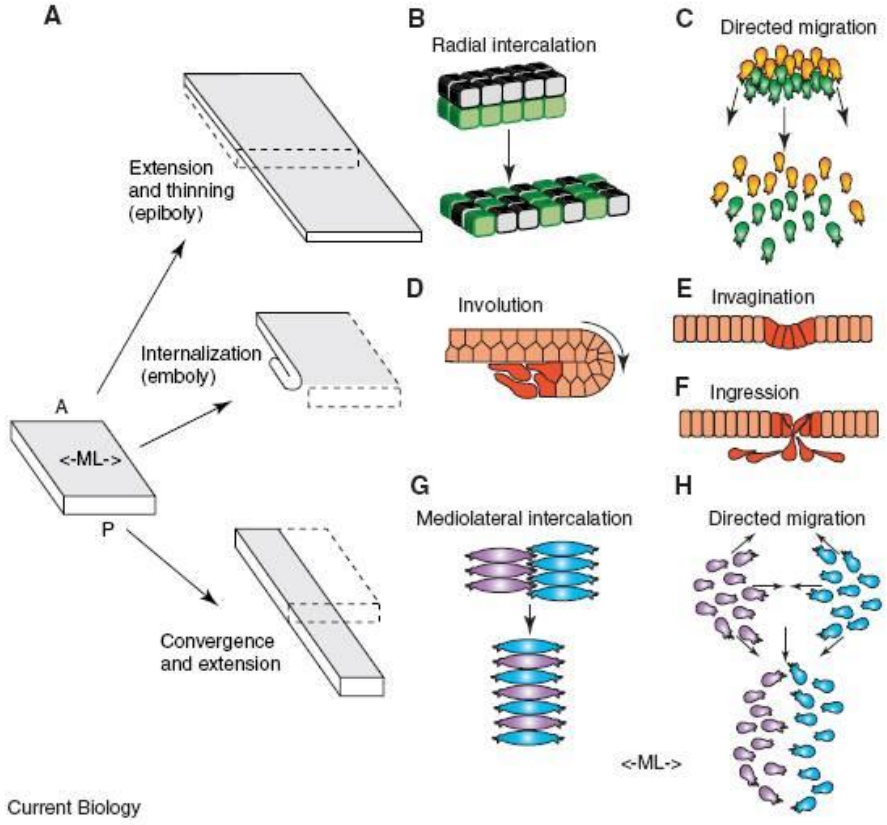

Figure 2.1.2 Morphogenetic movements of cells during gastrualtion. (A) Gastrulation movements can be classified based on the morphogenetic changes they produce. Epiboly leads to expansion of tissue, often accompanied by thinning. Emboly or internalization entails movement of mesodermal and endodermal precursors from the blastula surface beneath the prospective ectodermal layer. Convergence narrows tissues mediolaterally, whereas extension elongates them from head to tail. (B–H) Each class of gastrulation movements can be achieved by a variety of morphogenic cell movements. (Adapted from [24])

2.1.2 Biochemical control during gastrulation

Due to the fact that basic events in embryogenesis are believed to be highly conserved across species, many studies have been done using different species to understand mammalian embryogenesis. Biochemical signalling has been shown to be essential in cell fate determination for decades. Activin/Nodal, Wnt, and BMP signalling pathways are reported to be important for the mesoendoderm differentiation in gastrulation stage [25, 26]. Nostro et. al. (2007) found that Activin/Nodal and Wnt signalling are essential for the induction of primitive streak, the formation of which marks the start of gastrulation [25]. BMP signalling, however, although not required for primitive streak induction, has a strong posteriorizing effect on this population to correctly induce $F1k^{+}$ mesoderm.

Nodal signalling actually influences the embryogenesis since blastula stage [27]. There are three lineages in a mammalian blastula. The epiblast give rise to the embryo and later the fetus itself, the trophoblast develops into part of the placenta, and the primitive endoderm becomes the yolk sac. Nodal is activated through the developing epiblast by convertase enzymes secreted from the extraembryonic ectoderm and helps establishing the proximal-distal (PD) axis during blastula stage, which rotates and becomes the anterior-posterior (AD) axis [28, 29]. After Nodal is activated, it can autoregulate itself and activate BMP in the extraembryonic ectoderm. The activated BMP will then induce Wnt in the adjacent epiblast [30]. Wnt signals can concentrate

Nodal to the proximal epiblast by activating the proximal epiblast enhancer (PEE) in the Nodal gene [31]. A Nodal PD gradient will eventually form through the induction of the endogenous inhibitors Lefty1 and Cerberus in the distal visceral endoderm (DVE) by activated Nodal in the proximal epiblast. Nodal expression will be restricted to the proximal side of the embryo, where the primitive streak will locate. The PD axis will rotate to be the AP axis. Nodal is then expressed in the primitive endoderm and co-ordinates its directional migration and elongation [32]. When gastrulation is complete, Nodal expression will be restricted to the periphery of the node at the anterior end of the primitive streak [33].

On the other hand, Wnt signals can be transduced either to the canonical pathway for cell fate determination, or to the noncanonical pathway for control of cell movement and tissue polarity [34]. Canonical Wnt signals are transduced to the downstream β-catenin signaling cascade through Frizzled (FZD) family receptors and LRP5/LRP6 coreceptor [35, 36]. Noncanonical Wnt signals are transduced through FZD family receptors and coreceptors to a variety of Dishevelled- or Ca^{2+}-dependent signalling cascades, regulating processes such as convergent extension and planar cell polarity in vertebrates, and the polarity of hairs, bristles and ommatidia in Drosophila [34, 37]. In the context of gastrulation, studies have shown that the posterior expression of certain Wnt ligands and Wnt signaling components is indispensable for the formations of primitive streak, anteroposterior polarity and mesoderm [38-40].

In vitro, local activation of the Wnt pathway can induce the anteroposterior polarity establishment in the embryoid body (EB), which is a 3D aggregate formed in suspension by pluripotent stem cells. It can help to form a primitive streak-like region within the EB, and promote regional mesoendoderm differentiation [41]. This local activation of Wnt signaling requires external signals but is self-reinforcing after initiation [41].

FGF2 is also essential in mesoendoderm formation during gatrulation. It sustains Nanog through the MEK-ERK pathway, and switches BMP4-induced hPSC differentiation outcome from extraembryonic lineages to mesoendoderm [42]. FGF signalling also regulates morphogenetic movement at the primitive streak [43].

To sum up, Nodal signalling, Wnt signalling and FGF signalling are all essential for mesoendoderm formation and correct morphogenetic movements during gastrulation. Once Nodal is activated during blastula, it can activate Wnt which can inversely concentrate more Nodal. On the other hand, Nodal can also be maintained and concentrated by BMP signals. Once Wnt signalling is activated either by Nodal or other external signals, it can be self-reinforcing. FGF signalling is essential for switching BMP4-induced differentiation from extraembryonic lineages to mesoendoderm during gastrulation.

2.1.3 Mechanical control in cell fate determination and morphogenesis during gastrulation

Apart from biochemical signalling, recent studies have also shown an indispensible role of mechanical signalling in embryogenesis, especially during gastrulation [44]. This mechanical signalling is not only critical in cell fate determination such as mesoendoderm differentiation, but also indispensible for the various morphogenetic movements occurring during gastrulation. In amphibian embryos, the coordinated and differently located morphogenetic movements during gastrulation are believed to be mediated by biomechanical interactions between different parts of a gastrulating embryo [44, 45]. Series of Drosophila embryos studies also demonstrate a critical role of mechanical signalling in gastrulation such as cell sorting [46, 47], germ band extension [48, 49], anterior midgut differentiation [50], and mesoendoderm differentiation [51].

Farge (2011) suggests that mechanical signals actually can pattern gene expression within the developing embryo, therefore inducing the following morphogenetic movement sequence [52]. Morphogenetic movements require correctly patterned gene expression. For instance, mesoderm invagination in Drosophila embryos during gastrulation requires the transcription factor Twist, and the expression of Fog and Snail in the mesoderm [51, 53]. In fact, there are two waves of constriction occurring in the apical ventral cells which lead to Drosophila mesoderm invagination**.** The first wave is a Snail-dependent

stochastic process, whereas the second wave is controlled by Twist and requires Fog protein [51]. Twist expression is found to be mechanically induced by stomodeal cell compression due to germ-band extension during endogenous development [50, 54].

In order to understand how mechanical signalling controls the gene expression and apply it for basic and clinical research, a lot of *in vitro* cell-based studies other than embryo studies have been done. One major part of these studies is related to how mechanical signals affect cell fates under same biochemical induction environment. For instance, matrix elasticity and geometric cues can direct mesenchymal stem cell (MSC) lineage specification [55-57]. Naive single MSCs can sense the elasticity of the matrix and become neurogenic, myogenic or osteogenic when sitting on soft (0.1-1kPa), stiffer (8-17 kPa) and rigid (25-40 kPa) matrices respectively [55]. Geometric shapes which can increase cytoskeletal tension of single adherent MSCs promote osteogenesis relative to adipogenesis [57]. Two studies also show the critical role of mechanical gradients in spatial patterning of cells into specified lineages at appropriate locations [58]. In the presence of soluble factors inducing both osteogenic and adipogenic differentiation, MSCs at the edge of multicellular islands corresponding to regions of high mechanical stress differentiated into the osteocytes, while those in the centre which corresponds to low stress became adipocytes [58]. Similarly, gradients of mechanical stress within multicellular islands of mouse mammary epithelial cells (SCp2) can

define the spatial locations at which EMT occurs [59]. EMT is a phenotypic change in which epithelial cells lose their cell polarity and cell-cell adhesion and become migratory and invasive mesenchymal cells. It is important for early cell differentiation and collective cell migration during morphogenesis [26, 60-62]. When treated with transforming growth factor (TGF)-β, cells within regions of highest mechanical stress such as colony edges and corners expressed EMT markers, whereas those in the centre did not [59].

In summary, while biochemical cues are essential for stem cell differentiation, mechanical signalling is also critical in spatially defining cell fates both *in vitro* and *in vivo*. At the same time, it is also indispensable for morphogenetic movements induction during development such as gastrulation. Current *in vitro* studies related to spatial cell fate control are most done in MSCs or adult mammalian cells, no hPSC-based studies are available. Due to the cell property differences between MSCs/adult mammalian cells and hPSCs which may lead to different underlying mechanisms, studies on hPSCs are needed to study the effects and mechanisms of mechanical signalling in early hPSC differentiation. In addition, no *in vitro* studies to date have shown the role of mechanical signalling in morphogenetic movement control in the context of stem cell differentiation. Therefore, a hPSC-based model showing the dual role of mechanical signalling would be most helpful to recapitulate and study human embryogenesis.

2.2 Developmental toxicity

After knowing the basics of mammalian development and embryogenesis in Section 2.1, this section enters into the developmental toxicity testing field. It first gives a clear definition of developmental toxicity, then follows the introduction of *in vivo* animal studies for developmental toxicity testing, which are still the most widely accepted methods so far.

2.2.1 Birth defects and developmental toxicity

Major birth defects are conditions present at birth that cause structural changes in one or more parts of the body, which have a serious, adverse effect on health, development, or functional ability of the body. In United States, birth defects are one of the leading causes of infant death, accounting for more than one in every five infant deaths [63, 64]. In Singapore, birth defects constituted 13.6% of population stillbirths, 25.2% of population perinatal mortality, and 45.7% of population neonatal mortality between 1994 and 2000 [65]. In addition, babies born with birth defects have a greater chance of illness and long term disability than babies without birth defects. Birth defects actually occur before a baby is born, and most occur in the first 3 months of pregnancy, which is a very important stage of development when organs of the baby are forming.

Xenobiotics may cause developmental toxicity, which is the adverse effects on the developing embryo or fetus, resulting in severe birth defects.

Xenobiotics are chemicals which are found in an organism but not normally produced or expected to be present in it, or substances which are present in much higher concentrations than usual. In presence of xenobiotics such as certain drugs, deviant development may happen due to their teratogenicity, such as death, malformation, growth retardation, and functional deficiency. The manifestations of these deviant development increase in frequency and degree as dosage increases, from the no-effect to the totally-lethal level [1]. Potential Mech Developal toxicity of compounds include mitotic interference, altered membrane function/signal transduction, altered energy sources, enzyme inhibition, altered nucleic acid synthesis and mutations, as well as perturbations in gene or protein expression and programmed cell death [66].

In order to correctly classify those xenobiotics which may cause developmental toxicity to human, different drug screening methods, including both *in vivo* and *in vitro* models, have been developed. *In vitro* models mainly use cells or animal embryos as the experiment materials. Due to the complexity of embryo development, these models so far could only recapitulate some major developmental events within certain critical phases during embryogenesis. Therefore, *in vivo* animal studies are still the most commonly applied methods to date.

2.2.2 *In vivo* animal studies for developmental toxicity testing

The application of *in vivo* animal studies for human teratogen screening is based on a series of assumptions [1]. One of the key assumption is that an agent which can cause developmental toxicity to the tested animals will potentially pose a hazard to humans as well. However, the types of effects seen in animals are not necessarily the same as those may be seen in humans. This could be due to the inter-species variations in critical periods, timing of exposure, metabolism, developmental patterns, placetation, or mechanisms of action. Because of these existing differences, the most appropriate species should be used when applicable. The rat or the rabbit are normally the preferred species for developmental toxicity testing to date unless other species are considered as more relevant for certain xenobiotics. Usually animals are treated with test chemicals during pregnancy, and different toxicity endpoints, such as litter size, fetal weight, prenatal mortality, sex ratio as well as different malformations, are evaluated shortly before parturition.

There are different readout parameters in animal studies. Normally the no observable adverse effect level (NOAEL) and the lowest observable adverse effect level (LOAEL) are identified based on statistical tests as well as their biological significance. Appropriate dose selection is very important to make these two endpoints meaningful. Another readout is the benchmark dose (BMD), which is defined as the lower confidence limit on a dose that produces a particular effect size (e.g. 1%, 5% or 10% change compared with the

controls) and calculated by mathematical modelling. This BMD approach makes use of the entirety of the data and accounts for data variability.

The advantage of *in vivo* animal studies using either rodents or non-rodents compared with all *in vitro* developmental toxicity testing platforms are quite easy to interpret. First, it can test the adverse effects of compounds throughout the whole cycle of offspring development. Second, in the presence of placenta, it has similar compound adsorption, distribution, metabolism and activation capacity as human. However, the disadvantages of using *in vivo* models are quite obvious at the same time. First, *in vivo* models are quite expensive, need long experiment cycle, and more importantly, require a large number of animals for testing [2]. Second, for abnormal embryo development observed in the presence of maternal toxicity, it's difficult to rule out the possibility that the abnormality is due to indirect maternal toxicity instead of developmental toxicity of the compound [67]. Last but not least, the existence of high inter-species variation (~40%) in developmental toxicity response limits the accuracy of prediction for all *in vivo* studies [3, 4]. Simply adding a second species for compound testing will lead to higher false positive rates (40-60%) [68].

2.3 *In vitro* animal-based models for developmental toxicity testing

Despite the advantages of *in vivo* animal models introduced above, the need to reduce animal consumption, testing time and cost associated with *in*

vivo models have galvanized the development of alternative *in vitro* models. Before hPSCs were successfully derived in 1998 [11], main *in vitro* animal-based drug screening platforms for developmental toxicity testing include the frog embryo teratogenesis assay (FETAX) on xenopus [5], the chicken embryo toxicity screening test (CHEST) [6], the micromass (MM) assay using mouse embryonic mesenchymal cells [7], the mammalian whole embryo culture (WEC) assay using mouse [8] or rat, the zebrafish developmental toxicity assay [9], and the mouse embryonic stem cell test (mEST) [10]. According to the ECVAM Scientific Advisory Committee (ESAC), only MM assay, WEC and mEST for embryotoxicity testing are scientifically validated using twenty chemicals of known teratogenicity and ready for consideration for regulatory acceptance and application [69-71]. The accuracies of the three assays were 80% for WEC, 78% for mouse EST and 71% for the MM assay. The zebra fish model, on the other hand, has recently been proven to have comparable screening performance compared with all the above three assays [72-74]. In the following part of this section, I will introduce these four *in vitro* animal-based assays. The protocols, main applications as well as advantages and drawbacks will be covered for each of the assay.

2.3.1 The MM assay

The rodent micromass (MM) assay is based on the technique developed by Umansky to study the development and differentiation of chick embryo limb cells [75]. When cultured at high density (micromass), limb bud

mesenchyme cells isolated from 13-day rat embryos will form foci of differentiating chondrocytes [76], a fundamental step in the morphogenesis of the skeleton (Fig. 2.3.1). The MM assay can identify particular teratogenic compounds which can disrupt this cartilage histogenesis. The number of foci and the total surface of foci are calculated after compound treatment. The concentrations that produced 50% inhibition (IC_{50}) are then identified and used for the compound classification. Based on the results of the ECVAM validation study, the MM assay has a relatively good accuracy of prediction (70%) in general, with a best performance in identifying strongly teratogenic compounds [69]. However, currently studies using the MM assay for developmental toxicity screening are quite limited, possibly due to its laborious nature and the use of animal embryos.

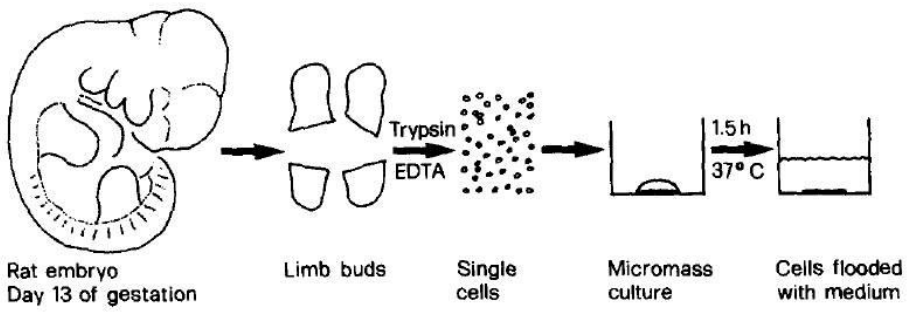

Figure 2.3.1 Schematic representation of limb bud cell preparation. Limbs are dissected from the embryo, trypsinized into single cell suspension, plated at high density (micromass) and flooded with medium. (Adapted from [76])

2.3.2 The WEC assay

The rat whole embryo culture (WEC) technique was mainly developed by Denis New in the 1960s [77]. The rat or mouse embryo and amnion enclosed within the visceral yolk sac (VYS) are explanted intact and cultured in an all-liquid media consisting mainly of heat-inactivated rat serum. A defined gas mixture is provided to the culture, whose oxygen content increased as a function of embryo age [77]. To drive more oxygen into the embryos, the whole culture system is in roller bottles, which can provide continuous turnover of the gas-liquid interface [78]. Morphological scoring system is applied to evaluate the development of the postimplantation embryos.

In the field of developmental toxicology, the enduring studied using WEC is mainly due to its flexibility [79]. It can be used for identification of a wide range of teratogenic agents including both chemicals and physical factors such as hyper/hypothermia [80] and oxidative stress [81]. By adding a metabolic activation system [82], or culturing embryos in serum obtained from animals even humans dosed *in vivo* [83, 84], WEC can also identify proximate teratogens whose toxicity are due to their metabolites instead of themselves without knowing the exact metabolic pathways. In addition, WEC could also be applied in rabbit other than rat or mouse, which can be used together with rat WEC to study the mechanisms underlying discordant responses between these two species (Fig. 2.3.2). Last but not least, the WEC could also be used

to study the *in vivo-in vitro* correlations of the developmental toxicity responses [85].

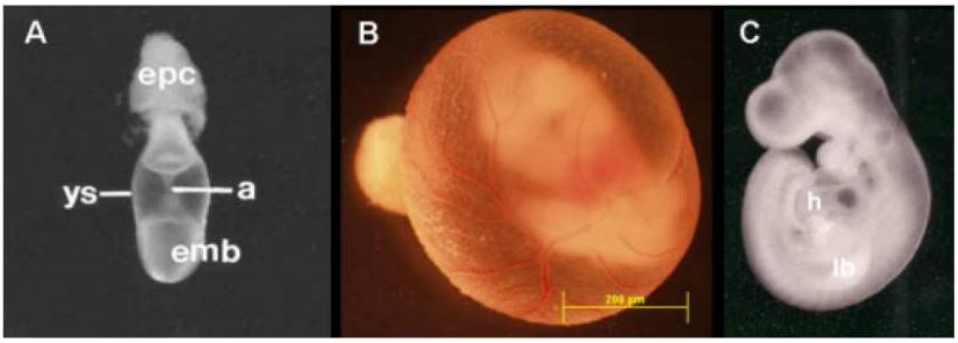

Figure 2.3.2 Embryos showing range of development possible in WEC. A: Gastation day (GD) -9 rat embryo. epc, ectoplacental cone; a, allantois; emb, embryo; ys, visceral yolk sac. B: GD-12 rat embryo in enclosed visceral yolk sac. C: GD-12 rat embryo with visceral yolk sac removed.h, heart; lb, limb bud. (Adapted from [79])

Despite the various advantages it could offer in developmental toxicology studies, WEC still suffers from some drawbacks. First of all, it uses animal embryos as the experiment objects, and the serum required to culture the embryos still need to sacrifice a lot of animals. Secondly, WEC is low throughput compared with the mouse EST and the zebrafish model, which makes its application for early screening quite limited. Thirdly, although the rat WEC could be used together with rabbit WEC, it still remains the question regarding human relevance of animal data, which exists in all animal-based *in vivo* and *in vitro* models.

2.3.3 The zebrafish model

The zebrafish model is a popular vertebrate model for developmental biology studies and toxicity screening of environmental contaminants as well as pharmaceutical compounds. It has several experimental advantages, such as the transparency of embryo and larva, test period, low cost, as well as easy manipulation [86]. The zebrafish finishes its embryogenesis in 72 hr, and can develop discrete organs and tissues in 120 hr after fertilization [87]. For developmental toxicity screening, the zebrafish embryos are exposed to test compounds with multiple concentrations for certain time period, which usually varies from 6-8 hr to 144 hr after fertilization, and evaluated for death and abnormal morphological changes [74, 88, 89] (Fig. 2.3.3). A morphological scoring system is applied with a score of 5-0.5. Score of 5 indicates normal morphology, while score of 1 represents severe malformations and score of 0.5 represents missing structures. The LOAEL and NOAEL values are identified together with the concentration of test compound which results in a 25% lethality rate (LC25). The LOAEL corresponds to a morphological score of no more than 3, and the NOAEL corresponds to a morphological score of 4. Compound with LC25 to NOAEL ratios of 10 or greater will be classified as a teratogen.

Currently studies using zebrafish models for developmental toxicity testing generally showed an accuracy of 83-87% [73, 89, 90]. However, one study published in 2011 only showed an accuracy of 60% when testing 15

compounds of known teratogenicity [91], which raises the necessity of further improvement and validation of the current model. It also has limitations compared to *in vivo* animal studies using mammals. Despite comparable development processes, the phenotypic differences between zebrafish and mammals are quite obvious, making it difficult to correlate abnormalities observed in zebrafish with those in mammals. More importantly, the lack of placenta makes the exposure to drugs from indirect to direct, leading to potential differences in drug adsorption, distribution, adsorption, distribution, metabolism and activation capacity compared with mammals.

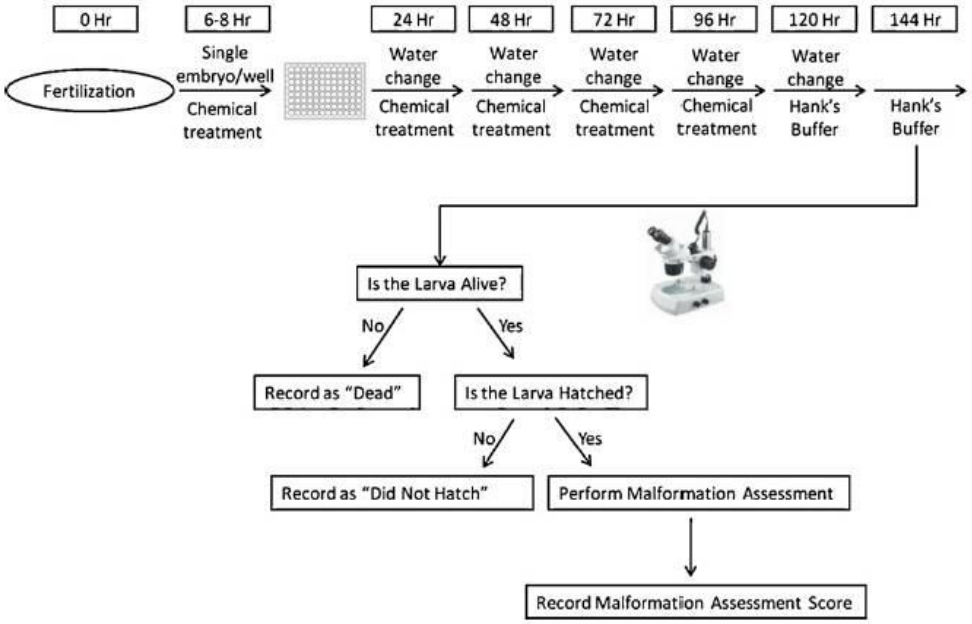

Figure 2.3.3 Experimental design of zebrafish developmental assay. (Adapted from [73])

2.3.4 The mEST

The core standard of mEST is to evaluate the toxicity of compounds based on their effect on mouse embryonic stem cell (mESC) differentiation to beating cardiomyocytes [10]. The assay is based on the fact that in the presence of fetal bovine serum (FBS) and absence of the leukemia inhibitory factor (LIF) in the maintenance medium, majority of the mESCs would spontaneously differentiate into cardiac lineage. According to the standard protocol, the mESC line D3 cells are first formed into embryoid bodies (EBs), which are multicellular aggregates of cells, using hanging drop method (Fig. 2.3.4). These EBs are harvested on day 3 and kept in suspension culture for 2 days before seeded into 24-well plates for further outgrowth and differentiation. Drug dosing starts at the very first beginning of EB formation and continues until the end of the cell culture. On day 7 or day10, all the cells would be accessed for cardiac differentiation either using FACS to check the cardiac gene expression levels or using traditional microscope observation, and an 50% of inhibition of differentiation (ID_{50}) value would be acquired for each test compound. Together with the 50% of inhibition of cytotoxicity (IC_{50}) values of each drug for mESCs as well as mouse embryonic fibroblast cell line 3T3 cells, they could classify the test compounds into three classes as "non-embryotoxic", "weakly embyotoxic" and "strongly embryotoxic" using the validated prediction model.

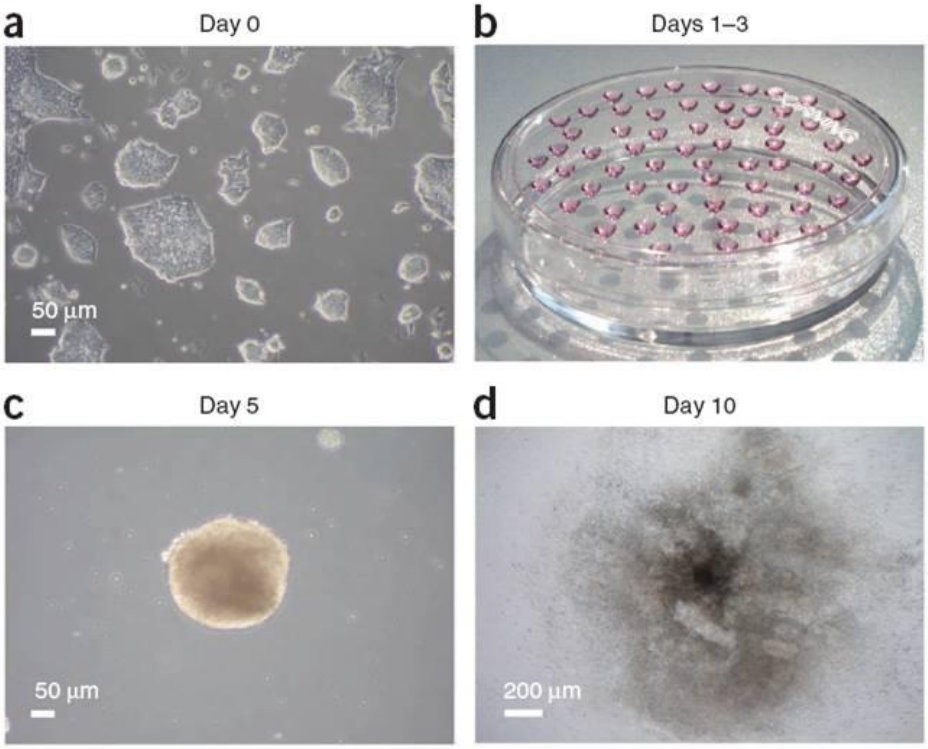

Figure 2.3.4 Different time points in cardiac differentiation of mESCs. (a) Undifferentiated mESCs cultured in maintenance medium in the presence of LIF. (b) Hanging drop culture from day 1 to 3 of differentiation. (c) Embryoid body at day 5 of differentiation in suspension culture. (d) Embryoid body outgrowth at day 10 of differentiation in 24-well plates. The center of the picture in d shows the area at which beating cardiomyocytes were located. (Adapted from [10])

Although mEST has been validated by ESAC, there are still many limitations and disadvantages of this assay [10]. The whole test spans 7 or 10 days, which is relatively long, and the differentiation process is quite labour-intensive. One of the main limitations is the high inter-species variation (~40%) [3], which means toxicity tests using animals are not representative for human

beings due to species-specific pharmaco-toxicological responses, and also exists in all of the other methods listed earlier. Famous examples have been shown in the cases of thalidomide [92], 13-cis retinoic acid and isotretinoin, which all demonstrated no obvious effects in mice but led to severe malformations in human embryos [93, 94].

Besides inter-species variation problem, a recent study using the mEST showed that the moue EST could only identified two out of thirteen substances tested, resulting an accuracy of only 15% [95]. None of the thirteen chemicals have inter-species variation in developmental toxicity between mouse and human. A further detailed study on these eleven misclassified compounds found that the lack of other endpoints such as developmental neurotoxicity and osteotoxicity might be the cause of misclassification for seven of these drugs [96]. The application domain of the mEST was limited to compounds that function in cardiac development and do not need metabolic conversion [96].

2.4 *In vitro* hPSC-based models for developmental toxicity testing

Since human embryonic stem cells (hESCs) were successfully derived from human blastocysts in 1998 [11], people are trying to replace mESC with hESCs in developmental toxicity testing in order to avoid inter-species variation [94, 97]. Also, the generation of induced pluripotent stem cells (iPSCs) from human adult cells [98] has provided more and cheaper cell

sources for compound testing, and made it possible to study patient-specific drug responses.

Up to now, few assays using hPSCs (hESCs & iPSCs) for developmental toxicity testing have been developed to screen a wide range of teratogens. The metabolite biomarker-based hPSC teratogenicity assay [99] and the human pluripotent stem cell test (hPST) [100] are probably the only two most promising ones. In the following sections, I will first introduce these two assays in more detail, and then summarize the main advantages and limitations of current hPSC-based models for developmental toxicity testing.

2.4.1 The metabolite biomarker-based hPSC teratogenicity assay

Currently the most developed assay using hPSCs should be metabolite biomarker-based hPSC teratogenicity assay. It's first developed in 2010 by Stemina Biomarker Discovery, Inc. and kept being optimized afterwards [13, 99, 101]. Basically they cultured the WA09 hESCs in undifferentiated state during compound exposure of 72 hrs, and collected the spent media from the last 24-hr treatment for liquid chromatography high resolution mass spectrometry (LC-HRMS) analysis. Various metabolites were then recognized by mass feature detection and targeted metabolite biomarkers were identified as indicators of developmental toxicity. In their study, by using two metabolite biomarkers ornithine and cystine, which are indicators of polyamine metabolism and reactive oxygen species (ROS)-related pathways, they could

classify the potential teratogens in the test set (13 drugs) with 77% accuracy [99]. Together with the training set data, the classification accuracy could be as high as 89% with 36 drugs tested.

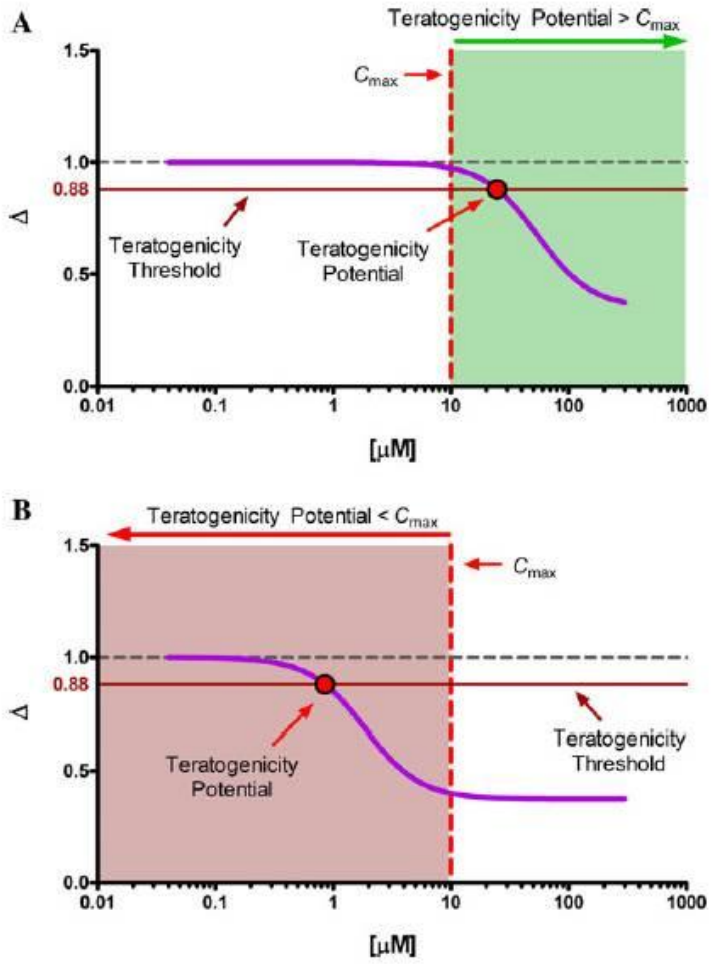

Figure 2.4.1 Graphical representation of the classification scheme for known human teratogens and nonteratogens utilizing the therapeutic C_{max} concentration to set the classification windows. The dose-response curve for the o/c ratio (purple curve) was fit using a four-parameter log-logistic model and used to interpolate the concentration where the o/c ratio crosses the teratogenicity threshold (i.e., teratogenicity potential, black-bordered red circle). A test compound was predicted as a nonteratogen when the

teratogenicity potential concentration is higher than the human therapeutic C_{max} (A). A test compound was predicted as a teratogen when the teratogenicity potential concentration is lower than the human therapeutic C_{max} (B). The x-axis is the concentration (μM) of the compound. The y-axis value of the o/c ratio is the ratio of the reference treatment normalized (fold change) values (ornithine/cystine) (Adapted from [99])

The above figure shows how this assay classified individual developmental toxicants. They used the ornithine/cystine ratio (o/c ratio), which is the fold change of ornithine for treatment x divided by the fold change of cystine for treatment x, as the experiment readout. A teratogenicity threshold of 0.88 was set to this ratio. If the exposure levels are greater than the concentration corresponding to the teratogenicity threshold, which is called the teratogenicity potential concentration, the treatment would be considered as teratogenic (Fig. 2.4.1). After that, the teratogenicity potential concentration was compared with the peak plasma *in vivo* concentration (C_{max}) of the test compound. If the teratogenicity potential concentration is lower than C_{max}, the test compound would be classified as a teratogen; otherwise it would be a non-teratogen.

One of the main advantages of the metabolite biomarker-based hPSC teratogenicity assay is that it can detect human teratogenicity of chemicals at their C_{max} following therapeutic doses, which is considered to be more clinically relevant. In addition, this assay has the highest accuracy (89%) for the same set/subset of test compounds when compared with most of the

animal-based *in vivo* and *in vitro* assays such as rodent (86%) and rabbit (79%) *in vivo* assays, as well as mEST (74%), WEC (73%) and the zebrafish model (75%) [99]. In addition, this assay might also be used to understand the Mech Developal toxicity of certain compounds. Last but not least, the metabolite biomarker-based hPSC teratogenicity assay is high-throughput, as well as time and cost-effective.

However, the metabolite biomarker-based hPSC teratogenicity assay may still suffer from several drawbacks. First, all the hPSCs were cultured in maintenance medium without any differentiation, compounds which adversely affect differentiation into specific lineages may not be correctly classified. For example, Diphenylhydantoin and Bosentan, which of both could disrupts the cardiovascular and craniofacial development in human, were misclassified as non-teratogens using the metabolite biomarker-based hPSC teratogenicity assay [99]. Second, no spatial and morphological endpoints were included, primarily due to no spatial and temporal control of the culture system. Besides, by only using the o/c ratio as the model readout, the model may be most applicable in finding compounds which could disrupt the ROS-related pathways and polyamine metabolism.

2.4.2 The hPST using mesoendoderm differentiation

The human pluripotent stem cell test (hPST) was developed by Hoffman-La Roche in New Jersey in 2013, which evaluated compounds' teratogenicity

in the context of mesoendoderm differentiation of hPSCs [100]. The whole test was done in monolayer cell culture condition in a 96-well plate format, and the cells were differentiated in a chemically-defined media for 3 days before fixation and immunostained for mesoendoderm markers for data analysis (Fig. 2.4.2a). The concentration of the test compound which could result in 50% inhibition of endoderm marker Sox17 expression relative to DMSO control, i.e. IC_{50} of Sox17, was calculated for each compound. By applying a IC_{50} threshold of 30 μM, the hPST could acquire an accuracy of 94% in screening of 71 pharmaceutical compounds (Fig. 2.4.2b). If changing the threshold from 30 μM to 35 μM, it could correctly classify 13 of 15 environment toxicants with an accuracy of 87%.

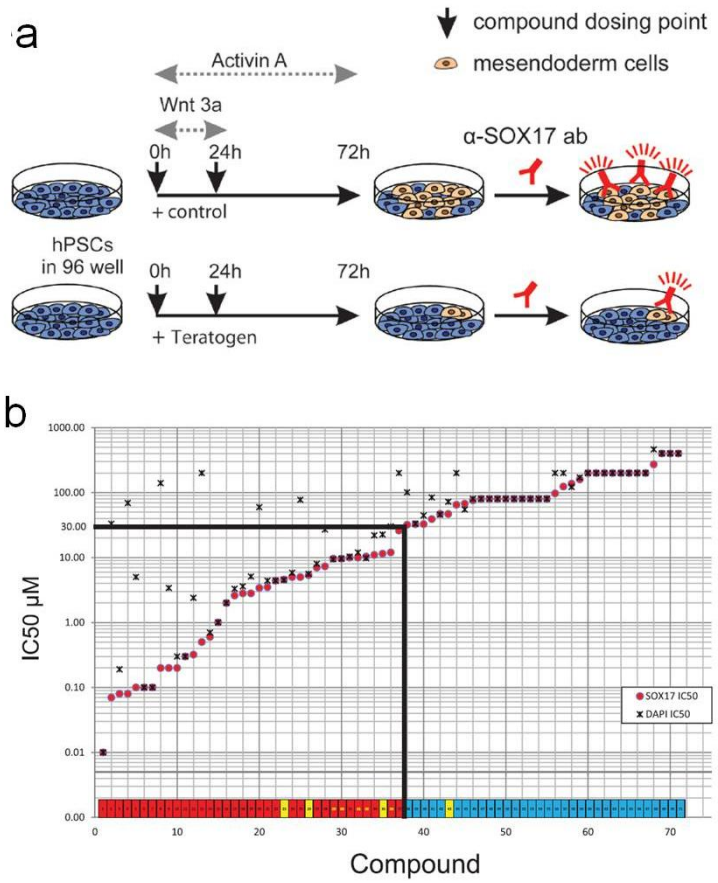

Figure 2.4.2 The hPST model (a) Schematic figure showing the time line of mesendoderm differentiation, compound dosing, and immunostaining. (Adapted from , Fig. 2a). (b) Plot of SOX17 and DAPI IC_{50} values for 71 tested pharmaceutical compounds. The colored boxes on the x-axis delineate the compounds tested. Boxes in red are true positives, blue boxes are true negatives, and yellow boxes are incorrectly classified at the 30µM SOX17 IC_{50} threshold. (Adapted from [100])

Although the hPST has been shown a high accuracy in compound screening, it still need further improvement in several aspects. First, the assay so far only has different test sets of compounds without any application sets. The thresholds shown here are kind of artificial without further validation. No

explanation was given regarding the inconsistency of IC_{50} thresholds between pharmaceutical compounds and environmental toxicants. Second, the quality control of the hPST assay is not trivial due to stochastic factors involved in hPSC differentiation or inherent passage-to-passage variation. The failure rate of a 96-well plate was near 20% even after fully optimization and quality screen of frozen cell stocks. In addition, when changing the hPSC line from current H9 to other hPSC lines such as LSJ-1, the concentration as well as duration of growth factor treatment for differentiation must be recharacterized due to line-to-line variability.

2.4.3 Summary

Despite of various aspects required for further development, it's kind of surprising that hPSC-based assays could actually show a decent accuracy (~90%) of developmental toxicity testing so far by only focusing on undifferentiated maintenance culture or the early stages of organogenesis since embryo development is so complex. There are some possible supporting bases behind it. First, the elimination of inter-species variation existing in all animal-based *in vivo* and *in vitro* assays improves the accuracy of all hPSC-based assays. Second, hPSCs are derived from human embryo and capable of differentiation into every cell type in the body. This broad transcriptional competence allows the interrogation the broadest milieu of signalling pathways when early stages of differentiation were captured [100]. Lineage-

specific differentiation may limit an assay's capability in predicting developmental toxins which affect development of a different lineage [99].

The hPSC-based assays can be best used in early discovery-phase detection of potential teratogenic xenobiotics due to their human-specific, high-throughput, time and cost-efficient features. Focusing on early stages of embryo development in developmental toxicity testing significantly reduces the time duration of *in vitro* hPSC-based assays from one week to 3 days without sacrificing the assay accuracy. However, current hPSC-based assays still need further optimization and validation. More importantly, these models only focus on the differentiation capabilities of hPSCs without considering the indispensible spatial and temporal control of cell differentiation and morphogenesis during embryo development, which was mentioned in Section 2.1. Therefore, new hPSC-based models are needed to recapitulate this important feature during early embryo development, which may show a higher predictivity for teratogen screening.

3. Specific aims

As mentioned in Chapter 2, cell differentiation and tissue morphogenesis characterize the whole embryo development process. The correct embryo development needs not only the correct cell fate control, but also needs the correct spatial control within the embryo. However, current *in vitro* hPSC-based models for developmental toxicity testing are all established based on

differentiation or maintenance culture-only platforms without any spatial control of the differentiation. In addition, no specific morphogenetic movements have been captured. Here, we hypothesize that a new hPSC-based model which captures both spatial controlled cell differentiation and morphogenetic movements may be more sensitive to teratogen treatment and show a better prediction performance compared with existing *in vitro* models.

In order to establish such a model, the mechanism behind the spatial controlled differentiation and morphogenesis needs to be studied and applied. Studies have shown that while biochemical cues are essential for stem cell differentiation, mechanical signalling is actually critical in spatially defining cell fates *in vivo*. However, so far the relevant *in vitro* studies have only been done in MSCs or adult mammalian cells. Due to the cell property differences between MSCs/adult mammalian cells and hPSCs which may lead to different underlying mechanisms, studies on hPSCs are needed.

Once this new hPSC-based model which captures both spatial controlled cell differentiation and morphogenetic movements is established, its sensitivity to known teratogens needs to be tested. Proper data analysis is also needed to quantify the drug testing results and correctly differentiate teratogenic compounds from the non-teratogens.

Therefore, there are three main aims presented in this dissertation:

1) To establish a hPSC-based spatially patterned mesoendoderm differentiation model and study the underlying mechanism.

2) To mimic both spatially patterned mesoendoderm differentiation and morphogenesis within the differentiation model and verify its sensitivity to existing developmental toxic drugs.

3) To correctly classify drugs into teratogenic and non-teratogenic ones and scale up the system if possible.

This dissertation would provide insights into the mechanism of spatially patterned differentiation in hPSCs, which refers to Aim 1 specifically; and show for the first time an *in vitro* model capturing both spatial differentiation patterning and morphogenesis (Aim 2). This model opens up the mindset of platform designing for developmental toxicity testing application and probably provides a better system for more accurate and robust developmental toxicity screening (Aim 2 & 3). In the following chapters (Chapter 4-6), experiment designs and results of each aim are presented respectively.

4. E-cadherin mediated spatial differentiation of hPSCs within 2D cell colony

4.1 Introduction

The stem cell microenvironment is a critical determinant in cell fate specification. A precise understanding of how different environmental cues affect decision rules during cell fate instruction can provide insights in mechanisms controlling spatially organized differentiation during actual

embryo development. So far, researchers have focused on how local paracrine signaling leads to stem cell fate heterogeneity [102, 103], as well as the effects of mechanical forces generated by cell adhesions in the stem cell niche on cell fate determinations. Asymmetry in cell-cell and cell-matrix adhesions in the developing embryo is known to be an important determinant for patterning tissues [104]. However, its corresponding role in generating heterogeneity in a PSC culture is currently unknown.

Most of the current understanding on the effects of mechanical force in human stem cell fate specification is based on studies with adult human stem cells [105, 106]. Asymmetry in integrin mediated mechanical forces between the periphery and interior of a MSC population can spatially direct osteogenic-adipogenic [57, 58] or chondrogenic-myogenic [107] differentiation decisions. However, since hPSCs are epithelial in nature, fundamental differences in mechanical force transmission between MSCs and hPSCs may alter the underlying mechanisms of cell fate instruction. Besides integrin adhesion, E-cadherin adhesion has been demonstrated to specifically affect hPSC fates. E-cadherin adhesion is required to maintain pluripotency [108, 109] whereas increased integrin adhesion-mediated forces promote differentiation [110]. Interestingly, the instructions of the two opposing cell fates by integrin and E-cadherin adhesions both act through the activation of Rho-ROCK myosin II signaling [108-110]. This is contrary to the conventional paradigm of integrin-cadherin crosstalk observed in adult epithelial cells (*e.g.*, MDCK), where

integrin activated Rho-ROCK-myosin II signaling antagonizes E-cadherin activated Rho-Dia [111] or Rac [112, 113] signaling. Therefore, it is unclear how the two modes of cell adhesion signal through a common downstream effector to control hPSC pluripotency-differentiation decision; and how their relative spatial distribution leads to heterogeneous cell fate patterning in a hPSC culture.

Here, we investigated the collective effects of integrin and E-cadherin adhesions in patterning mesoendoderm differentiation decision in hPSCs, which marks one of the earliest differentiation events in the epiblast [114]. Cell micropattering was utilized to control and modulate the relative spatial distribution and strength of integrin and E-cadherin adhesions within a cohesive hPSC colony so as to probe their crosstalk mechanism. Our data indicated that E-cadherin adhesion signaling is the dominant mediator in patterning pluripotent-differentiation decisions. Spatially polarized integrin adhesion in a cohesive hPSC colony compete to recruit Rho-ROCK activated myosin II away from E-cadherin mediated cell-cell junctions to promote differentiation at that locality, resulting in a heterogeneous cell population.

4.2 Materials and Methods

4.2.1 hPSC maintenance and differentiation

The hESC line H9 was obtained from WiCell Research Institute, Inc., (Madison, WI, USA) and cultured in hPSC-qualified Matrigel^{TM} (354277, BD

Biosciences, Singapore) coated cell culture plates using mTeSR^{TM}1 medium (05850, StemCell^{TM} Technologies, Singapore). Mechanical scraping was applied during normal subculture in order to only get undifferentiated hES colonies after Dispase (07923, StemCell^{TM} Technologies, Singapore) treatment. To induce mesoendodermal differentiation, cells were cultured in basal STEMdiff^{TM} APEL^{TM} medium (05210, StemCell^{TM} Technologies, Singapore) supplemented with 100 ng/ml Activin A (338-AC-025, R&D Systems, USA), 25 ng/ml BMP4 (314-BP-010, R&D Systems, USA) and 10 ng/ml FGF2 (233-FB-025, R&D Systems, USA).

4.2.2 Fabrication of PDMS stencils for micropatterning

Polydimethylsiloxane (PDMS) stencil components were designed with L-edit Pro software (Tanner, USA). A laser-cutter Epilog Helix 24 Laser System, USA) was used to cut the designed patterns on a 127 μm thick PDMS sheet (Specialty Silicone Products Inc.), and then the PDMS sheet was bonded to a laser-cut, 2mm thick PDMS gasket using liquid PDMS and baked at 60 ℃ for 3-4 hr to finally get the PDMS stencil for micropatterning (Fig. 4.2.1). The stencils were sterilized by autoclaving at 120 ℃ for 30 min every time before use.

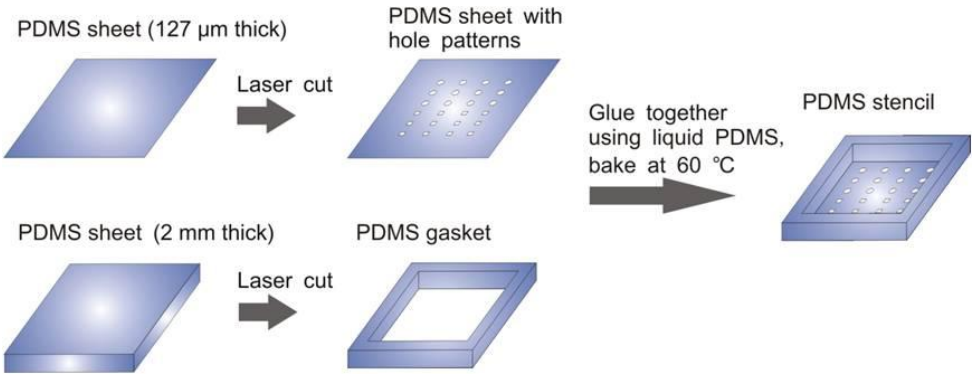

Figure 4.2.1 Generation of PDMS stencil for micropatterning.

4.2.3 Generation of micropatterned hPSC (μP-hPSC) colonies

The autoclaved PDMS stencil was first sealed onto a 60 mm petri dish using 200 μl of 70% ethanol. After drying in the cell culture hood, 450 μl Matrigel™ in DMEM/F12 (Life Technologies) was then added into each stencil and incubated for 5 hr at 37 ℃ before use. To obtain single-cell suspension, the hPSC culture was treated with Accutase (Merck Millipore) for about 10 min, and the cells were resuspended in mTeSR1 supplemented with 10 μM Y27632 (Calbiochem). The cells were seeded onto the PDMS stencils at 100% confluence density of 4.44×10^5 cells/cm^2. For a stencil with a surface area of 4.5 cm^2, 2 million cells were seeded every time. After 1 hr incubation for cell attachment, the stencil was removed and the unpatterned substrate was passivated with 0.5% pluronic acid (Sigma) in DMEM/F12. After 10 min incubation, the μP-hPSC colonies were washed 3 times with DMEM/F12 (Gibco), incubated for another 4 hr in mTeSR1 medium supplemented with 10

μM Y27632 before switching to mTeSR1 medium. Differentiation was initiated after overnight incubation by changing to mesoendoderm differentiation medium.

4.2.4 Immunofluorescence staining

Samples were fixed for 20 min in 3.7% paraformaldehyde, and permeabilized for 15 min with 0.5% Triton X-100 in PBS. After overnight incubation at 4 ℃ in blocking buffer (2% BSA and 0.1% Triton X-100 in TBS buffer), they were incubated overnight at 4 ℃ with primary antibodies (5-10 μg/ml in blocking buffer). The primary antibodies used in this study include: goat-anti-Brachyury (10 μg/ml, AF2085, R&D systems); rabbit-anti-phospho-myosin light chain 2 (1:200 dilution, 3674, Cell Signaling); rabbit-anti-E-cadherin (1:50 dilution, sc-7870, Santa Cruz Biotechnology); rabbit-anti-β-catenin (1:50 dilution, sc-1496, Santa Cruz Biotechnology); mouse-anti-paxillin (1 μg/ml, BD610052, BD BioSciences); mouse-anti-vinculin (1:200 dilution, V4505, Sigma); mouse-anti-integrin β1 (5 μg/ml, MAB2253Z, Merck Millipore); rabbit-anti-Nanog (4 μg/ml, ab21624, Abcam), rabbit-anti-Fgf8 (10 μg/ml, ab81384, Abcam), and rabbitanti-Eomes (10 μg/ml, ab23345, Abcam). The samples were washed 5 times with 15 min interval before adding the Alexa Fluor dye-conjugated secondary antibodies (1:1000, Molecular Probes). F-actin was stained by incubating with Alexa Fluor 488 Phalloidin (1:200 dilution, A12379, Molecular Probes). After 1 hr incubation at room temperature, samples were washed for 5 times with 15 min interval and

counter-stained with Hoechst 33342 (10 μg/ml, Molecular Probes) for 5 min. After that, samples were washed 3 times with PBS and then mounted using Fluorsave™ (Calbiochem).

4.2.5 Image acquisition and analysis

Immunofluorescence images of entire μP-hPSC colonies were acquired with an epifluorescence microscope (Olympus IX81, Olympus) with a motorized stage (Prior Scientific). Confocal images were acquired using Zeiss LSM 5 DUO microscope (Zeiss). Image processing and analysis was performed using ImageJ (version 1.46r, NIH).

Quantification of Brachyury (T) expression

The percentage of T^+ cells in a μP-hPSC colony was determined from 8-bit phase contrast and T immunofluorescence images. A region of interest (ROI) depicting the colony boundary was determined from the phase contrast image and applied to the fluorescence image, which had been subjected to contrast adjustment (LUT = 20-100) and binary conversion processing steps. The percentage of the ROI with positive fluorescence signal was measured.

The T expression profiles in specific regions of the μP-hPSC colonies were obtained by defining an arbitrary line on 8-bit fluorescence images with adjusted contrast (LUT = 20-100), and determining the intensity profile along that line.

Quantification of ppMLC expression and fiber length

The expression levels of ppMLC at the apical, lateral and basal intracellular domains were measured from a 3D confocal section spanning the height of the colony. The stack of confocal z-sections was divided into three sections to represent the apical, lateral and basal domains of the cell, and corresponding maximum projection images were generated. The percentage of $ppMLC^+$ area was determined as described above for T^+ area quantification.

To quantify ppMLC fiber length at different regions of the μP-hPSC colonies, a 8-bit projection image of a 3D confocal stack of ppMLC was despeckled, converted to a binary image using Otsu's method, and subjected to medial axis skeletonization to obtain a morphological skeleton of the ppMLC fiber distribution. A ROI mask was then applied to select for the desired colony region to be analyzed. The fiber length was determined by measuring the branch length of each skeleton using the Analyze Skeleton plugin. The mean of the 20 longest branches was taken to be the representative fiber length at the particular region of the colony.

Quantification of E-cadherin localization

To compare the diffusiveness of E-cadherin localization within or among μP-hPSC colonies in different treatment groups, the average $E\text{-cadherin}^+$ area per cell was quantified. A ROI of a fixed area was applied onto 8-bit maximum projection images of 3D confocal stacks for Hoechst 33342 and E-cadherin, followed by image segmentation, despeckling and binarization using Otsu's method to acquire the total percentage of $E\text{-cadherin}^+$ area as well as

the total cell number within each ROI. After that, the average E-cadherin^{+} area per cell was calculated. The higher of the average E-cadherin^{+} area per cell, the more diffusive of E-cadherin's localization was within the ROI.

4.2.6 Inhibition studies

Monoclonal antibodies against integrin-β1 (MAB1951Z, Merck Millipore), -α5 (MAB1956Z, Merck Millipore), -α6 (MAB1378, Merck Millipore), -α2β1 (MAB1998Z, Merck Millipore) and E-cadherin (MAB3199Z, Merck Millipore) were used to functionally block integrin and Ecadherin-mediated adhesions. Goat-anti-mouse IgG (sc-2055, Santa Cruz Biotechnology) was used as a control antibody. The antibodies were diluted to desired concentrations in culture media and added during both the cell seeding and differentiation steps.

For all other inhibition studies, the inhibitors were added at the initiation of mesoendoderm differentiation and incubated for 24 hr. Blebbistatin (203390, Merck Millipore) and Y27362 were used to inhibit myosin heavy chain and ROCK activation respectively; Cytochalasin D (C8273, Sigma) was inhibit the actin network; EHT1864 (3872, Tocris BioSciences) and ML141 (4266, Tocris BioSciences) were used as inhibitors for Rac and Cdc42 respectively.

4.2.7 E-cadherin Fc (EcadFc)-coated substrates

To generate μP-hPSC colonies on EcadFc-coated substrates, 10 μg/ml of E-cadherin Fc (648-EC-100, R&D Systems) in calcium-containing PBS was added to a PDMS stencil that has been sealed onto a 60 mm petri dish and incubated for 3 hr at 37 ℃. Cell seeding was performed as described above for μP-hPSC colonies on Matrigel™-coated substrate. Substrates with alternating strips of Matrigel™/EcadFc coating were obtained by sealing a PDMS stencil with 800 μm-wide strips onto a 35 mm tissue culture dish. 10 μg/ml of EcadFc solution in calcium-containing PBS was added to the stencil and incubated for 3 hr incubation at 37 ℃. The stencil was then removed and backfilled with Matrigel™ solution to coat the remaining unpatterned substrate. After 3 hr of incubation, cell seeding was performed as described above.

4.2.8 RNA isolation, cDNA synthesis and quantitative RT-PCR

Total RNA was extracted from the samples on day 3 of the differentiation using the RNeasy® Plus Micro Kit (Qiagen) according to manufacturer's protocol. Then cDNA was then synthesized from the extracted RNA using High Capacity RNA-to-cDNA Kit (Applied Biosystems). To analyze the gene expression levels of each sample, quantitative RT-PCR was performed using FastStart Universal SYBR Green Master (ROX) (Roche) on the ABI 7500 Fast Real-Time PCR system (Applied Biosystems) according to the manufacturer's standard protocol. The relative quantitative expressions values

of target genes were calculated after normalization with housekeeping gene GAPDH.

4.3 Results

4.3.1 Spatial heterogeneity in mesoendoderm differentiation corresponds to spatial polarization of cell adhesion and actomyosin networks

Cell micropatterning has been used extensively to spatially control the magnitudes of cell adhesion forces within a cohesive cell population [105, 115]. Similarly, we employed stencil micropatterning to generate circular hPSC colonies so as to impose polarized cell adhesions between the periphery and interior regions of the colony. Matrigel™ islands were first patterned onto a petri dish before single-dissociated hPSCs were seeded. The non-patterned area was passivated to spatially confine the cell population (Fig. 4.3.1). Cells in μP-hPSC colonies could maintain pluripotency and show similar gene and protein expression levels compared to conventionally cultured hPSCs cultured in mTeSR™1 maintenance medium (Appendices, Fig. 9.1.1, Appendices, Fig. 9.1.2). The colonies were cultured overnight in hPSC maintenance medium before mesoendoderm differentiation was initiated using a serum-free induction medium supplemented with Activin A, FGF2 and BMP4.

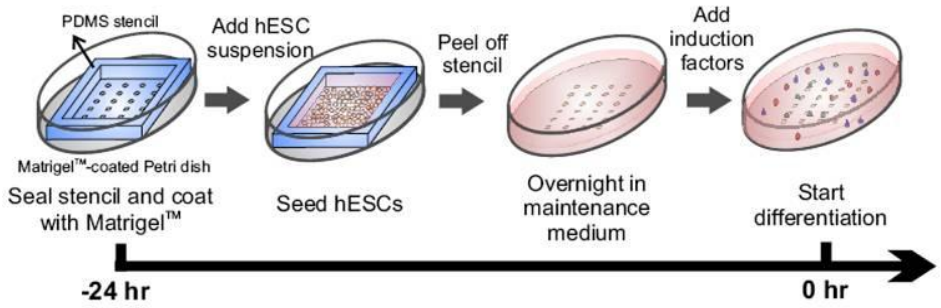

Figure 4.3.1 Schematic representation of micropatterning of hPSC colonies and mesoendoderm induction.

To ascertain that cell adhesion and actomyosin networks were spatially polarized in the micropatterned-hPSC (μP-hPSC) colony, we examined the localization patterns of cell adhesion molecules and activated myosin II before differentiation was initiated (*i.e.,* at 0 hr). We observed tissue-level spatial asymmetry in the distribution of the force-transmitting molecules. Integrin β1, vinculin and paxillin were preferentially localized to the colony periphery (Fig. 4.3.2), suggesting stronger cell-matrix adhesions at the colony periphery than interior. Correspondingly, the distribution of E-cadherin was diffusive near the colony periphery, while their localization at the inter-cellular junctions was maintained at the colony interior (Fig. 4.3.3). Phosphorylated myosin light chain (ppMLC) was localized to a circumferential actomyosin contractile cable at the colony periphery (Fig. 4.3.3, white arrows). In the colony interior,

ppMLC was localized at the cell-cell junctions (Fig. 4.3.3).

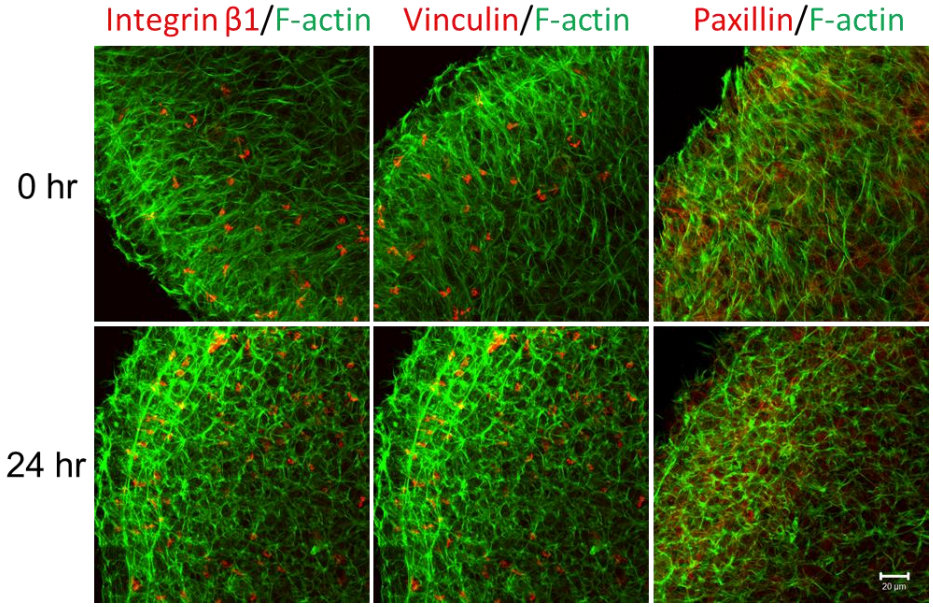

Figure 4.3.2 Asymmetric spatial localization of integrin mediated cell-matrix adhesion in the μP-hPSC colony. Images are immunofluorescence projections of 3D confocal sections of integrin β1, vinculin and paxillin before (0 hr) and after (24 hr) mesoendoderm differentiation. All samples were counter-stained for F-actin (blue). Scale bar, 20 μm.

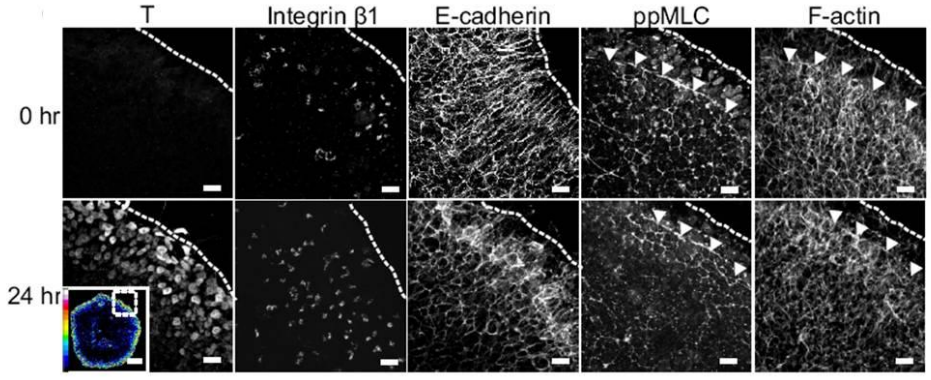

Figure 4.3.3 Asymmetric spatial localization of cell adhesion and actomyosin contractile networks components preceded and persisted during

mesoendoderm differentiation. Images are immunofluorescence staining of Brachyuary (T), integrin β1, E-cadherin, phosphorylated myosin light chain (ppMLC) and F-actin before (0 hr) and after (24 hr) mesoendoderm differentiation. Inset show intensity map of T expression in the entire colony. Dotted white lines denote colony edge. Scale bar, 20 μm in (b), 200 μm in (b, inset).

After 24 hours of differentiation, we observed positive immunostaining for the mesoendoderm marker, Brachyury (T) at the colony periphery (Fig. 4.3.3, lower panel) while the colony interior remained pluripotent *i.e.*, $Nanog^{+}$ (Fig. 4.3.4a). The localization of T was coincidental with the cell adhesion polarization patterns in the μP-hPSCs, which persisted after differentiation (Fig. 4.3.2, Fig. 4.3.3).

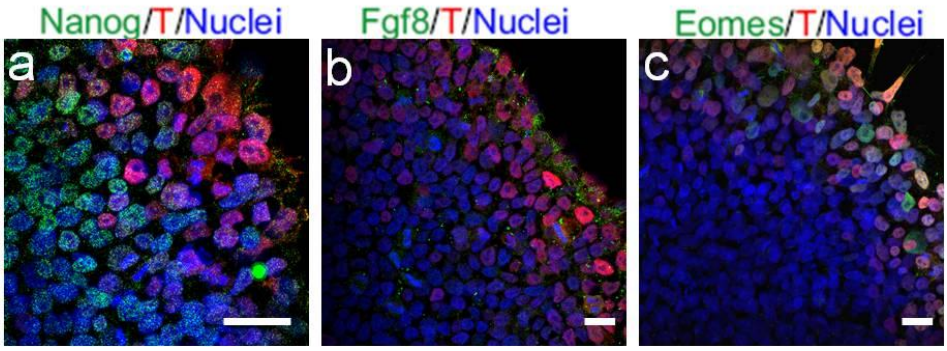

Figure 4.3.4 Expression of pluripotency and mesododerm markers in μP-hPSC colonies after 24 hr of differentiation. (a) Nanog, (b) Fgf8, (c) Eomes. All samples are counter-stained for Brachyuary, T (red) and nuclei (blue). Scale bar, 20 μm in (a-c).

We also observed that T^{+} cells at the colony periphery had more distinct intracellular apical-basal polarization of the actomyosin contractility (Fig.

4.3.5a). In the T^+ cells, ppMLC expression at the apical cellular domain was significantly higher than that of the basolateral domains (Fig. 4.3.5c). ppMLC and F-actin in the T^- interior cells were sequestered to the cadherin adherens junctions (AJs) indicated by -catenin co-localization (Fig. 4.3.5a,b). Other mesoendoderm markers, including Fgf8, and Eomes showed similar expression patterns as T (Fig. 4.3.4b,c). These data collectively suggested that spatial localization of mesoendoderm differentiation was coincidental with the spatial polarization patterns of the cell adhesion and actomyosin networks.

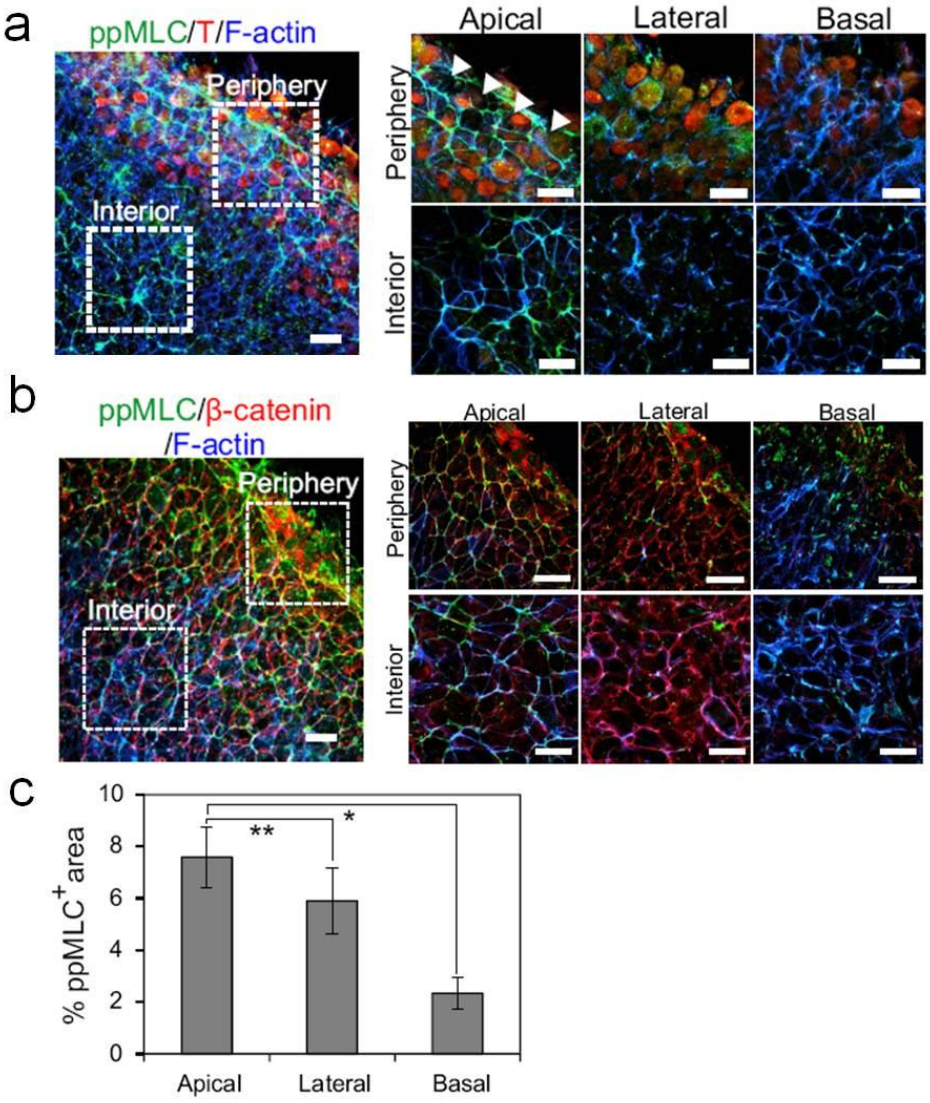

Figure 4.3.5 Apical-basal polarization of the actomyosin and actin cytoskeleton networks within μP-hPSC colonies after 24 hr of differentiation. (a) T^+ cells at the colony periphery had more distinct apical-basal intracellular polarization of actomyosin and F-actin cytoskeleton networks. Co-immunostaining of T (red), ppMLC (green) and F-actin (blue) shows their respective intracellular localization at the colony periphery and interior. White arrows denote circumferential actomyosin contractile cable. (b) Co-immunostaining of ppMLC (green), β-catenin (red) and F-actin (blue)

showing their respective subcellular localization at the periphery and interior of the μP-hPSC colonies. Scale bar, 20 μm in (a, b). (c) Quantification of ppMLC expression at the apical, lateral and basal cellular domains of T^+ cells at the periphery of μP-hPSC colonies. Data are average ± s.e.m of 7 images. *p<005, **p<0.01 (Student's t-test).

4.3.2 Control over mesoendoderm differentiation patterns by modulating integrin and E-cadherin adhesions

We then demonstrate that one can modulate the relative magnitudes and spatial distribution of integrin and E-cadherin adhesions as a mean to control the ensuing differentiation process. Geometrical anisotropy of ECM substrates leads to a higher concentration of integrin-mediated traction forces at sharp corners or regions of convex curvatures [115, 116] (Fig. 4.3.6a). When the hPSCs were micropatterned onto Matrigel™ islands of different geometries at a constant colony area, T localization was still restricted to the colony periphery (Fig. 4.3.6b). By mapping T expression intensity at different localities within a single colony, we found that the extent of mesoendoderm induction was higher in sharp corners of square and rectangular colonies (Fig. 4.3.6c) and at convex curvatures of a semi-circular arc (Fig. 4.3.6d), which corresponded to reported high integrin-mediated stress regions in an anisotropic geometry [115, 116].

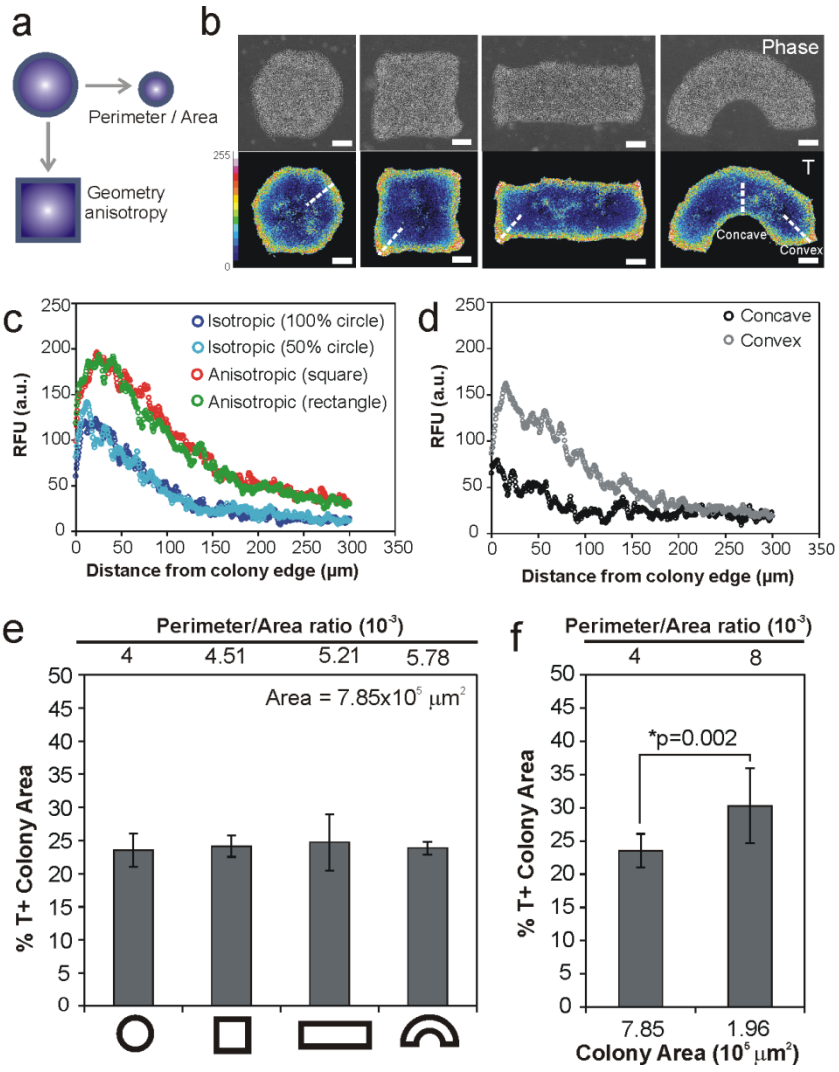

Figure 4.3.6 (a) Modulating mesoendoderm differentiation by changing the relative magnitude (with anisotropic geometries) and ratio (with increased perimeter) of integrin and E-cadherin adhesions. (b) μP-hPSC colonies of different geometrical shapes but same colony area. Phase images (top panel) and intensity maps of T expression (bottom panel) after 24 hr induction. (c) Average T intensity profiles (along white dotted lines in (a)) in isometric circular colonies or anisometric square and rectangular colonies. All colonies had the same area except for one of the circular colonies, which was 50% smaller (i.e., 50% circle). (d) Average T intensity profiles from the concave or

convex edges into the colony interior in a semi-circular arc, as indicated by white dotted lines in (a). Each intensity profile in (c-d) is an average of 16 intensity profiles obtained from 4 colonies. (e) Percentage of T+ colony area in different colony geometries of the same area. Data are average ± s.e.m of respective sample sizes (n): circle (n=8), square (n=8), rectangle (n=7), arc (n=8). (f) Percentage of T+ colony area in circular colonies of different sizes. Data are average ± s.e.m of 8 colonies. **$p<0.01$ (Student's t-test). Scale bar, 200 μm in (b).

While there were geometry-dependent spatial fluctuations within a colony, the overall extent of mesoendoderm differentiation in μP-hPSC colonies of a given area was not affected by their geometries (ANOVA, p=0.84) (Fig. 4.3.6e). This may be due to the fact all the colonies had similar ratios of periphery-to-interior cells, which was indicated by similar perimeter-to-area (P/A) ratios in different colony geometries ($4 – 5.8 \times 10^{-3}$), and therefore were subjected to similar ratios of integrin and E-cadherin adhesions. Increasing the ratio of periphery-to-interior cells by reducing the size of colonies of a given geometry (*i.e.,* having a higher P/A ratio) would increase mesoendoderm differentiation. When we doubled the P/A ratio for a given (circular) geometry by reducing the colony area by 50%, there was no change in the spatial distribution of T expression within the colony (Fig. 4.3.6c). However, the overall extent of mesoendoderm differentiation in the colony was significantly increased (Student's t-test, p = 0.002) (Fig. 4.3.6f). Hence, physical attributes of tissue boundary, such as geometry and P/A ratio, can alter the relative

magnitudes or ratios of integrin and E-cadherin adhesions to affect mesoendoderm differentiation within a μP-hPSC colony.

To directly demonstrate that modulating cell adhesion is sufficient to pattern mesoendoderm differentiation, we exogenously imposed asymmetry in the adhesive mode by which hPSCs attach onto a substrate. This was achieved by micropatterning alternating strips of Matrigel™ and E-cadherin-tagged with human Fc fragment (EcadFc) (Fig. 4.3.7a). EcadFc has been used to mimic E-cadherin-mediated adhesion on tissue culture polystyrene substrates in a concentration-dependent manner [117, 118] (Appendices, Fig. 9.2.1). We first confirmed that hPSCs on EcadFc-coated substrates were still able to proliferate and maintain their pluripotency (Appendices, Fig. 9.2.2). hPSCs cultured as micropatterned colonies on EcadFc-coated substrate had more diffusive E-cadherin distribution with an appreciable increase at the basal domain of the cell in contact with the EcadFc-coated substrate (Fig. 4.3.7b). This was accompanied by a significant increase in ppMLC being sequestered as plaques at the basal domain of the cell (Fig. 4.3.7b,c). Mesoendoderm differentiation was less efficient on the EcadFc-coated substrate (Fig. 4.3.7b), which was consistent with previous report that EcadFc-coated substrate promotes ESC pluripotency [118]. Hence, the EcadFc-coated substrate could elicit a *bona fida* E-cadherin-mediated adhesive response despite the fact that cells did not exhibit a typical epithelial morphology with compact cell-cell junctions.

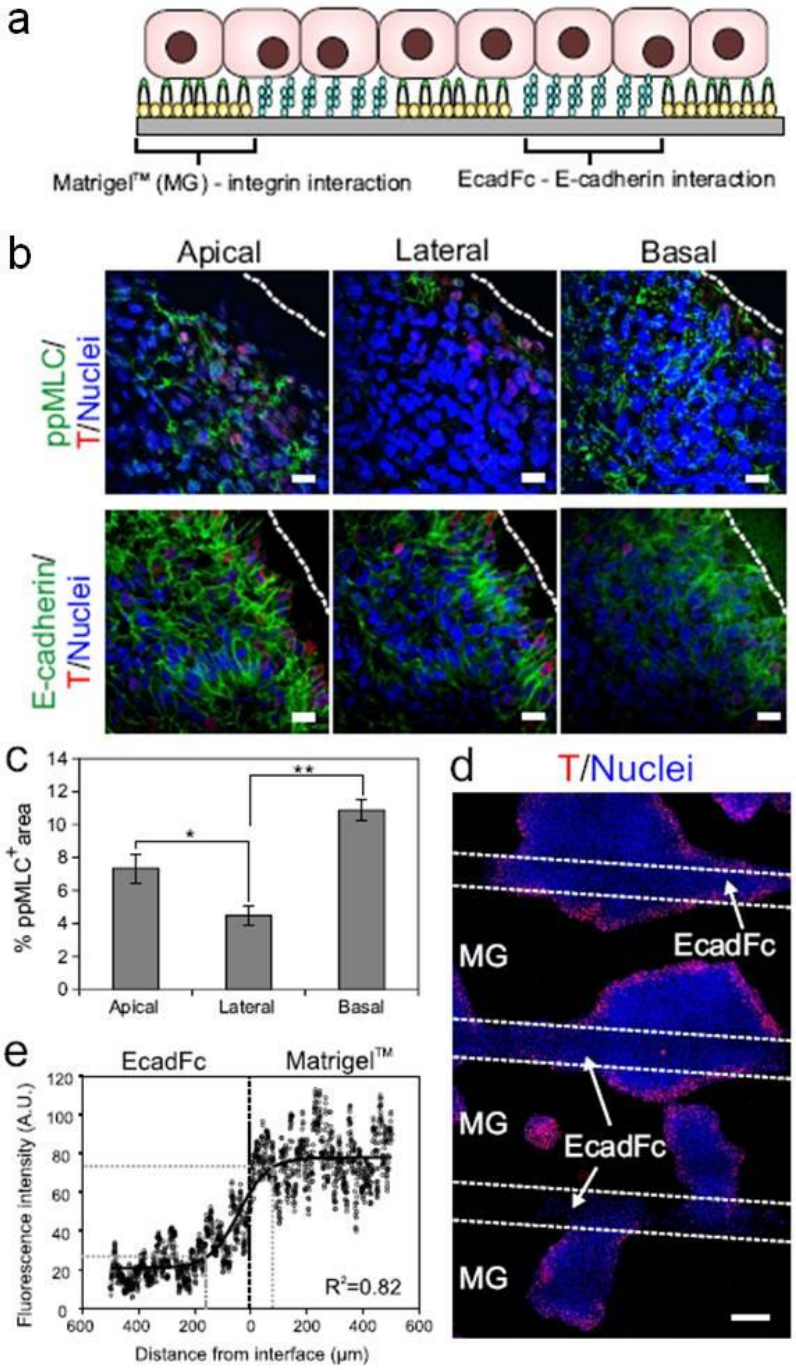

Figure 4.3.7 Exogenously imposed mechanical polarization by micropatterning alternating strips of Matrigel™ (MG) and E-cadherin tagged with human Fc fragments (EcadFc) on substrate. **(a)** Schematic illustrating

asymmetry in cell adhesion modes within a hPSC colony. **(b)** µP-hPSC colonies on E-cadherin Fc (EcadFc)-coated substrates exhibited E-cadherin and ppMLC that were localized to basal domain in contact with substrate, and attenuated T expression. Images are confocal sections showing sub-cellular localization of T, ppMLC and E-cadherin after 24 of differentiation. White dotted line denotes colony edges. **(c)** Quantification of ppMLC expression at the apical, lateral and basal domains of cells cultured on EcadFc substrates. Data are average ± s.e.m of 6 images from different colonies. *$p<0.05$, **$p<0.01$ (Student's t-test). **(d)** Immunofluorescence image of T expression on alternating MG-EcadFc substrates after 24 hr of differentiation. **(e)** T intensity profile along the colony edges from the MG-EcadFc interface to the respective adhesive substrates. The transition distance was measured as the distance where deviation from the plateau RFU values were >10%. Data points are average of 15 profiles and fitted to a 4-parameter sigmoidal model (black solid line). Scale bar, 20 µm in (b), 200 µm in (d).

After micropatterning alternating strips of Matrigel™ and EcadFc, we seeded hPSC colonies and cultured them in maintenance medium for 24 hours before inducing mesoendoderm differentiation. Upon examining mesoendoderm differentiation by immunostaining for T^+ cells, we found that patterns of mesoendoderm differentiation within a single hPSC colony corresponded to the underlying alternating Matrigel™/EcadFc strips (Fig. 4.3.7d). Part of the colony experiencing integrin-mediated adhesion (*i.e.,* on Matrigel™) maintained compact colony morphology with distinct boundary, and exhibited mesoendoderm patterning at the colony periphery. In comparison, cells in regions of the colony subjected to E-cadherin-mediated adhesion (*i.e.,* on EcadFc) were more scattered and had attenuated T

expression. We tracked the T fluorescence intensity profile along the colony edges from the Matrigel™-EcadFc interface to the respective adhesive substrates. The distance over which the switch from a T^{high} region on Matrigel™ to a T^{low} region on EcadFc occurred was approximately 230 μm (Fig. 4.3.7e). This relatively short transition distance relative to the colony length scale (> 1 mm) indicated that spatial asymmetry in the substrate cell adhesion modes can be an effective modulator in controlling the spatial heterogeneity of pluripotency-differentiation fates in a hPSC culture.

4.3.3 Spatial patterning of mesoendoderm differentiation requires both integrin and E-cadherin adhesions

We next determine if integrin and E-cadherin-mediated adhesions acted in an independent or collective manner in generating spatial heterogeneity in mesoendoderm differentiation. First, we used specific integrin antibodies to block integrin-mediated adhesions. Attachment of hPSCs onto micropatterned Matrigel™ islands was mainly mediated by $\alpha_6\beta_1$-laminin binding, while inhibition of $\alpha_2\beta_1$-laminin/collagen or $\alpha_5\beta_1$-fibronectin interactions [119, 120] had no significant effects on cell attachment to the Matrigel™ substrate (Appendices, Fig. 9.3.1, Fig. 9.3.3). The weakening of cell-matrix interaction by $\alpha_6\beta_1$ antibody caused contraction of the μP-hPSC colonies in a dose dependent manner (Appendices, Fig. 9.3.2). For subsequent experiments, inhibition of integrin-mediated adhesion was performed with 0.1 μg/ml $\alpha_6\beta_1$

antibody, where we observed a 50% decrease in colony area (Appendices, Fig. 9.3.3).

The localization of ppMLC to a circumferential actomyosin cable at the colony periphery, which was indicative of integrin adhesion generated traction forces, was significantly attenuated in the $\alpha_6\beta_1$ antibody-treated μP-hPSC colonies (Fig. 4.3.8aii), whereas the cable was still present in $\alpha_5\beta_1$ or $\alpha_2\beta_1$ antibody-treated colonies (Fig. 4.3.8aiv, vi). This was indicated by a significant decrease in the ppMLC fiber length at the $\alpha_6\beta_1$ antibody-treated colony periphery relative to the colony interior (Fig. 4.3.8c). We observed that ppMLC in $\alpha_6\beta_1$ antibody-treated colonies was sequestered mainly at the cell-cell junctions both at the colony periphery and interior (Fig. 4.3.8aii). The inhibition of integrin-mediated adhesion was specific since the E-cadherin AJ network remained intact in all samples (Fig. 4.3.8a, left panel). However, spatial polarization of E-cadherin in $\alpha_6\beta_1$ antibody-treated colonies was abolished. E-cadherin was localized to the cell-cell junctions at both the colony periphery and interior (Fig. 4.3.8ai), which was supported by a lower E-cadherin$^+$ area per cell at both the colony periphery and interior (Fig. 4.3.8b). This was in contrast to a more diffusive E-cadherin localization, as indicated by a significantly higher E-cadherin$^+$ area per cell (Fig. 4.3.8b), observed at the periphery of untreated (Fig. 4.3.3), $\alpha_2\beta_1$ or $\alpha_5\beta_1$ antibody-treated colonies (Fig. 4.3.8aiii, v,). The disruption of integrin-mediated adhesion in the $\alpha_6\beta_1$ antibody-treated μP-hPSC colonies abolished the polarized distribution of the

cell adhesion molecules and activated myosin II, resulting in uniformly undifferentiated colonies, where the percentage of T^+ area decreased to 6.4 ± 0.5% (Fig. 4.3.9d). In $\alpha_2\beta_1$ and $\alpha_5\beta_1$ antibody-treated colonies, where we did not observed changes in the spatial polarization of E-cadherin and ppMLC, there were no significant changes in the percentage of T^+ area and their distribution compared to untreated colonies (Fig. 4.3.9d).

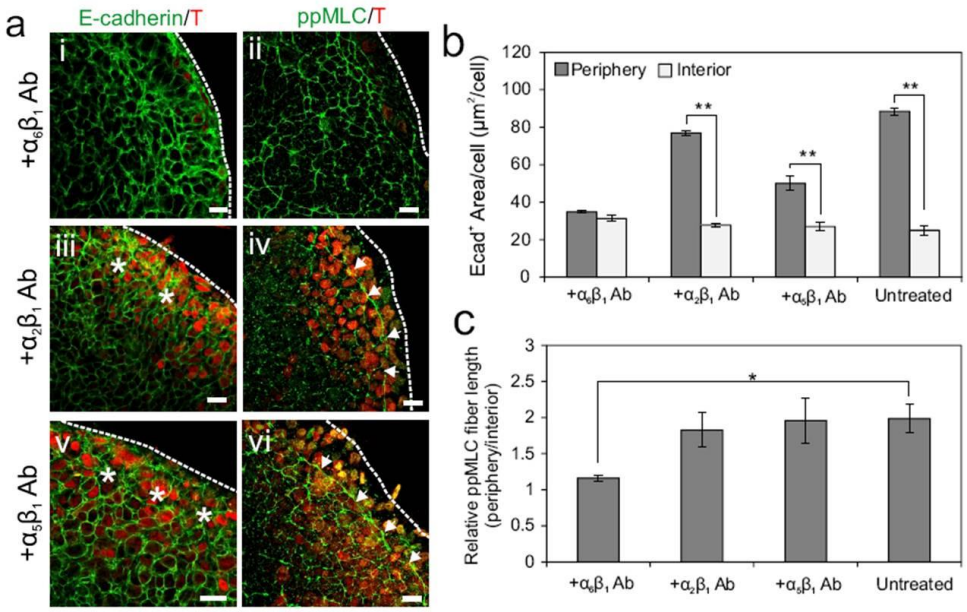

Figure 4.3.8 Integrin adhesions was required to generate spatial polarization of actomyosin contractility and mesoendoderm differentiation. (a) E-cadherin, ppMLC and T localization in μP-hPSC colonies treated with (i-ii) α6β1, (iii-iv) α2β1, and (v-vi) α5β1 integrin antibodies. Images are immunofluorescence confocal images after 24 hr of differentiation. Dotted white lines indicate colony edges. Asterisks (*) denote periphery regions with more diffusive E-cadherin localization as compared to colony interior. White arrows denote circumferential actomyosin cable. Scale bar, 20 μm. (b) E-cadherin localization area per cell at the periphery and interior regions of μP-hPSC colonies after integrin antibody blocking. A higher E-cadherin+ area per cell

corresponds to a more diffusive E-cadherin localization. (c) Relative ppMLC fiber length between periphery and interior of colonies after integrin antibody blocking. Data in (b-c) are average ± s.e.m of at least 3 images from different colonies. *p<0.05; **p<0.01 (Student's t-test).

Conversely, inhibition of cell-cell adhesion by the addition of E-cadherin antibody resulted in scattered colonies (Appendices, Fig. 9.3.4) that were uniformly differentiated (Fig. 4.3.9ai-ii). The percentage of T^+ colony area increased significantly to 73.6 ± 4.9% (Fig. 4.3.9d). Attenuation of cell-cell interaction was confirmed by a significantly more diffusive localization of E-cadherin throughout the entire colony (Fig. 4.3.9ai,b). Colonies treated with unspecific IgG antibody did not affect E-cadherin localization at the cell-cell junctions as compared to untreated control (Fig. 4.3.9b). The localization of ppMLC in the E-cadherin antibody-treated colonies was diffusive throughout the colony and there was a concomitant loss of the circumferential actomyosin cable (Fig. 4.3.9aii, c). Control IgG antibody-treated colonies still retained the polarized distribution of ppMLC between the circumferential actomyosin cable at the colony periphery and cell-cell junctions at the colony interior (Fig. 4.3.9aiv, c). This observation is consistent with that of Mertz *et al*, where E-cadherin adhesion is required to reorganize and transmit integrin-adhesion generated traction forces to the periphery of an epithelial cell population [121]. Collectively, the antibody blocking experiments indicated that integrin and E-cadherin are dependent on each other to generate spatial polarization of activated myosin II. Inhibiting any one mode of cell adhesion in a PSC culture

was sufficient to abolish this mechanical spatial polarization to achieve a uniform cell population.

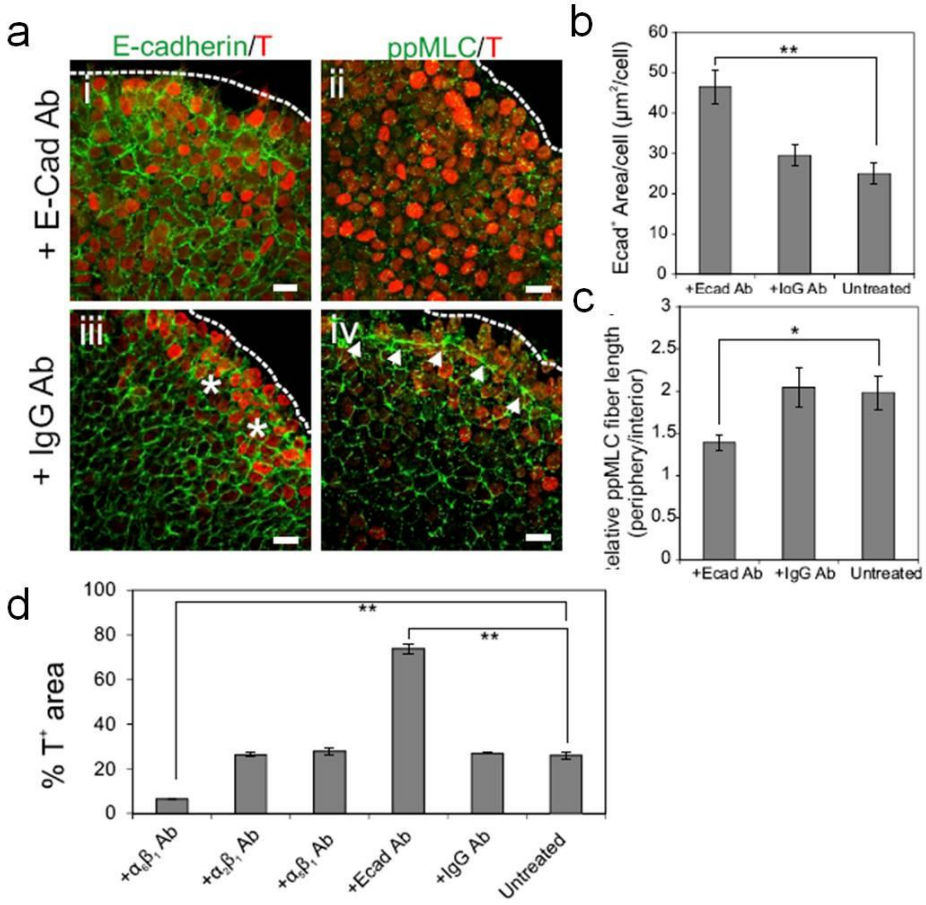

Figure 4.3.9 E-cadherin adhesion was required to generate spatial polarization of actomyosin contractility and mesoendoderm differentiation (a) E-cadherin, ppMLC and T localization in μP-hPSC colonies treated with (i-ii) E-cadherin antibody, (iii-iv) unspecific IgG antibody. Images are immunofluorescence confocal images after 24 hr of differentiation. Dotted white lines indicate colony edges. Asterisks (*) denote periphery regions with more diffusive E-cadherin localization as compared to colony interior. White arrows denote circumferential actomyosin cable. Scale bar, 20 μm. (b) E-cadherin localization area per cell at the interior of μP-hPSC colonies after E-cadherin

antibody blocking. (c) Relative ppMLC fiber length between periphery and interior of colonies after E-cadherin antibody blocking. (d) $\%T^+$ area in the presence of different blocking antibodies. Data in (b-c; e-g) are average ± s.e.m of at least 3 images from different colonies. *$p<0.05$; **$p<0.01$ (Student's t-test).

4.3.4 Integrin adhesion modulates E-cadherin adhesion signaling via Rho-ROCK-myosin II activity to determine pluripotency-differentiation cell fates

Since Rho-ROCK-myosin II signaling is implicated in both integrin and E-cadherin adhesions in hPSCs [108-110], the modulation of this common effector by pharmacological inhibitors in the μP-hPSC colonies should reveal whether integrin or E-cadherin functions as the dominant mechanical regulator in instructing pluripotency-differentiation decision. In the presence of the myosin motor inhibitor, blebbistatin, or the ROCK inhibitor, Y27632, at concentrations which did not result in significant cytotoxic effects, we observed that the restriction of mesoendoderm differentiation to the colony periphery was abolished (Fig. 4.3.10i-ii). We observed similar results when the actin cytoskeleton, which is required to generate actomyosin contractility, was destabilized with Cytochalasin D (Fig. 4.3.10iii). Inhibition of other GTPases, including Rac or Cdc42 by their specific inhibitors, EHT1864 and ML141, respectively did not affect mesoendoderm patterning (Fig. 4.3.10iv-v). This confirmed that Rho-ROCK-myosin II signaling was involved in patterning mesoendoderm differentiation to the colony periphery.

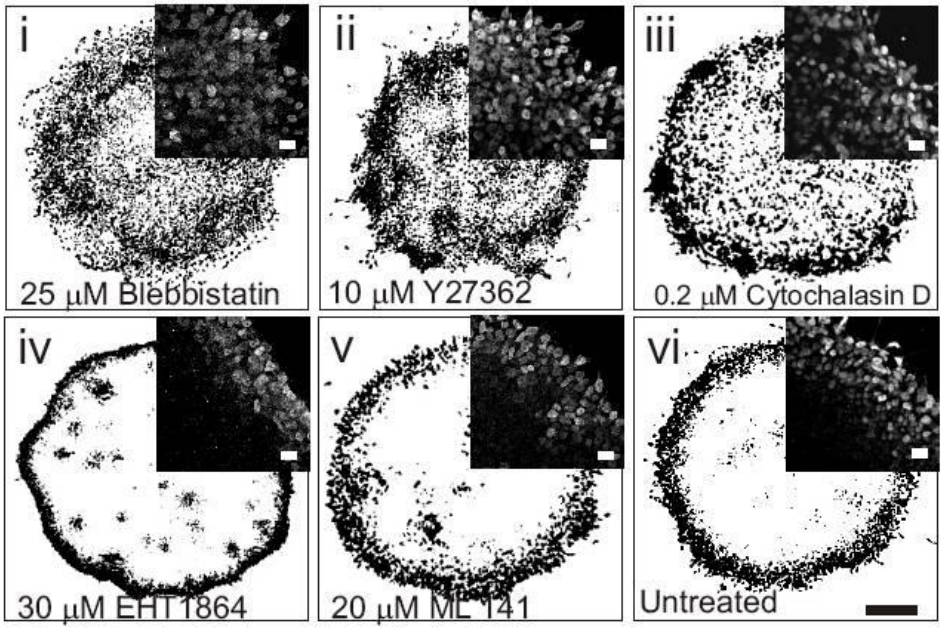

Figure 4.3.10 Binarized images showing distribution of T^+ cell in μP-hPSC colonies after 24 hr of mesoendoderm differentiation in the presence of (i) blebbistatin (myosin II inhibitor), (ii) Y27362 (ROCK inhibitor), (iii) cytochalasin D (actin polymerization inhibitor), (iv) EHT1864 (Rac inhibitor), (v) ML141 (Cdc42 inhibitor), and (vi) no drug treatment. Insets are immunofluorescence images showing T localization at colony periphery. Scale bar = 200 μm; scale bars in insets = 20 μm.

We note that the concomitant loss of integrin-mediated traction forces and E-cadherin AJs by Rho-ROCK-myosin II inhibition (Fig. 4.3.11a) phenocopied the results of E-cadherin antibody blocking instead of the integrin-blocking experiment. Colonies treated with blebbistatin resulted in a significant increase in E-cadherin$^+$ area per cell, indicating a more diffusive cellular distribution, as compared to untreated colonies (Fig. 4.3.11b). There was also a loss of the circumferential actomyosin cable, which was indicated

by a significant reduction in ppMLC fiber length at the colony periphery (Fig. 4.3.11c). This resulted in uniformly differentiated colonies, which corroborated with a significant increase in the proportion of T^+ area from 25.9 ± 3.8% in the untreated control μP-hPSC colonies to 73.6 ± 4.9% (Fig. 4.3.11d).

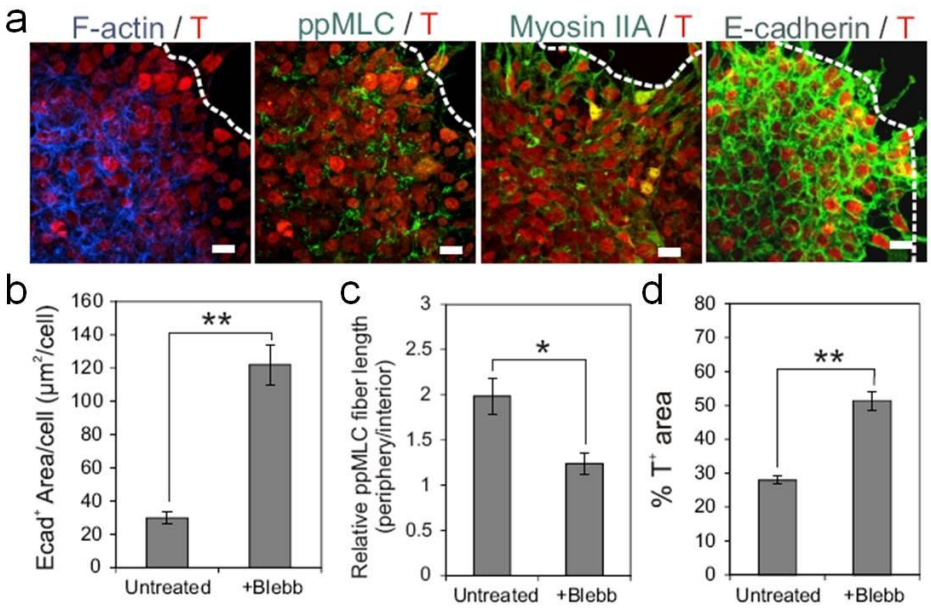

Figure 4.3.11 Effect of Rho-ROCK-myosin II inhibition by blebbistatin on mesoendoderm differentiation and patterning. (a) Immunofluorescence staining after 24 hr of mesoendoderm differentiation in the presence of 25 μM blebbistatin. (b-d) Quantitative comparison of (b) E-cadherin localization area per cell at colony interior, (c) relative ppMLC fiber length between periphery and interior colony regions, and (d) % T^+ colony area in blebbistatin-treated and untreated μP-hPSC colonies after 24 hr of differentiation. Scale bar, 20 μm in (a).

Our data suggested that E-cadherin-mediated signaling was a direct negative modulator of mesoendoderm differentiation and integrin-mediated signaling is likely coupled to E-cadherin-mediated signalling (Fig. 4.3.12). When activated myosin II was sequestered to the E-cadherin AJs, such as in the integrin-blocked (Fig. 4.3.8) or EcadFc (Fig. 4.3.7) colonies, mesoendoderm differentiation was inhibited. Conversely, the disruption of the AJs by E-cadherin antibody blocking (Fig. 4.3.9) or Rho-ROCK-actomyosin inhibitors (Fig. 4.3.10, 4.3.11) allowed for differentiation progression throughout the entire colony. Thus, the spatial correlation of mesoendoderm differentiation to regions of higher integrin-mediated adhesion was likely due to the corresponding destabilization of the E-cadherin AJs, and not a direct promotion of differentiation.

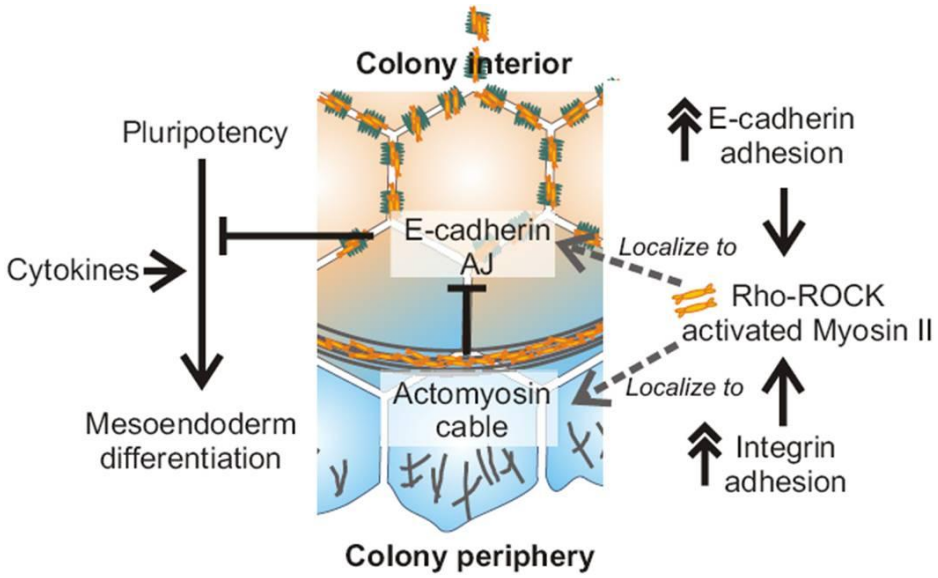

Figure 4.3.12 Cartoon illustrating how polarization of cell adhesions at boundary of a hPSC colony differentially localizes Rho-ROCK-myosin II to

either actomyosin contractile or E-cadherin AJ networks to pattern differentiation decisions.

4.4 Conclusion

The interplay between integrin and cadherin adhesions and their coupling via activated myosin II was mainly investigated in the context of collective cell migration in adult epithelial cell population [117, 122]. This present study is to our knowledge, a first report integrating the roles of integrin and E-cadherin adhesion-mediated Rho-ROCK-myosin II in human PSC pluripotency-differentiation cell fate decisions. We have shown that Rho-ROCK-myosin II played a pleiotropic role in establishing both integrin-mediated contractile stresses and E-cadherin AJs in the μP-hESC colonies. These differential functions of activated myosin II were modulated by spatial asymmetry in integrin and E-cadherin adhesions at the tissue boundary (Fig. 5e). When activated myosin II was mainly sequestered to the E-cadherin AJs, the pluripotency circuitry persisted and cells were prevented from undergoing differentiation even in induction medium. At regions with increased integrin adhesion-mediated contractile stresses, such as at colony periphery or sharp corners, activated myosin II preferentially localized to the actomyosin contractile cable instead of the E-cadherin AJ network and the cells underwent mesoendoderm differentiation. Obstructing the generation of contractile traction force at the colony edges either by inhibiting integrin adhesion or employing EcadFc-mediated adhesion attenuated mesoendoderm

differentiation and patterning, provided that the E-cadherin AJ network is largely intact. A universal abolishment of both integrin-mediated contractile and E-cadherin AJ networks by pharmacological inhibitors of Rho-ROCK-myosin II led to the robust differentiation of the entire colony instead, suggesting that E-cadherin signaling was the primary gatekeeper of pluripotency-differentiation decision. Hence, asymmetry in the localization of Rho-ROCK-myosin II resulting from spatial polarization of integrin and E-cadherin adhesions in a hPSC colony served to provide positional cues to determine if a cell in a particular locality within the colony should exit from pluripotency and differentiate according to biochemical induction factors.

A direct implication of this finding is that it allows for biomaterials to be tailored for human PSC maintenance or differentiation with minimal heterogeneity. In terms of hPSC model development for developmental toxicity testing, we could apply these spatially differentiated μP-hPSC colonies as the starting point of recapitulating both spatial differentiation and collective cell migration *in vitro*, and then use it for developmental toxicity screening. By controlling the colony size and shape, we could get a consistent extent of mesoendoderm differentiation at the colony periphery compared with unpatterned hPSC colonies. This is very important in drug screening application since it always needs a stable baseline to start with. Once we could also observe a consistent controlled collective cell migration process within

these colonies after further differentiation culture, we may acquire an ideal mesoendoderm pattern for teratogen screening.

5. *In vitro* mesoendoderm pattern formation by geometrically confined cell differentiation and migration

5.1 Introduction

In order to mimic human gastrulation process *in vitro*, only capturing spatially organized mesoendoderm differentiation is not enough. Another key feature during gastrulation is the extensive spatially and temporally controlled morphogenetic movements such as collective cell migration of cell populations. These morphogenetic movements play critical roles in correctly forming embryonic structures at desired positions. Here, after the initial mesoendoderm induction only to the periphery of the μP-hPSC colonies as shown in Chapter 4, we further cultured the cells and found that these spatially induced mesoendoderm cells could undergo directed collective cell migration process and form an *in vivo*-like mesoendoderm pattern on day 3. The migration speed and the corresponding morphologic localization of the mesoendoderm pattern depended on the coating concentration of Matrigel. Despite the existence of inherent line-to-line variability, the mesoendoderm pattern could be formed at similar positions across different hPSC lines without protocol optimization.

5.2 Materials and Methods

Most of the materials and methods were the same as stated in Section 4.2.

5.2.1 Cell maintenance and differentiation

The hESC lines H9, H1 and the iPSC line IMR90 were all obtained from WiCell Research Institute, Inc., (Madison, WI, USA). The cell maintenance and differentiation protocols were the same as stated in 4.2.1.

5.2.2 Matrigel™ coating

Since the stock concentration of every lot of Matrigel™ (354277, BD Biosciences, Singapore) acquired from the vendor was different, there was a suggested dilution factor for each lot to make consistent coating concentration by the vendor. We set this suggested coating concentration for hPSC culture as 1X. To evaluate the effect of coating concentration of Matrigel™ on the collective migration of the mesoendoderm cells, 1X, 1.5X and 2X Matrigel™ solution were used for testing. For consistently generating a mesoendoderm pattern at desired position and monitoring cell migration, hPSCs were cultured on surfaces coated with 1.5X Matrigel™.

5.2.3 Immunofluorescence staining and microscopy

The immunofluorescence staining process was quite similar as stated in 4.2.4. Samples were fixed with 3.7% paraformaldehyde, permeabilized with

0.5% Triton X-100 in PBS and incubated for 3 hr at room temperature (RT) in blocking buffer (2% BSA and 0.1% Triton X-100 in PBS). After that, they were incubated overnight at 4 ℃ with primary antibodies (5-10 μg/ml in blocking buffer). The primary antibodies used in this study were as follows: goat anti-Brachyury (AF2085, R&D Systems), rabbit anti-Eomes (ab23345, Abcam), rabbit anti-Cripto1 (ab19917, Abcam), and rabbit anti-FoxA2 (ab40874, Abcam). The samples were washed 4 times with 15 min interval before adding secondary antibodies (1:1000 dilution). The secondary antibodies used in this study were Alexa Fluor® 546 (A11056, Invitrogen, USA) and Alexa Fluor® 488 (A21206, Invitrogen, USA). Confocal images were acquired using Zeiss LSM 5 DUO microscope (Zeiss), and immunofluorescence images of entire μP-hPSC colonies for quantitative analysis were acquired using Olympus IX81 epifluorescence microscope (Olympus, Japan) with a motorized stage (Prior Scientific). For phase contrast live imaging, images were acquired every 20 min by BioStation CT (Nikon) using 10X objective. The imaging period started since the induction of differentiation and lasted for 3 days.

5.3 Results

5.3.1 Geometrically-confined collective cell migration in μP-hPSC colonies

Our goal is to spatially organize cellular events (*i.e.* differentiation and cell migration) characteristic of embryonic development in hPSC cultures. As mentioned in Chapter 4, we leveraged on asymmetry in the mechanical environment imposed by cell micropatterning to drive differential stem cell fates [123]. Instead of inducing mesoendoderm differentiation for only 24 hr, we monitored the expression patterns of Brachyury (T), an early mesoendoderm marker [124], over three days (Fig. 5.3.1). T was initially expressed on the periphery of the colony after one day of differentiation (Fig. 5.3.2). By day 3, the T^+ cells were displaced inwards by approximately 200 μm from the colony edges, and formed an annular pattern of multilayer cells, suggesting that these cells underwent collective cell migration (Fig. 5.3.2).

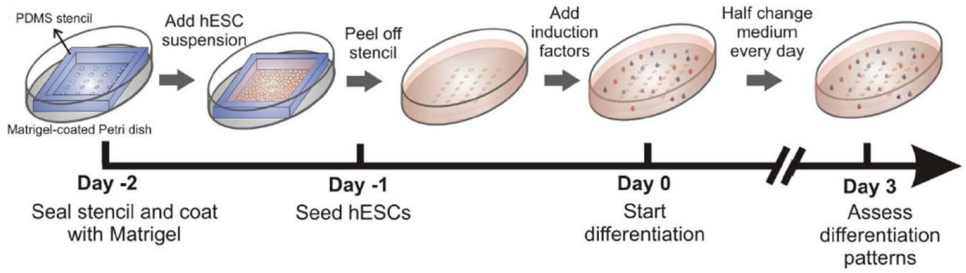

Figure 5.3.1 Schematic representation of the micropatterning of hPSC colonies and mesoendoderm induction over 3 days.

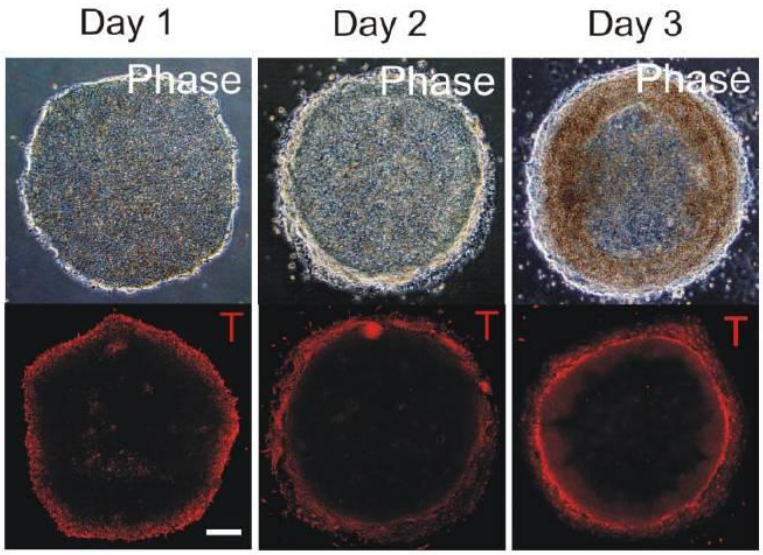

Figure 5.3.2 Fluorescent images of mesoendoderm marker Brachyury (T) on day 1- day 3. Scale bar, 200 μm.

To verify this, a 3-day live imaging under 10X objective using phase contrast was performed to track the cell movements (Fig. 5.3.3). Kymograph analysis gave a graphical representation of spatial position changes along a line over the three days of mesoendoderm induction [125]. Results showed that after one day induction, periphery cells became motile and migrated out from the main colony, While T^+ periphery cells in unpatterned hPSC colonies spread out from the colony continuously (Fig. 5.3.5), the physical constraints in the μP-hPSC colonies allowed the periphery cells to migrate outwards for only about ~150 μm. The majority of these motile cells then established contact with each other, and migrated for about 200 μm towards in the colony interior in an amoeboid manner on top of a cell layer in contact with the underlying substrate (Fig. 5.3.3). The spreading and retraction of

mesoendoderm cells in the μP-hPSC colonies during the 3-day time frame was manifested as a major migratory front in the kymograph, which was consistently observed in different colonies (Fig. 5.3.4).

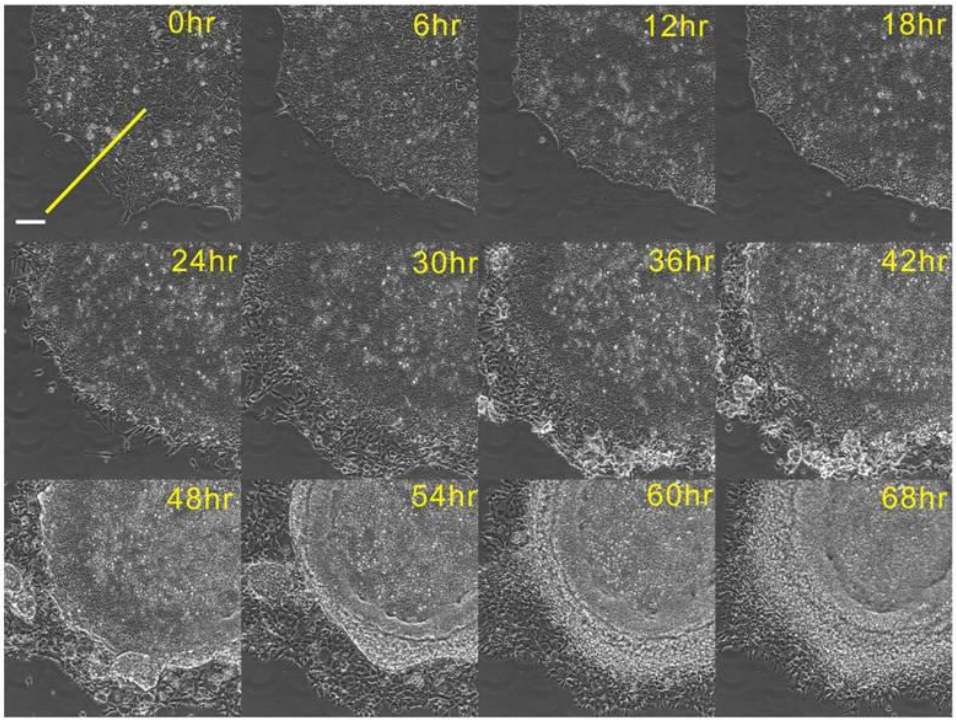

Figure 5.3.3 Montage from a 3-day phase imaging on about one quarter of a circular μP-hPSC colony. Scale bar, 100 μm.

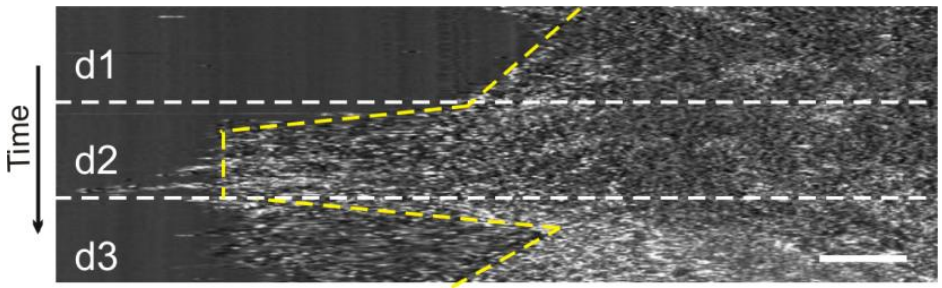

Figure 5.3.4 Kymograph analysis showing the movement of cells along the yellow line shown in Fig. 5.2 throughout the 3-day live imaging time frame. Scale bar, 50 μm.

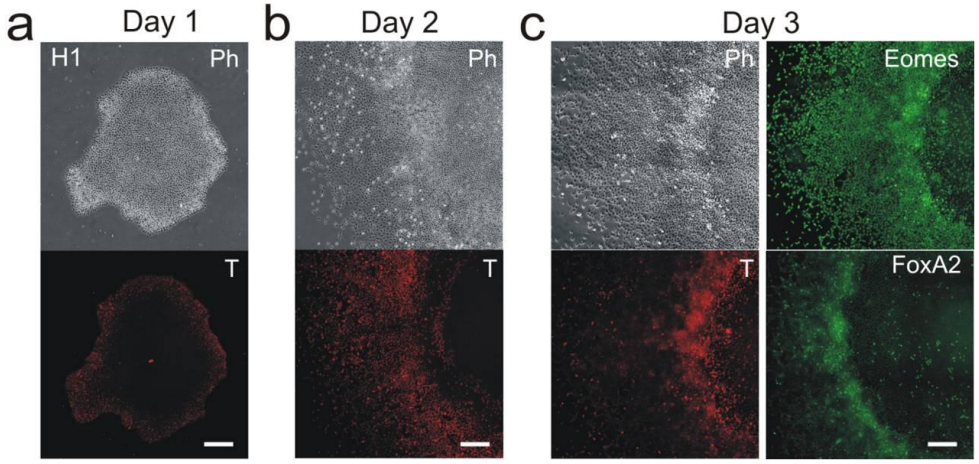

Figure 5.3.5 Mesoendoderm differentiation in unpatterned hPSC colonies. (a-c) Phase and fluorescent images of mesoendoderm markers for samples fixed on day 1 (a), day 2 (b) and day 3 (c). Scale bar, 200 μm.

To confirm that the annular multicellular pattern is formed as a result of mesoendoderm cell differentiation and migration, we cultured μP-hPSC colonies in a basal differentiation medium without adding any mesoendoderm induction factors. Immunostaining results of fixed samples from day 1 to 3 showed no detectable T expression (Fig. 5.3.6 a,b). Live imaging and kymograph analysis indicated that cell migration at the colony periphery was negligible in the absence of mesoendoderm induction (Fig. 5.3.6 c,d). Cells proliferated and distributed relatively evenly throughout the whole colony during the 3-day time frame with no annular pattern being formed (Fig. 5.3.6 c,d). These data confirmed that the formation of an annular mesoendoderm pattern in the μP-hPSC colonies was specifically a result of mesoendoderm cells differentiating and migrating in a geometrically confined space.

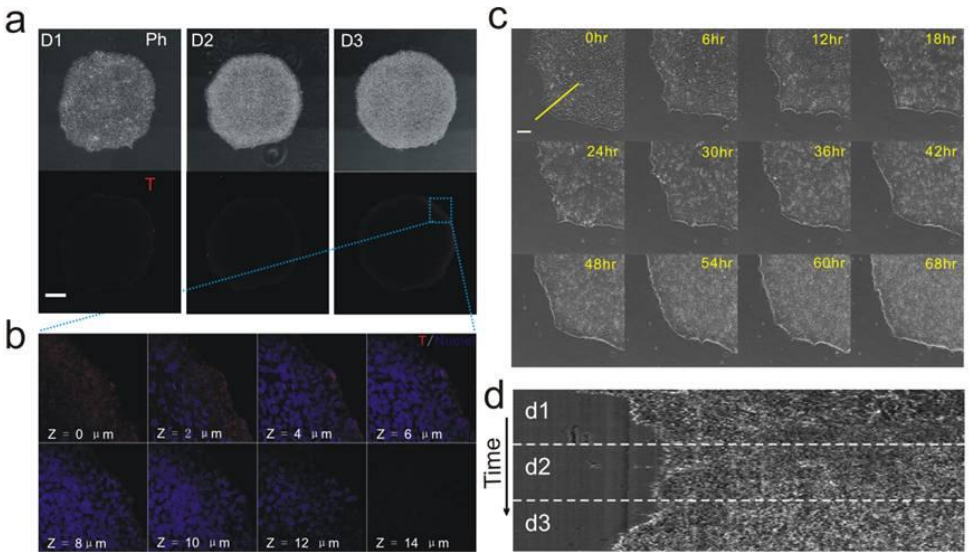

Figure 5.3.6 No similar annular mesoendoderm pattern formed after 3-day culture in basal STEMdiff™ APEL™ medium. (a) Phase and fluorescent mesoendoderm marker T images on day 1 to day 3. Scale bar, 200 µm. (b) Confocal z-stack images of T and cell nuclei within a µP-hPSC colony fixed on day 3. (c) Montage from a 3-day phase imaging on about one quarter of a circular µP-hPSC colony. Scale bar, 100 µm. d) Kymograph analysis showing the movement of cells along the yellow line shown in (c) throughout the 3-day live imaging time frame.

5.3.2 Formation of an annular mesoendoderm pattern in µP-hPSC colonies

To study the annular mesoendoderm pattern formed by both differentiation and cell migration, a confocal z-stack analysis of the periphery section of a T-labeled µP-hPSC colony was performed to reveal its internal structure (Fig. 5.3.7). The cross section of the mesoendoderm pattern resembled a ridge-like multicellular structure (Fig. 5.3.7 b), where the T^+ cells were mainly localized on top of the ridge, and a narrow furrow a few microns

in width ran underneath the ridge (Fig. 5.3.7 a). This ridge like structure appeared to resemble an invagination of the epiblast sheet [126] seen during primitive streak formation *in vivo*, which is approximately an *in vivo* equivalent of the hPSCs-derived mesoendoderm cells at the multicellular ridge.

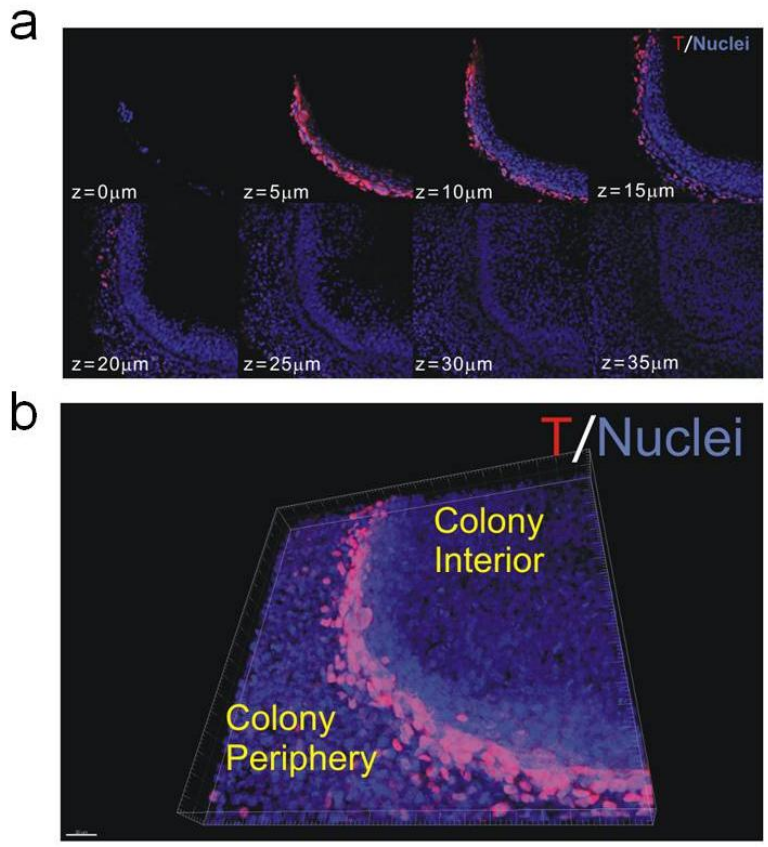

Figure 5.3.7 3D structure of the mesoendoderm pattern. Confocal z-stack images of T and cell nuclei (a) and its 3-D reconstruction image (b) within a μP-hPSC colony fixed on d3. Scale bar, 30 μm in (b).

Immunostaining of various other mesoendoderm markers was performed on day 3 to confirm that the migrating cells were mesoendoderm cells (Fig. 5.3.8). The expression of mesoendoderm markers Eomes and Cripto1, as well

as the early definitive endoderm marker FoxA2 all co-localized with T as an annular pattern, indicating that the motile cells were indeed mesoendoderm cells (Fig. 5.3.8). Epithelial-mesenchymal transition (EMT) interrelates mesoendoderm differentiation and cell morphogenesis during gastrulation [127]. Indeed, higher expression levels of EMT markers were also detected within the multicellular annular pattern. Cells were isolated from the periphery and center of the μP-hPSC colonies on day 3 and transcription levels of EMT markers were determined by RT-PCR (Fig. 5.3.9). Cells in the colony periphery exhibited a much lower level of E-cadherin expression, and a higher level of N-cadherin, Vimentin and Snail compared with those in the colony centre (Fig. 5.3.9), indicating that EMT was also preferentially localized near the colony periphery together with mesoendoderm differentiation.

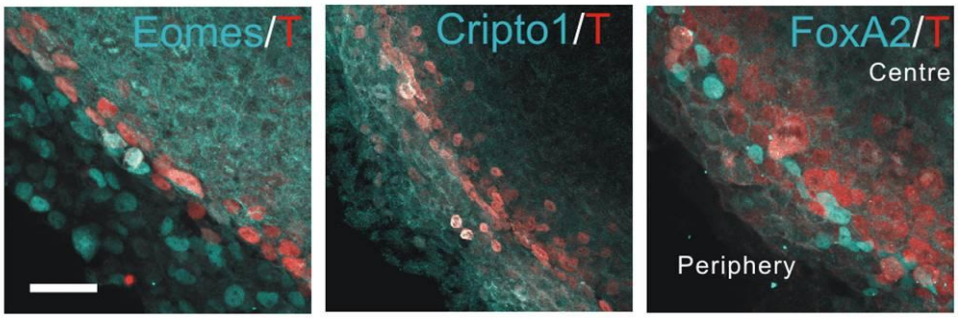

Figure 5.3.8 Fluorescent images of mesoendoderm markers Wnt3a, Eomes and Cripto1 within μP-hPSC colonies on day 3. Scale bar, 50 μm.

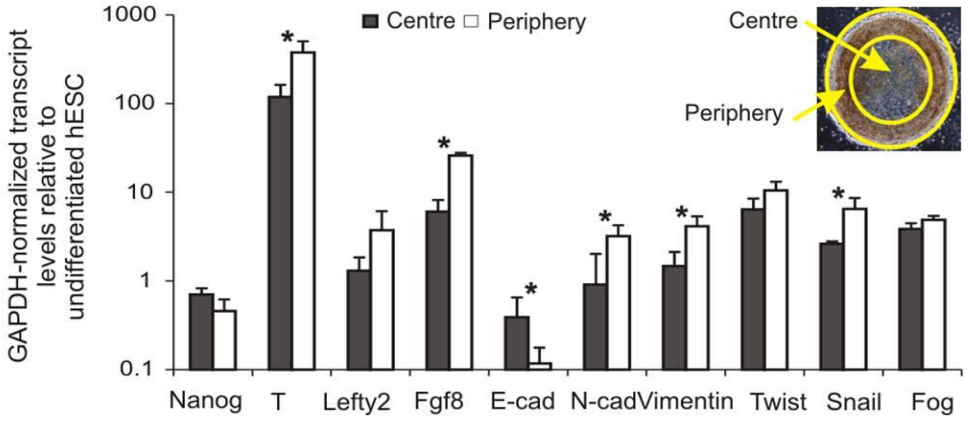

Figure 5.3.9 RT-PCR results of EMT marker expression levels in colony centre and colony edge (n = 3). *, $p < 0.05$ in paired t-test. Inset, phase image showing colony edge and centre.

5.3.3 Matrix concentration-dependent collective cell migration in μP-hPSC colonies

After we formed the annular mesoendoderm pattern within the μP-hPSC colonies, next we wanted to check whether the location of the mesoendoderm pattern was matrix concentration-dependent.

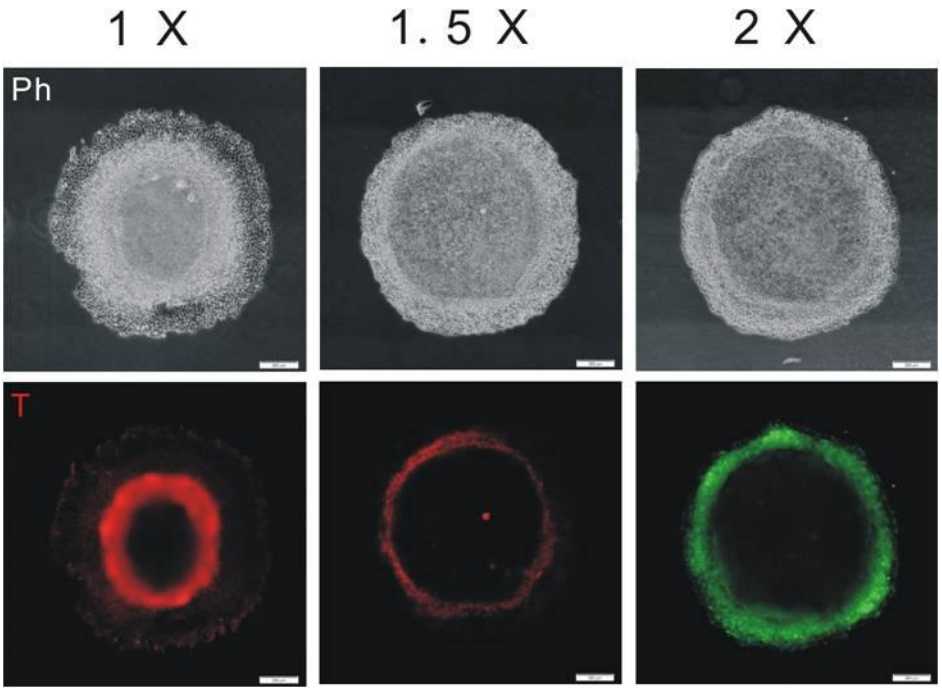

Figure 5.3.10 Matrix-concentration dependent collective cell migration. Phase and T images of μP-hPSC colonies on day 3 of mesoendoderm induction. Scale bar, 200 μm.

We found that by controlling the matrigel amount coated on the dish, we could control the position of the mesoendoderm pattern. The recommended Matrigel^{TM} concentration for hPSC cell culture from the product information was defined as 1X. Cells were seeded on 1X, 1.5X and 2X Matrigel^{TM} coated surfaces. After 3 days' mesoendoderm induction, the mesoendoderm patterns localized more outwards in dishes coated with higher concentrations of Matrigel^{TM} (Fig. 5.3.10). In fact, cells in 2X Matrigel^{TM} coated dishes hardly move inwards compared those in 1X and 1.5X Matrigel^{TM} coated dishes. This indicated that the tag of war between cell-matrix and cell-cell interactions could affect the collective cell migration. With more matrix and higher cell-

matrix interaction, cells would migration less distance. Therefore, it's better to recharacterize the amount of Matrigel^{TM} solution used for coating when changing the lot of Matrigel^{TM}.

5.3.4 Free of line-to-line variability in mesoendoderm pattern formation

As we know, hPSCs consist of hESCs and iPSCs. For each of them, there were different cell lines generated from different human embryos or adult cells. The existence of line-to-line variability may vary the mesoendoderm pattern formation when using a different hPSC line other than H9, and reduce the robustness and reproducibility of the current model [128]. Here, we wanted to check whether the mesoendoderm pattern formation processes observed in H9 cells could be maintained in other hPSC lines without protocol optimization. Another hESC line H1 and one human iPSC line IMR90 were patterned to form μP-hPSC colonies and cultured in mesoendoderm induction medium for 3 days. The expression patterns of mesoendoderm markers (T, FoxA2 and Eomes) were examined using immunofluorescence staining and fluorescence microscopy. Results showed that both cell lines could undergo spatial mesoendoderm differentiation at colony periphery after 1 day of culture (Fig. 5.3.11a,d), and form a similar mesoendoderm pattern on day 3 through collective cell migration (Fig. 5.3.11b-c, e-f). Therefore, the formation of mesoendoderm pattern by geometrically confined cell differentiation and

migration in our μP-hPSC colonies was not cell-line specific, and could be a common phenomena for all hPSCs including both hESCs and human iPSCs.

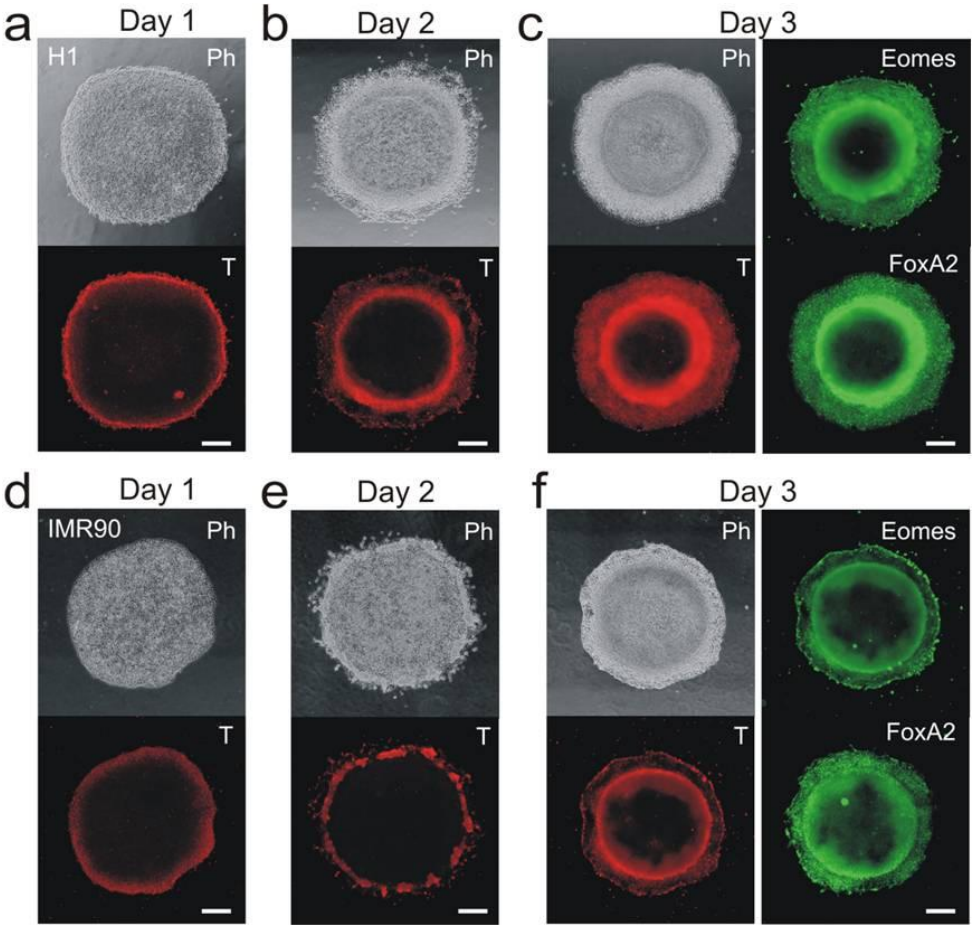

Figure 5.3.11 Generation of annular mesoendoderm pattern in H1 and IMR90 cells. (a-f) 3-day phase and fluorescent images of μP-hPSC colonies formed by H1 cells (a-c) and IMR90 cells (d-f). Scale bar, 200 μm.

5.4 Conclusion

Embryo development is more than just cell differentiation. Organized spatial control and morphogenic movements such as collective cell migration

play as important roles in correct embryo formation. Here we have shown a first *in vitro* cell model which could mimic both spatially controlled differentiation and collective cell migration processes during embryogenesis. This μP-hPSC model could be used to study the underlying mechanisms of mesoendoderm pattern formation in human embryos, or applied for human teratogen detection.

One key feature of the μP-PSC model that will facilitate its practical application is the consistency at which we could generate the annular mesoendoderm pattern, which provides a baseline to morphologically measure drug or other molecule-induced disruption effects. In an unpatterned hPSC colony, spatial patterns of mesoendoderm differentiation were heterogeneous and vary across cultures (Fig. 5.3.5). The use of geometric confinement by cell micropatterning could induce reproducible spatial patterning of mesoendoderm differentiation [129]. Our μP-hPSC model not only recapitulated spatially induced mesoendoderm differentiation, but also self-organized collective cell migration within the colony, forming reproducible mesoendoderm patterns. We have shown that such annular mesoendoderm pattern could be generated with different hPSC lines (Fig. 5.3.11). Compared with other methods of creating environmental gradient to pattern stem cell fates, such as microfluidic patterning of soluble factors [130, 131] or micropatterned feeder cells [132] or hydrogels [133], the μP-hPSC approach is

straightforward to implement, readily scalable, and is more amenable to high content imaging for downstream data collection and analysis.

6. A new method for human teratogen detection by geometrically confined cell differentiation and migration

6.1 Introduction

Teratogens are drugs or chemicals that can interfere with normal embryonic development and induce abnormalities in growth and functions [1], resulting in various birth defects. Due to the complexity of embryonic developmental processes, the identification of teratogens rely mostly on animal models [93]. However, the need to reduce the time and cost associated with animal testing as well as circumvent high inter-species variability (~40%) in teratogenic response [4] have galvanized the development of alternative *in vitro* models, especially those based on human pluripotent stem cells (hPSCs). The hPSC-based testing models developed so far employed temporally-controlled differentiating stem cell cultures using either directed differentiation (i.e., differentiation into mesoendodermal [128], neural [16] or cardiac cells [14]) or random differentiation in embryoid bodies [134]. Measurements of molecular biomarkers by gene expression [16, 128, 134], flow cytometry [14], or metabolite detection [13, 99] were used to determine the teratogenic potential of a compound.

While measuring the temporal expression of molecular biomarkers, such as transcription factors, surface markers or secretory proteins, are fairly successful in predicting drug-induced toxicity on terminally differentiated cells [135, 136], their utility in detecting teratogenic effects of compounds has been limited partially due to the transient, complex and spatially organized nature of molecular signaling events during embryonic development. Therefore, a small set of biomarkers cannot adequately describe developmental processes. Embryonic development is characterized by spatio-temporally regulated cell differentiation and tissue morphogenesis, which involves collective cell migration [20, 21]. Spatio-temporally regulated differentiation and morphogenesis are important in collectively forming developmental structures, such as the primitive streak, at the desired time and place during embryonic development [21], which are sensitive to disruption by teratogens. We hypothesize that constructing a spatial pattern of cell differentiation and migration in hPSC culture can provide a sensitive assay for detecting the teratogenic potential of compounds *in vitro*.

Asymmetries in both mechanical and biochemical environmental cues have been shown to play important roles in the spatial patterning of cell differentiation and collective cell migration both *in vivo* [21, 50, 51, 137] and *in vitro* [57, 58, 123]. As shown in Chapter 4 and Chapter 5, we used the inherent mechanical asymmetry in a micropatterned hPSC (μP-hPSC) colony as a simple and robust means to spatially localize the mesoendoderm

differentiation of hPSCs and allowed them to undergo collective cell migration. Cells at the periphery of the colony preferentially expressed the mesoendoderm marker, Brachyuary (T) after one day of differentiation. These mesoendoderm cells underwent collective cell migration to eventually form a multicellular annular pattern on day 3. Here, we further applied our μP-hPSC model for human teratogen detection. In presence of known teratogens, the formation of the annular mesoendoderm pattern was disrupted in a dose-dependent manner. Quantitative analysis of the mesoendoderm morphologic features across different compound treatment groups using feature clustering and one-way analysis of variance (ANOVA) could successfully distinguish known teratogens from the non-teratogens and avoid inter-species variation when compared with the traditional mouse embryonic stem cell test (mEST).

6.2 Materials and Methods

6.2.1 Cell maintenance and differentiation

The hPSC maintenance and differentiation protocols were the same as stated in 4.2.1. The adult human dermal fibroblast (aHDF) was obtained from Lonza (Singapore) and cultured in DMEM high glucose medium (10569-010, Gibco) supplemented with 10% FBS and 1% Pen-Strep (09367-34, Nacalai Tesque). To get single cell suspension for cell seeding, the cells were washed with 1X PBS three times and treated with 0.25% Trypsion-EDTA (25200-114, Gibco) at 37 ℃ for 3-4 min.

6.2.2 Drug preparation

The drugs tested in this study were Penicillin G (P3032-10MU, Sigma-Aldrich), Thalidomide (T144-100MG, Sigma-Aldrich), VPA (P4543-10G, Sigma-Aldrich), D-penicillamine (P4875-5G, Sigma-Aldrich) and RA (554720-500MGCN, Merck, Millipore). The stocks of Thalidomide and RA were dissolved in DMSO (D2650, Sigma-Aldrich), while others are dissolved in distilled water. The dilutions of thalidomide and RA for drug treatment in our μP-hPSC model were prepared such that DMSO concentration was less than 0.25%.

6.2.3 Cytotoxicity assay

The cytotoxicity test was done in 96-well tissue culture plates with 100 μl of medium with or without the drug. For each drug, 8 concentrations with 5-fold dilution were tested together with the vehicle controls. For H9 cells, the plates were coated with Matrigel^{TM} before cell seeding. 10,000 hES cells or 500 aHDF cells were plated into each well and cultured for 3 days in the test solution with half change of the medium with or without the drug every day. On day 3, cell viability was measured using CellTiter 96® AQueous One Solution Cell Proliferation Assay (MTS, G3580, Promega, USA). Three independent tests were done for each drug to finally acquire the cytotoxicity results. IC_{25} values were acquired from either logistic regression using OriginPro 9 or direct reading from the cytotoxicity curve.

6.2.4 Image analysis

Kymograph analysis

Kymographs were generated using ImageJ (Version 1.46r, NIH) with installed MultipleKymograph plugin. After importing the time series of μP-hPSC colony images, an average intensity Z-projection image was generated. A segmented line was drawn at the region of interest (ROI) (which was the colony periphery in our study) in the Z-projection image and then restored in the original time series image window using Restore Selection Tool. After that, a kymograph could be generated with a line width of 1 using MultipleKymograph Plugin, which shows the movement of cells along the segmented line within time of interest.

Morphological feature extraction

Morphological feature extraction from T fluorescence images was done in MATLAB Image Processing Toolbox (Mathworks). First, the outline of the μP-hPSC colony was identified by intensity difference compared with background and its centroid position was determined. The Otsu's method was then applied to segment the whole μP-hPSC colony into T^+ region and T^- region. The relative positions/distributions of each region were acquired. All of the 19 morphological features were extracted based on the distribution of the T^+ region, mainly including the area of the T^+ region, relative distance of the T^+ region to the colony centroid and outline, the standard deviation,

coefficient of variance, skewness, kurtosis, entropy and energy of the distribution of the T^+ region, etc.

Unsupervised Feature clustering

The feature clustering was done in R (Version 3.1.2). After excluding four extraneous features, which showed random trends, the remaining 15 features were clustered into seven morphologic clusters based on their feature correlations by hierarchical clustering using complete linkage method. Based on the clustering result, the feature average values for each morphologic cluster were calculated and plotted in boxplots.

6.2.5 Statistical analysis

One-way ANOVAs were used to access the effects of test compounds on the morphologic changes of mesoendoderm patterns in R. Post-hoc analysis was performed to verify significant ANOVA results and determine DC values of each drug using unpaired t-test and Bonferroni correction methods. Since there were four test groups for each compound screening, six comparisons using unpaired t-test were generated. According to Bonferroni correction, the adjusted critical p value for 0.05 significance would be 0.05 divided by the total number of comparisons, which was 0.0083 (0.05/6). Therefore, the acquired p values by unpaired t-tests were compared with the adjusted critical p value 0.0083.

6.3 Results

6.3.1 Sensitivity and specificity of mesoendoderm pattern formation to teratogen treatment

Since the formation of the mesoendoderm pattern in μP-hPSC colony encompassed developmentally relevant processes (*i.e.*, differentiation and cell migration), we wanted to test if teratogens could disrupt its formation. We treated the μP-hPSC colonies with a paradigm teratogen, Thalidomide (800 μM), and a known non-teratogenic compound, Penicillin G (200 ug/ml), at their non-cytotoxic concentrations to both hPSCs and human adult fibroblasts. Although T^+ cells could be observed in both drug-treated colonies after 3 days, the resultant mesoendoderm patterns were distinctively different (Fig. 6.3.1a,c). The colonies treated with Penicillin G had a similar annular mesoendoderm pattern to the untreated colonies, whereas the colonies treated with Thalidomide showed a much wider mesoendoderm pattern that was displaced towards the colony center (Fig. 6.3.1a,c). Live imaging and kymograph analysis showed that Thalidomide treatment could disrupt the original collective cell migration trajectory (Fig. 6.3.1d). While cells in Penicillin G-treated colonies underwent similar migration trajectory as that in untreated colonies, cells in Thalidomide-treated μP-hPSC colonies migrated much more towards the colony center (Fig. 6.3.1b,d). Since the tested concentration of both compounds was not cytotoxic to the hPSCs, the disruption of the collective cell migration process and the final morphology of

the mesoendoderm pattern by Thalidomide was likely specific to its teratogenic effects. Therefore, our μP-hPSC model could successfully differentiate teratogenic compound Thalidomide from non-teratogenic compound Penicillin G.

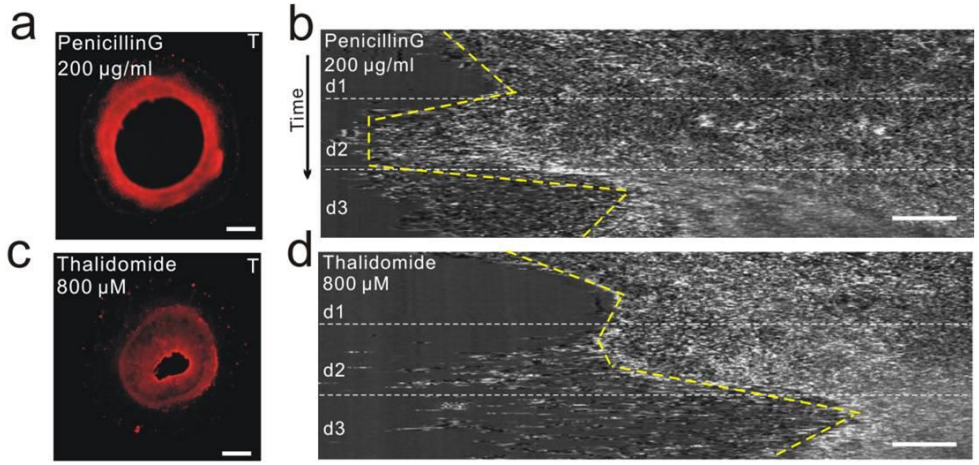

Figure 6.3.1 Disruption of annular mesoendoderm pattern by teratogen treatment. (a,c) Fluorescent images of T in μP-hPSC colonies under Penicillin G (a) and Thalidomide (c) treatment after 3-day mesoendoderm induction. Scale bar, 200 μm. (b,d) Kymographs of cell movements around colony edges during 3-day mesoendoderm induction under Penicillin G (b) and Thalidomdie (d) treatment. Scale bar, 50 μm.

On the contrary, it was difficult to differentiate the teratogenic effects of Thalidomide and Penicillin G by simply measuring the expression levels of molecular biomarkers for mesoendoderm differentiation. Cells from Penicillin G (200 μg/ml) and Thalidomide (800 μM) treated colonies as well as untreated control colonies were examined for the expression level of three germ layer markers using quantitative RT-PCR (Fig. 6.3.2). Results showed no significant

differences of the expression levels of both mesoendoderm markers T and Nkx 2.5, and ectoderm markers Pax 6 and Nestin between Penicillin G-treated and Thalidomide-treated colonies, although colonies in both conditions had an increased T expression level compared with untreated controls (Fig. 6.3.2). Thalidomide-treated samples showed lower expression levels of two other mesoendoderm markers FoxA2 and Sox17 than Penicillin G-treated colonies. However, there were no significant differences of these two markers for either of these two treated samples compared with untreated colonies (Fig. 6.3.2). Therefore, we reasoned that measuring changes in the mesoendoderm pattern, which is an assimilation of multiple cellular processes, as an assay readout for teratogenic potential, is sufficiently sensitive and may show better specificity as compared to the expression levels of a panel of molecular biomarkers for differentiation.

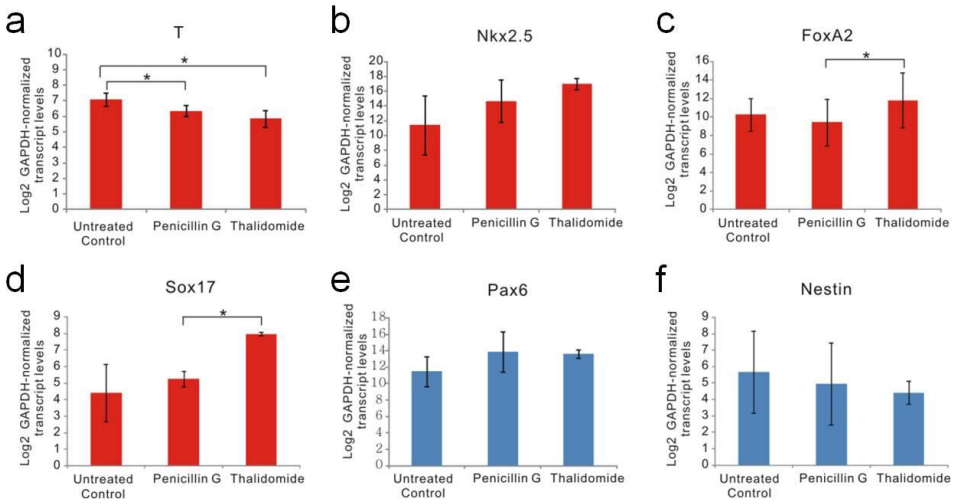

Figure 6.3.2 Expression levels of germ layer markers in untreated, Penicillin G-treated and Thalidomide-treated colonies. Mesoendoderm markers are T,

Nkx2.5, FoxA2 and Sox17; ectoderm markers are Pax6 and Nestin. *, $p < 0.05$ in paired t-test. n= 3.

6.3.2 A quantitative morphometric assay to classify teratogenic potential of compounds

Since the annular mesoendoderm pattern in our μP-hPSC model was sensitive to teratogen treatment, we next developed a quantitative assay to measure drug-induced morphological changes to the mesoendoderm pattern, so as to classify whether a compound is likely to be teratogenic or not.

The dose-dependent effect of each compound on the mesoendoderm pattern formation was determined by dosing at three different concentrations. The cytotoxicity of each compound was evaluated in order to find the appropriate range of testing concentrations. Since drugs or chemicals may have different cytotoxic effects on hPSCs and human adult cells, human embryonic stem cell line, H9 and adult human dermal fibroblasts (aHDFs) were tested for cytotoxicity of each drug. The results would represent specific cytotoxicity to embryonic and adult cells respectively. Based on the cytotoxicity data, three drug concentrations (designated as low, medium and high) were selected such that the lowest concentration tested was not toxic to both H9 cells and aHDFs, and the highest concentration should not be cytotoxic to aHDFs. The tested concentration was considered as not cytotoxic if it was less than the drug's 25% inhibitory concentration (IC_{25}) to the tested cell line [138].

A series of imaging processing and statistical analysis were developed to quantitatively measure the teratogenic effects of each drug (Fig. 6.3.3). For each compound, there were four test groups, consisting of zero, low, medium and high drug concentrations. After three days of culture in the mesoendoderm induction medium, immunofluorescence images of T were acquired. Morphologic features describing the T^+ region within the colony were extracted from the immunofluorescent images using image processing. After excluding extraneous features, which showed random trends, the remaining features were clustered into different morphologic clusters based on their feature correlations. One-way analysis of variance (ANOVA) was then performed on each morphologic cluster to determine whether there were significant morphologic differences among test groups for each drug. If no significant differences among groups were identified in all feature clusters, we could directly classify the tested drug as non-teratogenic.

On the contrary, if any morphologic clusters showed significant differences among four test groups, post-hoc analysis was then performed in those morphologic clusters to confirm the ANOVA results, as well as to find the lowest concentration showing significant mesoendoderm pattern disruption compared with the non-treated control group. This concentration was defined as the disruption concentration (DC). If $DC < IC_{25,H9}$, we can infer that the drug is teratogenic, where it affects embryonic development without being cytotoxic to embryonic cells [138].

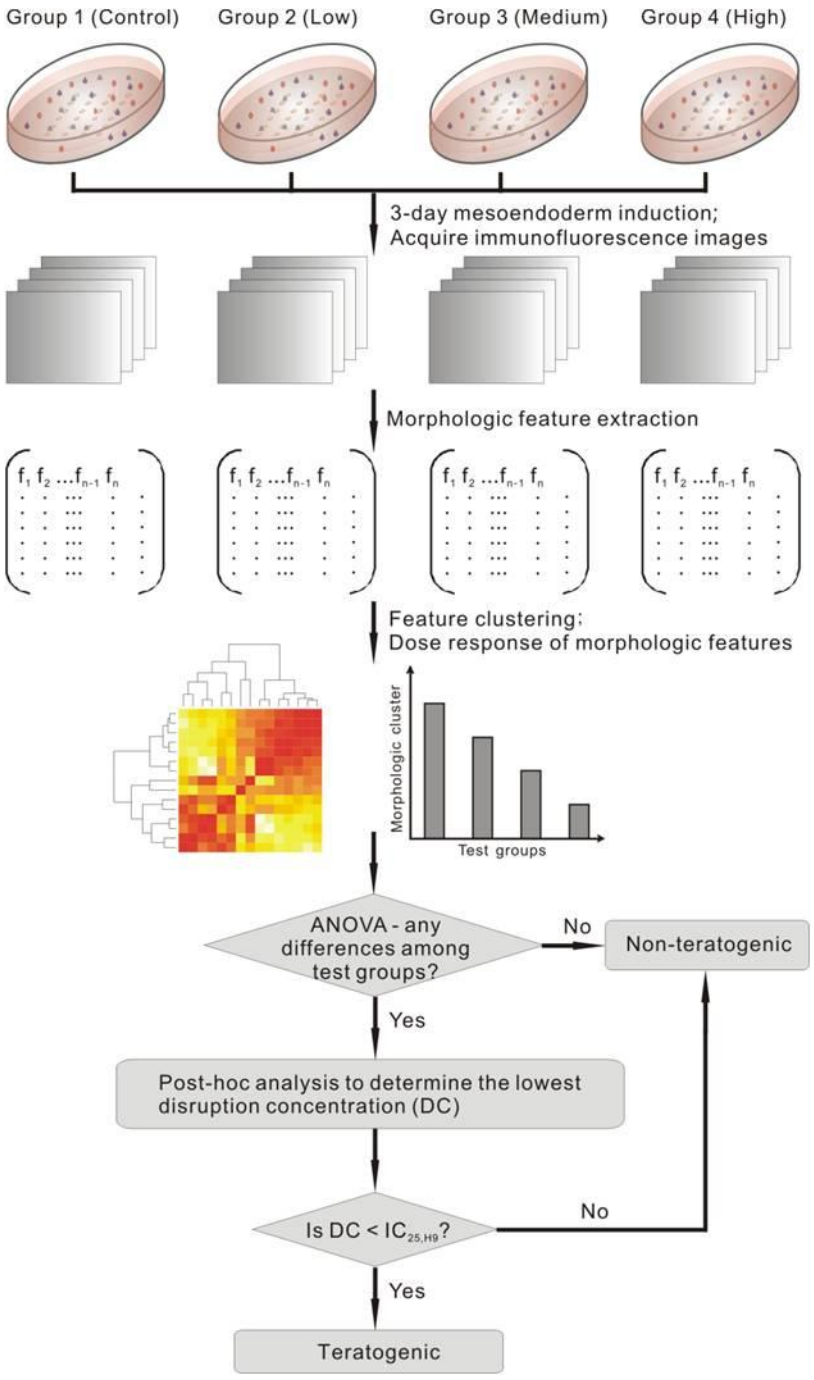

Figure 6.3.3 Development of a quantitative morphometric assay for teratogen screening. Details are provided in the main text. DC, disruption concentration, the lowest concentration which morphologically disrupts the mesoendoderm pattern.

6.3.3 Evaluation of the morphometric μP-hPSC model in classifying teratogens

We evaluated the drug testing performance of the μP-hPSC model by comparing with a well-established stem cell-based assay, the mouse embryonic stem cell test (mEST). The mEST measures whether a drug or chemical can disrupt beating cardiomyocytes formation using mESCs, and is currently one of the leading *in vitro* models being validated for teratogenicity screening [10, 71]. Here, five drugs were selected according to the United States (US) FDA Pharmaceutical Pregnancy Risk Categories based on animal and/or human data (Table 6.3.1).

Table 6.3.1 Compound list for teratogen screening in the μP-hPSC model

No.	Compounds	Drug Application	US FDA Pharmaceutical Pregnancy Category*	*In vivo* human data	In mEST
1	Thalidomide	Anti-nausea and sedative drug	Pregnancy risk category X	Teratogenic [92]	N.A.
2	Retinoic acid (RA)	Antineoplastic drug	Pregnancy risk category D	Teratogenic [139]	Teratogenic
3	D-Penicillamine	For Wilson's disease and heavy metal intoxication	Pregnancy risk category D	Teratogenic [140]	Non-teratogenic

4	Valproic acid (VPA)	Anticonvulsant and mood-stabilizing drug	Pregnancy risk category D	Teratogenic [141]	Teratogenic
5	Penicillin G	Antibotics, antibacterial drug	Pregnancy risk category B	Non-teratogenic [142]	Non-teratogenic

*: There are five categories. Category A indicates no pregnancy risk in human, Category B indicates no risk in animal studies, Category C shows positive pregnancy risk in animals, and Category D & X indicate clear risks in pregnant women.

Four of the drugs are classified as teratogens *in vivo* [92, 139-141] (Category D or X) while a non-teratogenic [142] drug *in vivo* (Category B) was included as a negative control. The mEST can only accurately classify three out of the five selected drugs (Table 6.3.1). Thalidomide affects human but not mouse development and therefore cannot be detected in mEST [143]. D-penicillamine, on the other hand, was misclassified as non-terotogenic in mEST [95] due to the model's limitation in assessing only cardiogenesis endpoints [96]. By choosing this five model drugs, we aimed to evaluate whether our uP-hPSC model can potentially show better performance than the mEST.

First, the cytotoxicity data of each drug on both H9 cells and aHDFs were acquired to determine the low, medium and high concentrations for different test groups (Fig. 6.3.4). Results showed that hPSCs were more susceptive to drug treatments than adult cells in the cases of Penicillin G, VPA and D-

Penicillamine, exhibiting more cell death at high drug concentrations compared with aHDF cells (Fig. 5). In the case of RA, however, high concentration at about 2 μg/ml actually significantly promoted H9 cell proliferation whereas showed no effects on aHDFs. This is probably due to the fact that RA is a potent morphogen, high differentiation effects of RA which can induce hPSCs to differentiate into neuronal cells [144]. Thalidomide caused no cell death to both H9 and aHDF cells up to its highest soluble concentration.

Drug dosing, mesoendoderm induction as well as immunofluorescence images were acquired (Fig. 6.3.5) and processed as described above. Seven morphologic clusters were generated by clustering the extracted fifteen morphologic features based on their correlations with each other (Fig. 6.3.6a). These seven morphologic clusters collectively describe the dispersion (CL1 and CL3), position (CL2 and CL6), area (CL4), kurtosis (CL5) and energy (CL7) of the T^+ cell distribution within each μP-hPSC colony (Fig. 6.3.6b).

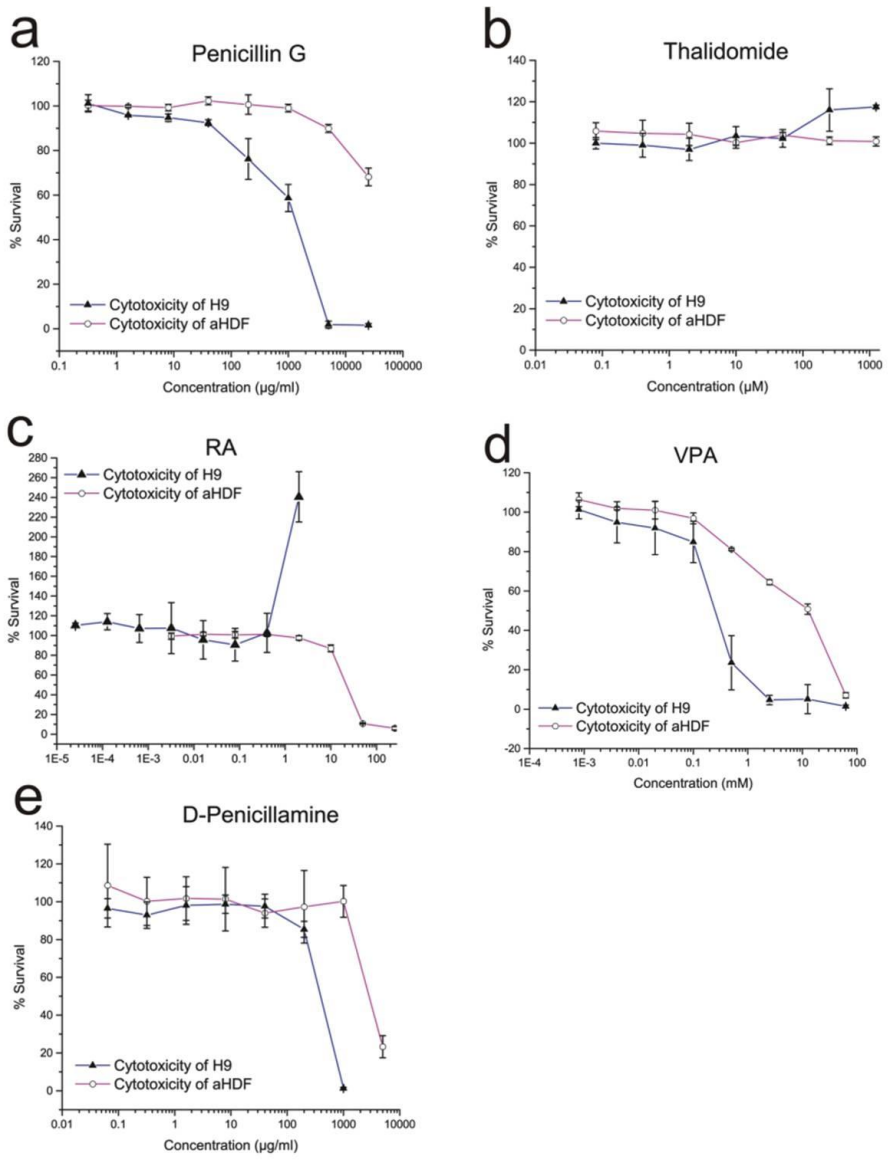

Figure 6.3.4 Cytotoxicity results of the five tested drugs. (a-e) Cell viability curves for drug treatment in h9 cells (blue line) and aHDFs (pink lines) (n = 3).

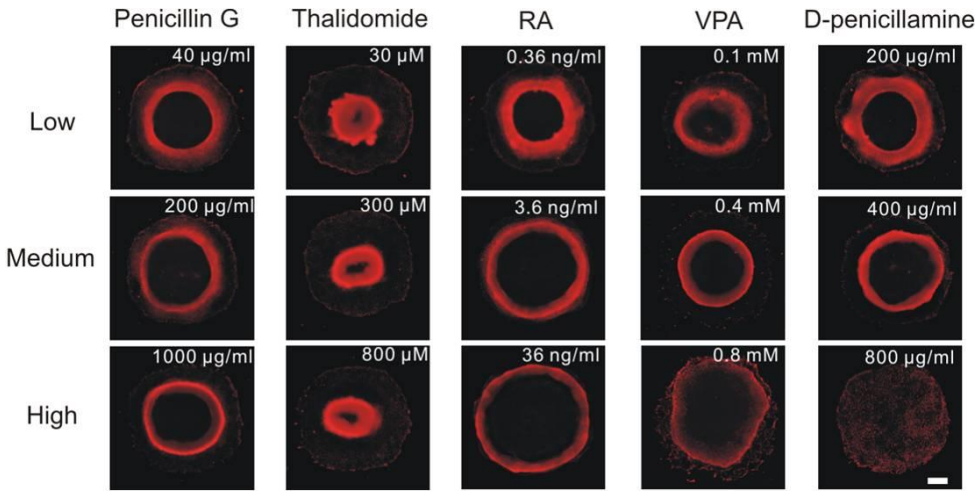

Figure 6.3.5 Fluorescent images of T in different drug test groups on day 3. Scale bar, 200 μm.

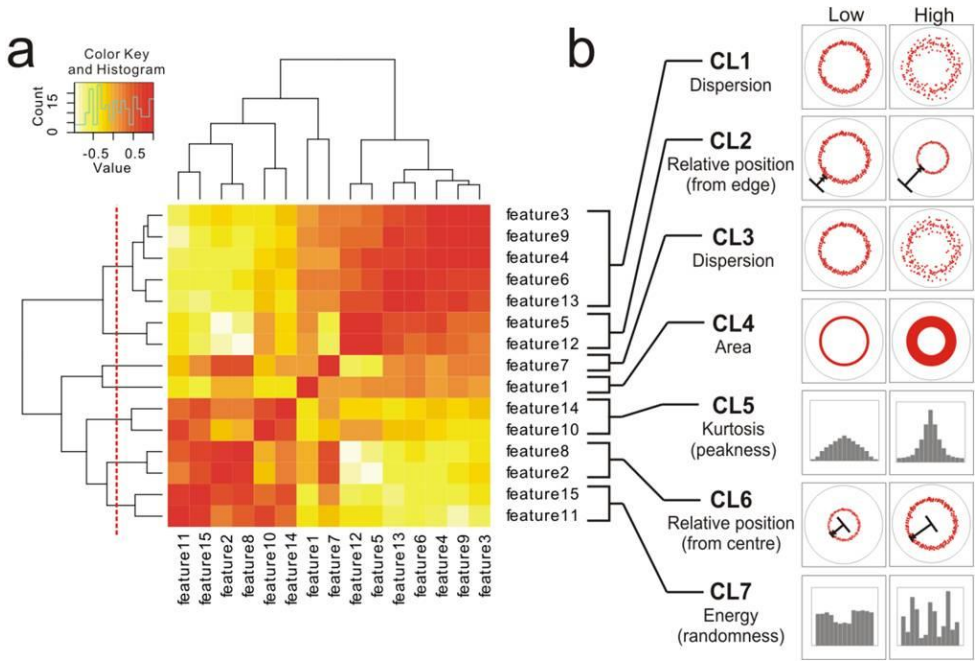

Figure 6.3.6 Generation of morphologic clusters by feature clustering. (a) Hierarchical clustering of morphologic features based on feature correlations. Dash line indicates that 7 clusters were acquired. (b) The morphologic interpretations of the 7 morphologic clusters.

The readouts of each morphologic cluster across the four test groups (*i.e.* control, low, medium, high) were plotted for each drug and one-way ANOVA was performed to determine whether there were significant differences across the test groups (Fig. 6.3.7-6.3.11). Post-hoc analysis was performed using unpaired t-test and Bonferroni correction methods to verify the ANOVA results and determine the DC values of each drug. Our assay based on the morphologic clusters showed that Thalidomide, Retinoic acid (RA), D-penicillamine, and Valproic acid (VPA) exhibited significant dose-dependent morphologic disruptions of the mesoendoderm pattern (Fig. 6.3.8-6.3.11). For each drug, at least one morphologic clusters showed significant disruption to the mesoendoderm pattern in the low concentration test groups (Fig. 6.3.8-6.3.11). Therefore, the DC values for these four drugs were 30 μM for Thalidomide, 0.36 ng/ml for RA, 200 μg/ml for D-penicillamine, and 0.1 mM for VPA (Table 6.3.2). In the case of the negative control drug Penicillin G, ANOVA results showed no significant differences among test groups in almost all morphologic clusters except CL6 ($p=0.0122$) (Fig. 6.3.7). The high concentration test group at 1000 μg/ml showed a significant inward mesoenoderm pattern position toward the colony centre compared with zero dose control group (Post-hoc analysis, $p=0.0014 < 0.0083$) (Fig. 6.3.7f). Therefore, the DC for Penicillin G was 1000 μg/ml (Table 6.3.2).

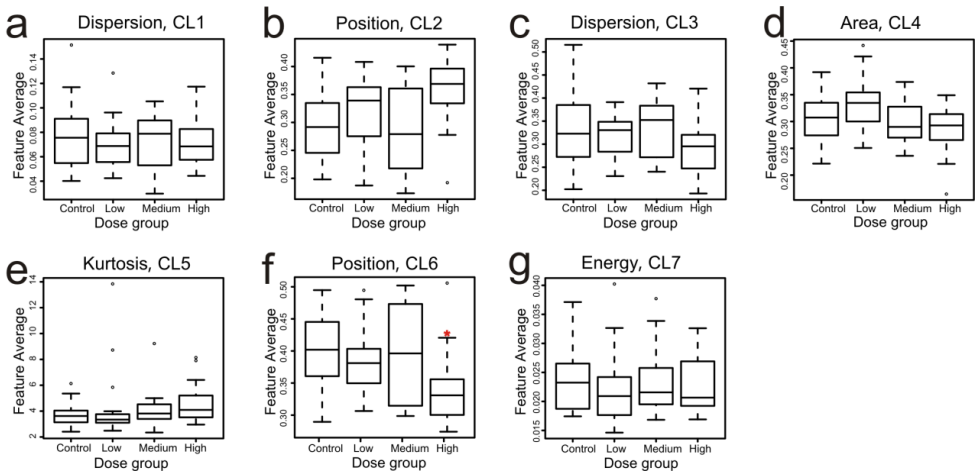

Figure 6.3.7 Boxplots of morphologic cluster readout in Penicillin G test groups. Low: 40 µg/ml; Medium: 200 µg/ml; High: 1000 µg/ml. *: p<0.0083 in post-hoc analysis for comparing the difference between the corresponding dose group and the untreated control group.

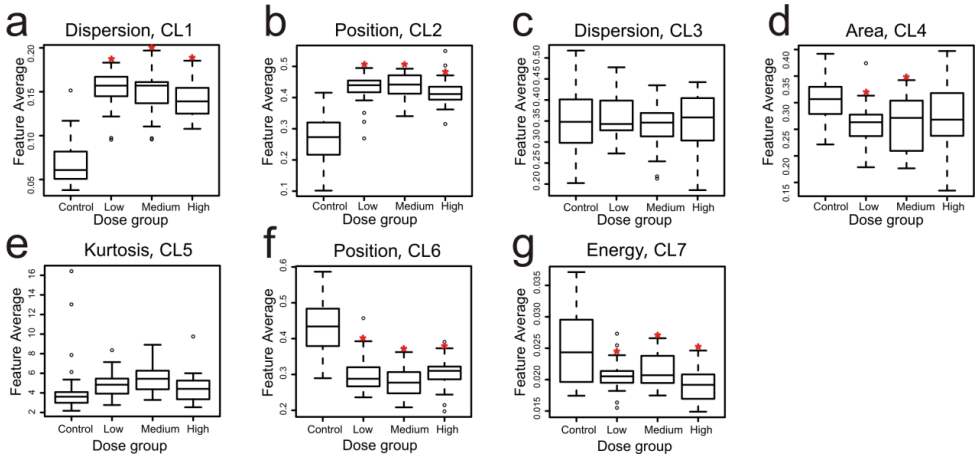

Figure 6.3.8 Boxplots of morphologic cluster readout in Thalidomide test groups. Low: 30 µM; Medium: 300 µM; High: 800 µM. *: p<0.0083 in post-hoc analysis for comparing the difference between the corresponding dose group and the untreated control group.

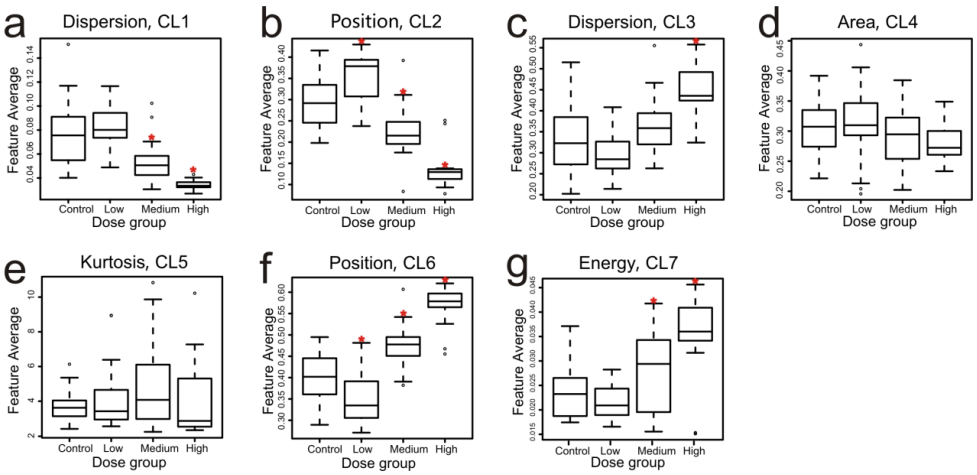

Figure 6.3.9 Boxplots of morphologic cluster readout in RA test groups. Low: 0.00036 μg/ml; Medium: 0.0036 μg/ml; High: 0.036 μg/ml. *: p<0.0083 in post-hoc analysis for comparing the difference between the corresponding dose group and the untreated control group.

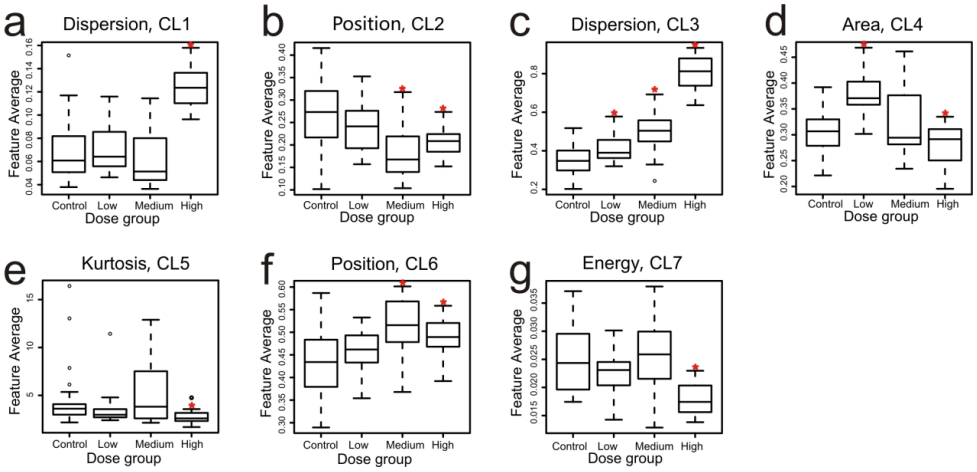

Figure 6.3.10 Boxplots of morphologic cluster readout in D-penicillamine test groups. Low: 200 μg/ml; Medium: 400 μg/ml; High: 800 μg/ml. *: p<0.0083 in post-hoc analysis for comparing the difference between the corresponding dose group and the untreated control group.

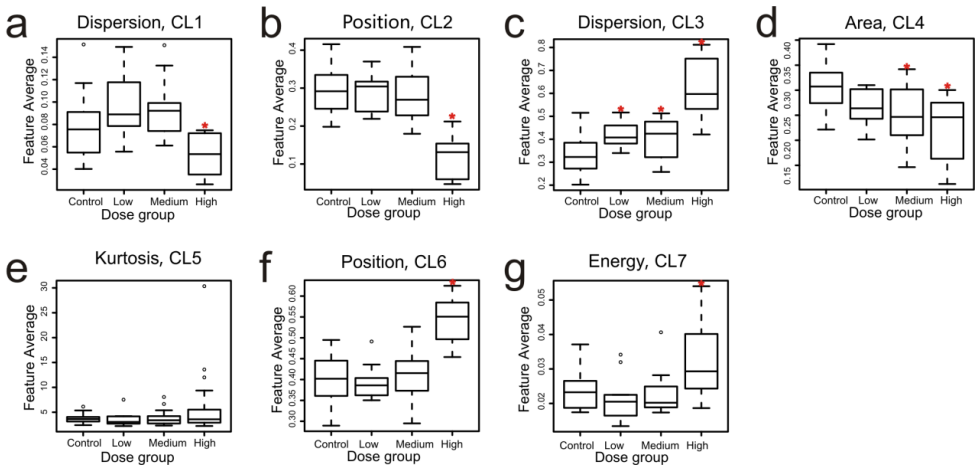

Figure 6.3.11 Boxplots of morphologic cluster readout in VPA test groups. Low: 0.1 mM; Medium: 0.4 mM; High: 0.8 mM. *: $p<0.0083$ in post-hoc analysis for comparing the difference between the corresponding dose group and the untreated control group.

Finally we compared the DC values of each drug with their IC_{25} values to H9 cells to determine whether they are teratogenic (Table 6.3.2). For Thalidomide, RA, D-penicillamine and VPA, the DC values were all less than their corresponsive $IC_{25,H9}$ values, indicating that the disruption of the mesoendoderm pattern was likely mediated by alterations to differentiation and migration rather than cytotoxicity effects on the embryonic cells. Therefore, they were identified as teratogenic in our model. In contrast, Penicillin G had a much higher DC value compared with its $IC_{25,H9}$ value, and was classified as non-teratogenic. Therefore, our quantitative morphometric assay based on the μP-hPSC model could correctly classify the five test compounds in accordance to their teratogenicity potential *in vivo* and showed a better performance when compared with the mEST.

Table 6.3.2 Teratogenicity screening results in the μP-hPSC model

Compound	**DC**	**IC_{25H9}**	**Does DC < IC_{25H9}?**	**In the μP-hPSC model**	**In mEST**
Thalidomide	30 μM	>1000 μM	Yes	Teratogenic	N.A.
RA	0.36 ng/ml	> 2000 ng/ml	Yes	Teratogenic	Teratogenic
D-penicillamine	200 μg/ml	278 μg/ml	Yes	Teratogenic	Non-teratogenic
VPA	0.1 mM	0.13 mM	Yes	Teratogenic	Teratogenic
Penicillin G	1000 μg/ml	787 μg/ml	No	Non-teratogenic	Non-teratogenic

6.3.4 Concentration-dependent teratogenicity of compounds

An important consideration when assessing for teratogenic potential is the dose-dependent response [1]. The effect of a potentially teratogenic compound may not be manifested *in vivo* due to a low therapeutic dose being used [128, 145]. Therefore, an ideal *in vitro* screening model should not only identify whether a drug is potentially teratogenic, it should also be able to detect its teratogenic effects at clinically-relevant concentrations. The drug testing results in this study demonstrated the potential of the μP-hPSC model to detect teratogenic effects of compounds at clinically-relevant concentrations. In fact, when compared with the compound's highest *in vivo* concentration (C_{max}) in human plasma following therapeutic dosing, the DC values we detected for RA, D-penicillamine and VPA were already lower than or equal to their known C_{max} values, indicating their strong clinical teratogenic effects (Table

6.3.3). In contrast, the DC value for Penicillin G was much higher than the highest clinical C_{max} value reported in literature, which was 400 μg/ml [146], confirming that it was non-teratogenic (Table 6.3.3).

Table 6.3.3 The DC and Cmax values of test compounds

No.	Compounds	DC in μP-hPSC model	C_{max}	Reference
1	Thalidomide	30 μM	10.922 μM	Teo et al. (2004) [147]
2	RA	0.36 ng/ml	347 ng/ml	Muindi et al. (1992) [148]
3	D-penicillamine	200 μg/ml	200 μg/ml	Netter et al. (1987) [149]
4	VPA	0.1 mM	0.574 mM	Reed et al. (2006) [150]
5	Penicillin G	1000 μg/ml	400 μg/ml	Plaut et al. (1969) [146]

6.4 Conclusion

Human-specific drug screening platforms for teratogenicity are needed to avoid inter-species variation problems [93]. However, current *in vitro* human PSC-based models only recapitulate temporal differentiation events [13, 14, 16, 99, 128, 134], and overlooked other key processes during embryonic development, including spatial organization of differentiation and morphogenic movements. Our μP-hPSC model is the first *in vitro* human developmental toxicity screening model, which recapitulated both spatially controlled differentiation and collective cell migration processes during

embryogenesis. Here, we demonstrated that this model was sensitive enough to distinguish compound's teratogenic potential, and exhibited better selectivity to human-specific effects than the mEST.

However, we must admit that so far the advantage of our μP-hPSC model has only been shown when compared with the mEST and other animal-based assays due to a small number of compounds tested. It avoids inter-species variation and can correctly classify D-penicillamine which was misclassified in mEST due to model limitations. Compared with other existing hPSC-based models such as the metabolite biomarker-based hPSC teratogenicity assay and the hPST model, our model has shown equal performance for all of the five drugs tested. In order to further validate the predicitivity of our model and statistically compare it with current hPSC models, more drugs need to be tested and the classification rules may also need to be further optimized to get better predicitivity performance.

7. Conclusions and Recommendations

This dissertation has documented the establishment of a new *in vitro* hPSC-based model, which could capture both spatial differentiation and collective cell migration in development, for developmental toxicity testing application.

Firstly, we spatially induced mesoendoderm differentiation to the periphery of a circular μP-hPSC colony, which possessed higher intergrin-

mediated adhesions compared with the interior. By studying the underlying mechanism, we found that instead of a direct promotion of differentiation, this spatial correlation of mesoendoderm differentiation was likely induced by the corresponding destabilization of the E-cadherin AJs in regions of higher integrin-mediated adhesion. The destabilization of the E-cadherin AJs was due to the position change of the activated myosion II from the E-cadherin AJs to the actomyosin contractile cable caused by increased integrin adhesion-mediated contractile stresses at the colony periphery. E-cadherin signaling was the primary gatekeeper of pluripotency-differentiation decision in hPSCs. Inhibition of Rho-ROCK-myosin II with pharmacological inhibitors (e.g. blebbistatin or Y27632) led to the robust differentiation of the entire μP-PSC colony instead of attenuated differentiation of MSCs even in an inductive soluble environment.

Secondly, we formed an annular mesoendoderm pattern in our μP-hPSC model by geometrically confined cell differentiation and migration. When culturing μP-hPSC colonies for 3 days instead of 1 day in mesoendoderm induction medium, the differentiated mesoendoderm cells at the colony periphery would undergo collective cell migration process towards colony centre and form a 3D *in vivo*-like mesoendoderm pattern on d3. The migration speed was matrix concentration-dependent. Higher Matrigel^{TM} concentration led to slower migration within the μP-hPSC colonies. Different hPSC lines

could generate similar mesoendoderm patterns without protocol optimization, showing the robustness of our μP-hPSC model.

Finally, we further applied our μP-hPSC model for human teratogen detection. In presence of known teratogens, the formation of the annular mesoendoderm pattern was disrupted in a dose-dependent manner. Quantitative analysis of the mesoendoderm morphologic features across different compound treatment groups using feature clustering and one-way analysis of variance (ANOVA) successfully distinguished known teratogens from the non-teratogens and avoid inter-species variation when compared with the traditional mouse embryonic stem cell test (mEST).

The μP-hPSC platform developed in this dissertation may serve as a great system to systematically study the signalling mechanisms of how mechano-sensory cues can modulate self-renewal and/or differentiation program of hPSCs. Here our results showed that E-cadherin was the main gatekeeper in hPSCs, and integrin signalling actually affected hPSC fate through destabilization of E-cadherin AJs (Chapter 4). In future studies, it would be interesting to investigate exactly how integrin-mediated tension signalling specifically activates the differentiation program through E-cadherin AJs. For example, it would be important to look at downstream integrin signaling, such as FAK activity, in μP-hPSCs treated with E-cadherin function blocking antibodies in order to correlate a gain of integrin signalling with loss of E-cadherin at the junctions. On the other hand, we could also try to uncouple the

adhesion functions and the signalling functions of E-cadherin, to provide a better understanding of its effect on hPSC differentiation. We can overexpress either the extra-cellular domain of E-cadherin which is competent for adhesion but deficient in signalling or just the intra-cellular domain that is signalling competent but adhesion deficient, and test whether the T expression pattern within the μP-hPSC colony is maintained.

The processes of spatial differentiation and coordinated collective cell migration of mesoendoderm cells in our μP-hPSC model are quite similar to *in vivo* embryo development. During gastrulation in mouse, Drosophila, or avian embryos, mesoendoderm cells all flow into the midline of the embryo to form the primitive streak and then migrate away from the streak to their desired location. However, the underlying mechanism of this directed migration process is still not fully understood so far [137, 151]. Possible mechanisms might involve morphological asymmetries, asymmetric signalling activities [137], actomyosin activity related intrinsic forces as well as extrinsic forces to the tissues [152]. In this dissertation, we showed that there were indeed asymemetries in cell-matrix, cell-cell interactions and actomyosin contractility within the μP-hPSC colony between the colony edge and interior (Chapter 4). And RT-PCR results also proved that the cells at the periphery did undergo EMT process and became migratory (Chapter 5). However, the exact mechanism of this collective cell migration process was not studied in our model. We only focused on mimicking and observing the collective cell

migration process and applied it for our drug testing application. It should be acceptable at this stage since the main purpose of this dissertation is to establish and apply this model for developmental toxicity testing. To fully understand the underlying mechanism of its migration process requires a lot of resources and effort, which can be conducted as a further extension of this study.

In terms of developmental toxicity testing application, further study could be conducted to scientifically validate the μP-hPSC model with more test compounds. In order to systematically compare the teratogen screening performance with other existing models, at least 20-30 compounds of known teratogenicity should be tested altogether. A test group with enough compounds is required to optimize the classification rules, and an application group is required to evaluate the actual prediction performance of the model. To facilitate this systematic validation process, a scale-up of the current μP-hPSC model may also be required. Luckily, the scalability and robustness of our μP-hPSC model should make it easy to implement. Our μP-hPSC model could also be easily combined with other data collection and analysis techniques applied in other hPSC models shown in Chapter 2 to study the mechanisms of teratogenicity for specific chemical compounds.

8. References

1. Haschek, W.M., C.G. Rousseaux, and M.A. Wallig, *Fundamentals of Toxicologic Pathology*. 2 ed. Developmental Pathology. 2010, London, UK: Academic Press.

2. Rovida, C. and T. Hartung, *Re-evaluation of animal numbers and costs for in vivo tests to accomplish REACH legislation requirements for chemicals - a report by the transatlantic think tank for toxicology (t(4)).* ALTEX, 2009. **26**(3): p. 187-208.

3. Basketter, D.A., et al., *A roadmap for the development of alternative (non-animal) methods for systemic toxicity testing - t4 report*.* ALTEX, 2012. **29**(1): p. 3-91.

4. Bremer, S., et al., *The development of new concepts for assessing reproductive toxicity applicable to large scale toxicological programmes.* Curr Pharm Des, 2007. **13**(29): p. 3047-58.

5. Bantle, J.A., et al., *Further validation of FETAX: evaluation of the developmental toxicity of five known mammalian teratogens and non-teratogens.* Drug Chem Toxicol, 1990. **13**(4): p. 267-82.

6. Jelinek, R., M. Peterka, and Z. Rychter, *Chick embryotoxicity screening test--130 substances tested.* Indian J Exp Biol, 1985. **23**(10): p. 588-95.

7. Flint, O.P., *In vitro tests for teratogens: desirable endpoints, test batteries and current status of the micromass teratogen test.* Reprod Toxicol, 1993. **7 Suppl 1**: p. 103-11.

8. Sadler, T.W., W.E. Horton, and C.W. Warner, *Whole embryo culture: a screening technique for teratogens?* Teratog Carcinog Mutagen, 1982. **2**(3-4): p. 243-53.

9. Hill, A.J., *Zebrafish as a model vertebrate for investigating chemical toxicity.* Toxicol Sci, 2005. **86**(1): p. 6-19.

10. Seiler, A.E.M. and H. Spielmann, *The validated embryonic stem cell test to predict embryotoxicity in vitro.* Nat Protoc, 2011. **6**(7): p. 961-978.

11. Thomson, J.A., *Embryonic stem cell lines derived from human blastocysts.* Science, 1998. **282**(5391): p. 1145-1147.

12. Jagtap, S., et al., *Cytosine arabinoside induces ectoderm and inhibits mesoderm expression in human embryonic stem cells during multilineage differentiation.* Brit J Pharmacol, 2011. **162**(8): p. 1743-1756.

13. West, P.R., et al., *Predicting human developmental toxicity of pharmaceuticals using human embryonic stem cells and metabolomics.* Toxicol Appl Pharm, 2010. **247**(1): p. 18-27.

14. Zhu, M.X., et al., *Early embryonic sensitivity to cyclophosphamide in cardiac differentiation from human embryonic stem cells.* Cell Biol Int, 2011. **35**(9): p. 927-38.

15. Colleoni, S., et al., *Development of a neural teratogenicity test based on human embryonic stem cells: response to retinoic acid exposure.* Toxicol Sci, 2011. **124**(2): p. 370-377.

16. Colleoni, S., et al., *Characterisation of a neural teratogenicity assay based on human ESCs differentiation following exposure to valproic acid.* Curr Med Chem, 2012. **19**(35): p. 6065-71.

17. Tang, Y.L., et al., *Identification of Thalidomide-specific transcriptomics and proteomics signatures during differentiation of human embryonic stem cells.* PLoS One, 2012. **7**(8): p. e44228.

18. Browder, L.W., C.A. Erickson, and W.R. Jeffery, *Developmental Biology*. 3 ed. 1991.

19. Bard, J., *Morphogenesis.* Scholarpedia, 2008. **3**: p. 2422.

20. Farge, E., *Mechanotransduction in development.* Curr Top Dev Biol, 2011. **95**: p. 243-265.

21. Mammoto, T. and D.E. Ingber, *Mechanical control of tissue and organ development.* Development, 2010. **137**(9): p. 1407-20.

22. Sadava, D., et al., *Life, the science of biology*. 8th ed. 2007: W. H. Freeman and Company.

23. Tam, P.P. and D.A. Loebel, *Gene function in mouse embryogenesis: get set for gastrulation.* Nat Rev Genet, 2007. **8**(5): p. 368-81.

24. Solnica-Krezel, L., *Conserved patterns of cell movements during vertebrate gastrulation.* Curr Biol, 2005. **15**(6): p. R213-R228.

25. Nostro, M.C., et al., *Wnt, Activin, and BMP signaling regulate distinct stages in the developmental pathway from embryonic stem cells to blood.* Cell Stem Cell, 2008. **2**(1): p. 60-71.

26. Evseenko, D., et al., *Mapping the first stages of mesoderm commitment during differentiation of human embryonic stem cells.* Proc Natl Acad Sci USA, 2010. **107**(31): p. 13742-7.

27. Quail, D.F., et al., *Nodal signalling in embryogenesis and tumourigenesis.* Int J Biochem Cell B, 2013. **45**(4): p. 885-898.

28. Beck, S., et al., *Extraembryonic proteases regulate Nodal signalling during gastrulation.* Nat Cell Biol, 2002. **4**(12): p. 981-5.

29. Schier, A.F., *Nodal morphogens.* Cold Spring Harb Perspect Biol, 2009. **1**(5): p. a003459.

30. Vincent, S.D., et al., *Cell fate decisions within the mouse organizer are governed by graded Nodal signals.* Genes Dev, 2003. **17**(13): p. 1646-62.

31. Brennan, J., et al., *Nodal signalling in the epiblast patterns the early mouse embryo.* Nature, 2001. **411**(6840): p. 965-9.

32. Conlon, F.L., et al., *A primary requirement for nodal in the formation and maintenance of the primitive streak in the mouse.* Development, 1994. **120**(7): p. 1919-28.

33. Schier, A.F., *Nodal signaling in vertebrate development.* Annu Rev Cell Dev Biol, 2003. **19**: p. 589-621.

34. Katoh, M., *WNT signaling pathway and stem cell signaling network.* Clin Cancer Res, 2007. **13**(14): p. 4042-4045.

35. Bhanot, P., et al., *A new member of the frizzled family from Drosophila functions as a Wingless receptor.* Nature, 1996. **382**(6588): p. 225-30.

36. Pinson, K.I., et al., *An LDL-receptor-related protein mediates Wnt signalling in mice.* Nature, 2000. **407**(6803): p. 535-8.

37. Eisenmann, D.M., *Wnt signaling.* WormBook, 2005.

38. Huelsken, J., et al., *Requirement for beta-catenin in anterior-posterior axis formation in mice.* J Cell Biol, 2000. **148**(3): p. 567-78.

39. Kelly, O.G., K.I. Pinson, and W.C. Skarnes, *The Wnt co-receptors Lrp5 and Lrp6 are essential for gastrulation in mice.* Development, 2004. **131**(12): p. 2803-15.

40. Greco, T.L., et al., *Analysis of the vestigial tail mutation demonstrates that Wnt-3a gene dosage regulates mouse axial development.* Genes Dev, 1996. **10**(3): p. 313-24.

41. ten Berge, D., et al., *Wnt signaling mediates self-organization and axis formation in embryoid bodies.* Cell Stem Cell, 2008. **3**(5): p. 508-518.

42. Yu, P., et al., *FGF2 sustains NANOG and switches the outcome of BMP4-induced human embryonic stem cell differentiation.* Cell Stem Cell, 2011. **8**(3): p. 326-334.

43. Ciruna, B. and J. Rossant, *FGF signaling regulates mesoderm cell fate specification and morphogenetic movement at the primitive streak.* Dev Cell, 2001. **1**(1): p. 37-49.

44. Keller, R., L.A. Davidson, and D.R. Shook, *How we are shaped: the biomechanics of gastrulation.* Differentiation, 2003. **71**(3): p. 171-205.

45. Beloussov, L.V. and V.I. Grabovsky, *Morphomechanics: goals, basic experiments and models.* Int J Dev Biol, 2006. **50**(2-3): p. 81-92.

46. Monier, B., et al., *An actomyosin-based barrier inhibits cell mixing at compartmental boundaries in Drosophila embryos.* Nat Cell Biol, 2010. **12**(1): p. 60-5; sup pp 1-9.

47. Landsberg, K.P., et al., *Increased cell bond tension governs cell sorting at the Drosophila anteroposterior compartment boundary.* Curr Biol, 2009. **19**(22): p. 1950-5.

48. Rauzi, M., P.-F. Lenne, and T. Lecuit, *Planar polarized actomyosin contractile flows control epithelial junction remodelling.* Nature, 2010. **468**(7327): p. 1110-1114.

49. Butler, L.C., et al., *Cell shape changes indicate a role for extrinsic tensile forces in Drosophila germ-band extension.* Nat Cell Biol, 2009. **11**(7): p. 859-864.

50. Desprat, N., et al., *Tissue deformation modulates twist expression to determine anterior midgut differentiation in Drosophila embryos.* Dev Cell, 2008. **15**(3): p. 470-477.

51. Pouille, P.A., et al., *Mechanical signals trigger myosin II redistribution and mesoderm invagination in Drosophila embryos.* Sci Signal, 2009. **2**(66): p. ra16-ra16.

52. Farge, E., *Mechanotransduction in development.* Curr Top Dev Biol, 2011. **95**: p. 243-65.

53. Seher, T.C., et al., *Analysis and reconstitution of the genetic cascade controlling early mesoderm morphogenesis in the Drosophila embryo.* Mech Dev, 2007. **124**(3): p. 167-79.

54. Farge, E., *Mechanical induction of Twist in the Drosophila foregut/stomodeal primordium.* Curr Biol, 2003. **13**(16): p. 1365-77.

55. Engler, A.J., et al., *Matrix elasticity directs stem cell lineage specification.* Cell, 2006. **126**(4): p. 677-89.

56. Wingate, K., et al., *Compressive elasticity of three-dimensional nanofiber matrix directs mesenchymal stem cell differentiation to vascular cells with endothelial or smooth muscle cell markers.* Acta Biomater, 2012. **8**(4): p. 1440-9.

57. Kilian, K.A., et al., *Geometric cues for directing the differentiation of mesenchymal stem cells.* Proc Natl Acad Sci USA, 2010. **107**(11): p. 4872-4877.

58. Ruiz, S.A. and C.S. Chen, *Emergence of patterned stem cell differentiation within multicellular structures.* Stem Cells, 2008. **26**(11): p. 2921-2927.

59. Gomez, E.W., et al., *Tissue geometry patterns epithelial-mesenchymal transition via intercellular mechanotransduction.* J Cell Biochem, 2010: p. n/a-n/a.

60. Eastham, A.M., et al., *Epithelial-mesenchymal transition events during human embryonic stem cell differentiation.* Cancer Res, 2007. **67**(23): p. 11254-11262.

61. Shook, D. and R. Keller, *Mechanisms, mechanics and function of epithelial–mesenchymal transitions in early development.* Mech Develop, 2003. **120**(11): p. 1351-1383.

62. Baum, B., J. Settleman, and M.P. Quinlan, *Transitions between epithelial and mesenchymal states in development and disease.* Semin Cell Dev Biol, 2008. **19**(3): p. 294-308.

63. Petrini, J., K. Damus, and R.B. Johnston, Jr., *An overview of infant mortality and birth defects in the United States.* Teratology, 1997. **56**(1-2): p. 8-10.

64. Heron, M., et al., *Deaths: final data for 2006.* Natl Vital Stat Rep, 2009. **57**(14): p. 1-134.

65. Tan, K.H., et al., *Birth defects in Singapore: 1994-2000.* Singap Med J, 2005. **46**(10): p. 545-52.

66. Faqi, A.S., et al., *Chapter 13 Developmental and reproductive toxicology*, in *a comprehensive guide to toxicology in preclinical drug development.* 2012, Academic Press. p. 345.

67. Paumgartten, F.J., *Influence of maternal toxicity on the outcome of developmental toxicity studies.* J Toxicol Env Heal A, 2010. **73**(13-14): p. 944-951.

68. Hartung, T. and C. Rovida, *Chemical regulators have overreached.* Nature, 2009. **460**(7259): p. 1080-1081.

69. Balls, M. and E. Hellsten, *Statement on the scientific validity of the mircromass test -- an in Vitro for embryotoxicity.* Altern Lab Anim, 2002. **30**(3): p. 268-70.

70. Balls, M. and E. Hellsten, *Statement on the scientific validity of the postimplantation rat whole-embryo culture assay -- an in vitro test for embryotoxicity.* Altern Lab Anim, 2002. **30**(3): p. 271-3.

71. Balls, M. and E. Hellsten, *Statement of the scientific validity of the embryonic stem cell test (EST) -- an in Vitro test for embryotoxicity.* Altern Lab Anim, 2002. **30**(3): p. 265-8.

72. Brannen, K.C., et al., *Development of a zebrafish embryo teratogenicity assay and quantitative prediction model.* Birth Defects Res B, 2010. **89**(1): p. 66-77.

73. Padilla, S., et al., *Zebrafish developmental screening of the ToxCast™ Phase I chemical library.* Reprod Toxicol, 2012. **33**(2): p. 174-187.

74. Gustafson, A.L., et al., *Inter-laboratory assessment of a harmonized zebrafish developmental toxicology assay – Progress report on phase I.* Reprod Toxicol, 2012. **33**(2): p. 155-164.

75. Umansky, R., *The effect of cell population density on the developmental fate of reaggregating mouse limb bud mesenchyme.* Dev Biol, 1966. **13**(1): p. 31-56.

76. Kistler, A. and W.B. Howard, *Testing of retinoids for teratogenicity in vitro: Use of micromass limb bud cell culture.* Method Enzymol, 1990. **190**: p. 427-433.

77. New, D.A., *Development of rat embryos cultured in blood sera.* J Reprod Fertil, 1966. **12**(3): p. 509-24.

78. New, D.A., P.T. Coppola, and S. Terry, *Culture of explanted rat embryos in rotating tubes.* J Reprod Fertil, 1973. **35**(1): p. 135-8.

79. Ellis-Hutchings, R.G. and E.W. Carney, *Whole embryo culture: a "New" technique that enabled decades of mechanistic discoveries.* Birth Defects Res B, 2010. **89**(4): p. 304-312.

80. Cockroft, D.L. and D.A. New, *Abnormalities induced in cultured rat embryos by hyperthermia.* Teratology, 1978. **17**(3): p. 277-83.

81. Manda, K., et al., *alpha-Lipoic acid attenuates x-irradiation-induced oxidative stress in mice.* Cell Biol Toxicol, 2007. **23**(2): p. 129-37.

82. Piersma, A.H., et al., *Biotransformation of cyclophosphamide in post-implantation rat embryo culture using maternal hepatocytes in co-culture.* Pharmacol Toxicol, 1991. **69**(1): p. 47-51.

83. Klein, N.W., et al., *The use of cultured rat embryos to evaluate the teratogenic activity of serum: cadmium and cyclophosphamide.* Teratology, 1980. **21**(2): p. 199-208.

84. Chatot, C.L., et al., *Human serum teratogenicity studied by rat embryo culture: epilepsy, anticonvulsant drugs, and nutrition.* Epilepsia, 1984. **25**(2): p. 205-216.

85. Piersma, A.H., et al., *Quantitative extrapolation of in vitro whole embryo culture embryotoxicity data to developmental toxicity in vivo using the benchmark dose approach.* Toxicol Sci, 2008. **101**(1): p. 91-100.

86. He, J.-H., et al., *Zebrafish models for assessing developmental and reproductive toxicity*. Neurotoxicol Teratol, 2014. **42**: p. 35-42.

87. Kimmel, C.B., et al., *Stages of embryonic development of the zebrafish.* Dev Dynam, 1995. **203**(3): p. 253-310.

88. Selderslaghs, I.W., et al., *Development of a screening assay to identify teratogenic and embryotoxic chemicals using the zebrafish embryo.* Reprod Toxicol, 2009. **28**(3): p. 308-320.

89. Brannen, K.C., et al., *Development of a zebrafish embryo teratogenicity assay and quantitative prediction model.* Birth Defects Res B, 2010. **89**(1): p. 66-77.

90. Gustafson, A.-L., et al., *Inter-laboratory assessment of a harmonized zebrafish developmental toxicology assay–Progress report on phase I.* Reprod Toxicol, 2012. **33**(2): p. 155-164.

91. Van den Bulck, K., et al., *Zebrafish developmental toxicity assay: a fishy solution to reproductive toxicity screening, or just a red herring?* Reprod Toxicol, 2011. **32**(2): p. 213-219.

92. Brent, R.L. and L.B. Holmes, *Clinical and basic science lessons from the thalidomide tragedy: what have we learned about the causes of limb defects?* Teratology, 1988. **38**(3): p. 241-51.

93. Wobus, A.M. and P. Löser, *Present state and future perspectives of using pluripotent stem cells in toxicology research.* Arch Toxicol, 2011. **85**(2): p. 79-117.

94. Adler, S., et al., *First steps in establishing a developmental toxicity test method based on human embryonic stem cells.* Toxicol In Vitro, 2008. **22**(1): p. 200-211.

95. Marx-Stoelting, P., et al., *A review of the implementation of the embryonic stem cell test (EST). The report and recommendations of an ECVAM/ReProTect Workshop.* Altern Lab Anim, 2009. **37**(3): p. 313-28.

96. Riebeling, C., et al., *Assaying embryotoxicity in the test tube: Current limitations of the embryonic stem cell test (EST) challenging its applicability domain.* Crit Rev Toxicol, 2012. **42**(5): p. 443-464.

97. Mehta, A., et al., *Assessment of drug induced developmental toxicity using human embryonic stem cells.* Cell Biol Int, 2008. **32**(11): p. 1412-1424.

98. Takahashi, K., et al., *Induction of pluripotent stem cells from adult human fibroblasts by defined factors.* Cell, 2007. **131**(5): p. 861-872.

99. Palmer, J.A., et al., *Establishment and assessment of a new human embryonic stem cell-based biomarker assay for developmental toxicity screening.* Birth Defects Res B, 2013. **98**(4): p. 343-363.

100. Kameoka, S., et al., *A high-hhroughput screen for teratogens using human pluripotent stem cells.* Toxicol Sci, 2014. **137**(1): p. 76-90.

101. Kleinstreuer, N.C., et al., *Identifying developmental toxicity pathways for a subset of ToxCast chemicals using human embryonic stem cells and metabolomics.* Toxicol Appl Pharm, 2011. **257**(1): p. 111-121.

102. Warmflash, A., et al., *A method to recapitulate early embryonic spatial patterning in human embryonic stem cells.* Nat Methods, 2014.

103. Peerani, R., et al., *Niche-mediated control of human embryonic stem cell self-renewal and differentiation.* EMBO J, 2007. **26**(22): p. 4744-4755.

104. Lecuit, T., P.F. Lenne, and E. Munro, *Force generation, transmission, and integration during cell and tissue morphogenesis.* Annu Rev Cell Dev Biol, 2011. **27**: p. 157-84.

105. Guilak, F., et al., *Control of stem cell fate by physical interactions with the extracellular matrix.* Cell Stem Cell, 2009. **5**(1): p. 17-26.

106. Gilbert, P.M., et al., *Substrate elasticity regulates skeletal muscle stem cell self-renewal in culture.* Science, 2010. **329**(5995): p. 1078-1081.

107. Gao, L., R. McBeath, and C.S. Chen, *Stem cell shape regulates a chondrogenic versus myogenic fate through Rac1 and N-cadherin.* Stem Cells, 2010. **28**(3): p. 564-572.

108. Li, D., et al., *Integrated biochemical and mechanical signals regulate multifaceted human embryonic stem cell functions.* J Cell Biol, 2010. **191**(3): p. 631-644.

109. Harb, N., T.K. Archer, and N. Sato, *The Rho-Rock-Myosin signaling axis determines cell-cell integrity of self-renewing pluripotent stem cells.* PLoS ONE, 2008. **3**(8): p. e3001.

110. Chowdhury, F., et al., *Material properties of the cell dictate stress-induced spreading and differentiation in embryonic stem cells.* Nat Mater, 2009. **9**(1): p. 82-88.

111. Sahai, E. and C.J. Marshall, *ROCK and Dia have opposing effects on adherens junctions downstream of Rho.* Nat Cell Biol, 2002. **4**(6): p. 408-415.

112. Noren, N.K., et al., *Cadherin engagement regulates Rho family GTPases.* J Biol Chem, 2001. **276**(36): p. 33305-33308.

113. Weber, G.F., M.A. Bjerke, and D.W. DeSimone, *Integrins and cadherins join forces to form adhesive networks.* J Cell Sci, 2011. **124**(8): p. 1183-1193.

114. Rossant, J. and P.P.L. Tam, *Blastocyst lineage formation, early embryonic asymmetries and axis patterning in the mouse.* Development, 2009. **136**(5): p. 701-713.

115. Gjorevski, N., E. Boghaert, and C.M. Nelson, *Regulation of epithelial-mesenchymal transition by transmission of mechanical stress through epithelial tissues.* Cancer Microenviron, 2012. **5**(1): p. 29-38.

116. Théry, M., *Micropatterning as a tool to decipher cell morphogenesis and functions.* J Cell Sci, 2010. **123**(24): p. 4201-4213.

117. Borghi, N., et al., *Regulation of cell motile behavior by crosstalk between cadherin-and integrin-mediated adhesions.* Proc Natl Acad Sci USA, 2010. **107**(30): p. 13324-13329.

118. Haque, A., et al., *Characterization and neural differentiation of mouse embryonic and induced pluripotent stem cells on cadherin-based substrata.* Biomaterials, 2012. **33**(20): p. 5094-5106.

119. Humphries, J.D., A. Byron, and M.J. Humphries, *Integrin ligands at a glance.* J Cell Sci, 2006. **119**(19): p. 3901-3903.

120. Meng, Y., et al., *Characterization of integrin engagement during defined human embryonic stem cell culture.* J FASEB, 2010. **24**(4): p. 1056-1065.

121. Mertz, A.F., et al., *Cadherin-based intercellular adhesions organize epithelial cell–matrix traction forces.* Proc Natl Acad Sci USA, 2013. **110**(3): p. 842-847.

122. Ng, M.R., et al., *Substrate stiffness regulates cadherin-dependent collective migration through myosin-II contractility.* J Cell Biol, 2012. **199**(3): p. 545-563.

123. Gomez, E.W., et al., *Tissue geometry patterns epithelial-mesenchymal transition via intercellular mechanotransduction.* J Cell Biochem, 2010. **110**(1): p. 44-51.

124. Kubo, A., *Development of definitive endoderm from embryonic stem cells in culture.* Development, 2004. **131**(7): p. 1651-1662.

125. Smal, I., et al., *Microtubule dynamics analysis using kymographs and variable-rate particle filters.* IEEE Trans Image Process, 2010. **19**(7): p. 1861-76.

126. Martin, A.C., et al., *Integration of contractile forces during tissue invagination.* J Cell Biol, 2010. **188**(5): p. 735-749.

127. Thiery, J.P., et al., *Epithelial-mesenchymal transitions in development and disease.* Cell, 2009. **139**(5): p. 871-90.

128. Kameoka, S., et al., *A high-throughput screen for teratogens using human pluripotent stem cells.* Toxicol Sci, 2014. **137**(1): p. 76-90.

129. Warmflash, A., et al., *A method to recapitulate early embryonic spatial patterning in human embryonic stem cells.* Nat Methods, 2014. **11**(8): p. 847-54.

130. Zhang, Y.S., et al., *Patterning pluripotency in embryonic stem cells.* Stem Cells, 2013. **31**(9): p. 1806-1815.

131. Suri, S., et al., *Microfluidic-based patterning of embryonic stem cells for in vitro development studies.* Lab Chip, 2013. **13**(23): p. 4617.

132. Toh, Y.-C., et al., *Spatially organized in vitro models instruct asymmetric stem cell differentiation.* Integr Biol, 2011. **3**(12): p. 1179.

133. Jeon, O. and E. Alsberg, *Regulation of stem cell fate in a three-dimensional micropatterned dual-crosslinked hydrogel system.* Adv Funct Mater, 2013. **23**(38): p. 4765-4775.

134. Meganathan, K., et al., *Identification of thalidomide-specific transcriptomics and proteomics signatures during differentiation of human embryonic stem cells.* PLoS One, 2012. **7**(8): p. e44228.

135. Amacher, D.E., *The discovery and development of proteomic safety biomarkers for the detection of drug-induced liver toxicity.* Toxicol Appl Pharmacol, 2010. **245**(1): p. 134-42.

136. Hoffmann, D., et al., *Performance of novel kidney biomarkers in preclinical toxicity studies.* Toxicol Sci, 2010. **116**(1): p. 8-22.

137. Tam, P.P.L., D.A.F. Loebel, and S.S. Tanaka, *Building the mouse gastrula: signals, asymmetry and lineages.* Curr Opin Genet Dev, 2006. **16**(4): p. 419-425.

138. Pinho, B.R., et al., *Is nitric oxide decrease observed with naphthoquinones in LPS stimulated RAW 264.7 macrophages a beneficial property?* PLoS One, 2011. **6**(8): p. e24098.

139. Lammer, E.J., et al., *Retinoic acid embryopathy.* N Engl J Med, 1985. **313**(14): p. 837-41.

140. Rosa, F.W., *Teratogen update: penicillamine.* Teratology, 1986. **33**(1): p. 127-31.

141. Lammer, E.J., L.E. Sever, and G.P. Oakley, Jr., *Teratogen update: valproic acid.* Teratology, 1987. **35**(3): p. 465-73.

142. Novartis, *Penicillin G Sodium injection*. 2009, New Zealand Medicines and Medical Devices Safety Authority.

143. Vargesson, N., *Thalidomide-induced limb defects: resolving a 50-year-old puzzle.* Bioessays, 2009. **31**(12): p. 1327-1336.

144. Jones-Villeneuve, E.M., et al., *Retinoic acid induces embryonal carcinoma cells to differentiate into neurons and glial cells.* J Cell Biol, 1982. **94**(2): p. 253-62.

145. *Teratology Society position paper: recommendations for vitamin A use during pregnancy.* Teratology, 1987. **35**(2): p. 269-75.

146. Plaut, M.E., et al., *Penicillin handling in normal and azotemic patients.* J Lab Clin Med, 1969. **74**(1): p. 12-8.

147. Teo, S.K., et al., *Clinical pharmacokinetics of thalidomide.* Clin Pharmacokinet, 2004. **43**(5): p. 311-27.

148. Muindi, J.R., et al., *Clinical pharmacology of oral all-trans retinoic acid in patients with acute promyelocytic leukemia.* Cancer Res, 1992. **52**(8): p. 2138-42.

149. Netter, P., et al., *Clinical pharmacokinetics of D-penicillamine.* Clin Pharmacokinet, 1987. **13**(5): p. 317-33.

150. Reed, R.C., et al., *Every-12-hour administration of extended-release divalproex in patients with epilepsy: impact on plasma valproic acid concentrations.* Epilepsy Behav, 2006. **8**(2): p. 391-6.

151. Chuai, M. and C.J. Weijer, *The mechanisms underlying primitive streak formation in the chick embryo.* Curr Top Dev Biol, 2008. **81**: p. 135-56.

152. Lye, C.M. and B. Sanson, *Tension and epithelial morphogenesis in Drosophila early embryos.* Curr Top Dev Biol, 2011. **95**: p. 145-87.

9. Appendices

9.1 Cells in μP-hPSC colonies maintained pluripotency in mTeSR™1 maintenance medium

Cells in μP-hPSC colonies could maintain pluripotency and show similar gene and protein expression levels compared to conventionally cultured hPSCs cultured in mTeSR™1 maintenance medium. Immunofluorescence staining showed that cells were positive for the pluripotency-associated transcription factors OCT4 and NANOG, and surface markers TRA-1-60 and SSEA-4 (Fig. 9.1.1). Compared with unpatterned hPSCs in conventional maintenance culture, the μP-hPSCs showed similar transcript levels of both pluripotency-associated and lineage-specific genes (Fig. 9.1.2).

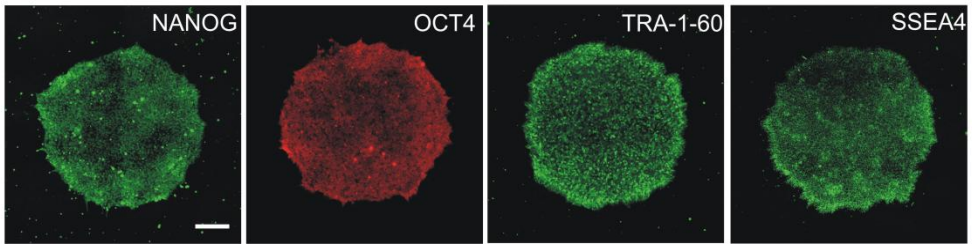

Figure 9.1.1 Immunofluorescence analysis of pluripotency markers in μP-hPSC colonies 24 hr after patterning. Expression of transcription factors OCT4 and NANOG and surface antigens TRA-1-60 and SSEA4 was observed. Scale bar = 200 μm.

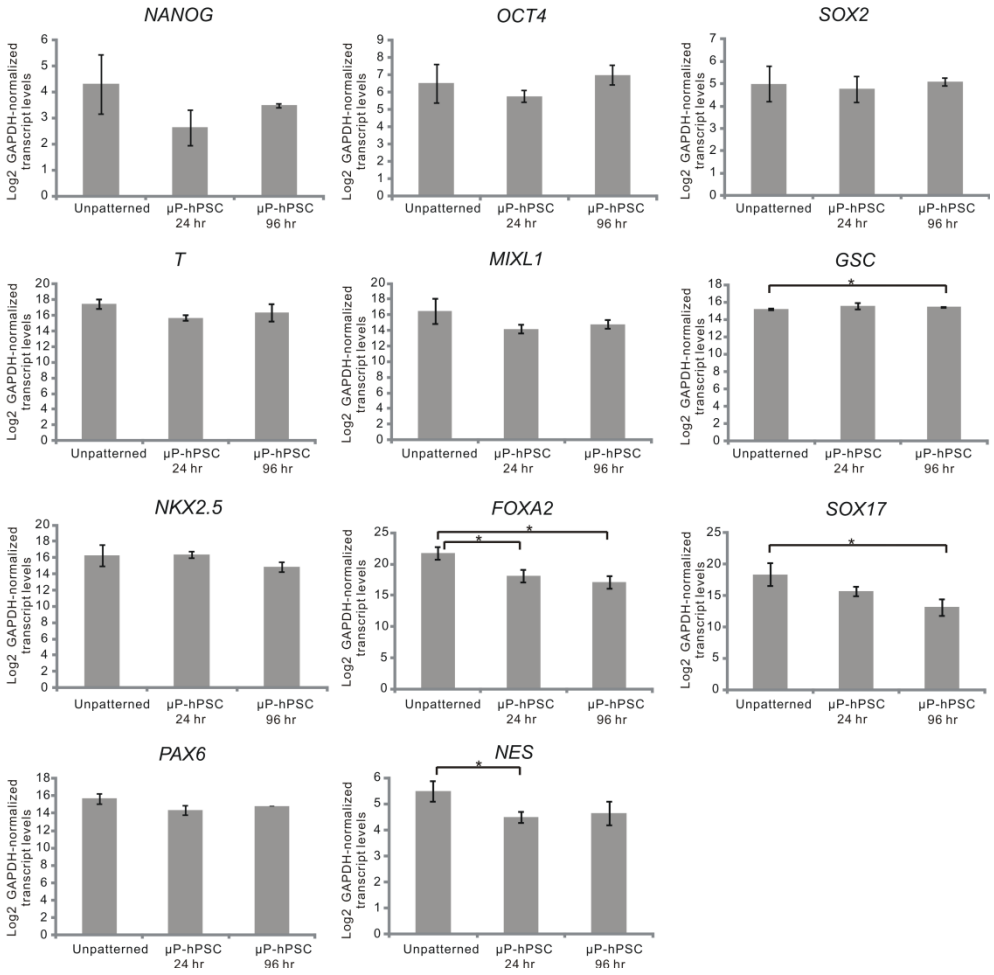

Figure 9.1.2 RT-PCR analysis of expression levels of pluripotency markers and lineage-specific markers in conventional unpatterned hPSCs and μP-hPSCs. Unpatterned hPSCs were lysed from normal hPSC culture when cells were 70%-80% confluent. The μP-hPSC colonies were cultured in mTeSR^{TM}1 maintenance medium and lysed for RT-PCR analysis 24 hr and 96 hr post patterning. Both unpatterned hPSCs and μP-hPSCs showed high expression levels of pluripotency markers and low expression levels of lineage-specific markers. Pluripotency markers: NANOG, OCT4, SOX2; Mesoendoderm markers: T, MIXL1, GSC, NKX2.5, FOXA2 and SOX17: Ectoderm markers: PAX6, NES (nestin). Data are average ± s.d of three experiments with duplicate samples. *, $p<0.05$ in paired t-test.

9.2 Culture of hPSCs on E-cadherin Fc-coated tissue culture polystyrene substrates

E-cadherin-Fc (EcadFc) could be used to culture hPSCs. hPSCs could attach to EcadFc-coated tissue culture polystyrene substrates in a dose-dependent manner (Fig. 9.2.1). Cells could attach, spread and proliferate well when the coating concentration of EcadFc was 10 μg/ml and 40 μg/ml without significant morphological differences between these two concentrations, while 2 μg/ml EcadFc coating concentration was too low for proper cell attachment and spreading (Fig. 9.2.1).

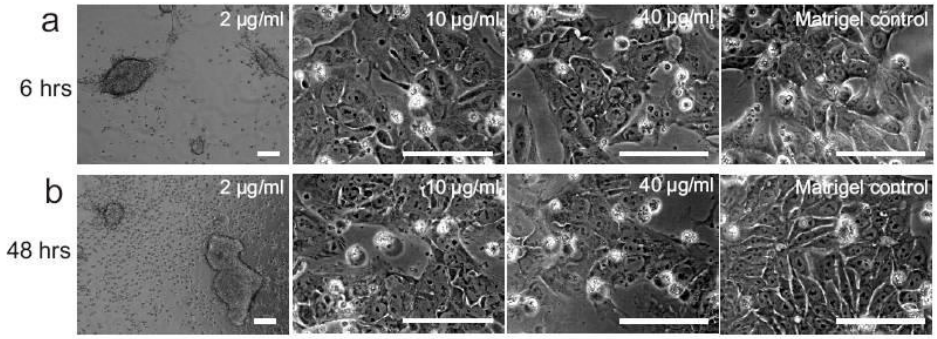

Figure 9.2.1 Attachment of hPSCs on different concentrations of E-cadherin Fc-coated tissue culture polystyrene. Single hPSCs were seeded and cultured in defined maintenance medium (mTeSR1, Stem Cell Technologies). Images were taken at (a) 6 hr and (b) 48 hr post seeding. Scale bars = 100 μm.

EcadFc could also maintain hPSC pluripotency when cells were cultured in defined maintenance medium (mTeSR1, Stem Cell Technologies) (Fig.

9.1.2). The expression levels of pluripotency markers Oct4 and Nanog were comparable with hPSCs cultured on Matrigel-coated substrate.

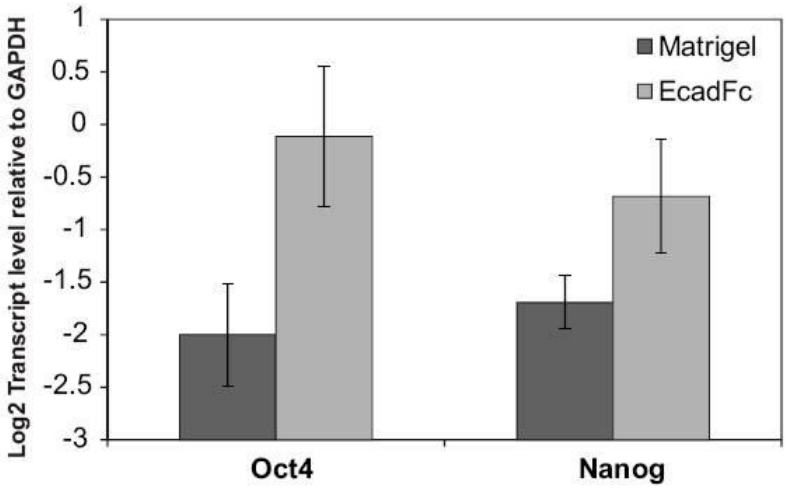

Figure 9.2.2 Pluripotency markers expression in hPSCs on Matrigel™ or EcadFc (10 μg/ml)-coated substrates 48 hr post seeding. Data are average ± s.e.m of 3 experiments.

9.3 Integrin and E-cadherin antibody blocking

In order to find the major integrins involved in hPSC attachment to Matrigel substrate, inhibition of cell-matrix adhersion by integrin antibodies was performed. Three integrin antibodies, $\alpha_5\beta_1$, $\alpha_2\beta_1$ and $\alpha_6\beta_1$ antibodies were added into the hPSC single cell suspension while cell seeding. After 4 hr incubation for cell attachment, untreated cells and cells treated with $\alpha_5\beta_1$ and $\alpha_2\beta_1$ antibodies spread more onto the substrate compared with cells treated with $\alpha_6\beta_1$ antibodies, indicating decreased cell-matrix adhesion in $\alpha_6\beta_1$ antibody-treated samples (Fig. 9.3.1). When mesoendoderm differentiation

was induced to these $\alpha_6\beta_1$ antibody-treated samples, a dose-dependent contraction of μP-hPSC colonies could be observed (Fig. 9.3.2). After 24 hr differentiation induction, the sizes of colonies treated with 0.1 μg/ml $\alpha_6\beta_1$ antibodies were about 50% of the untreated ones (Fig.9.3.2). In contrast, sizes of colonies treated with $\alpha_5\beta_1$ or $\alpha_2\beta_1$ antibodies showed no significant differences compared with untreated control samples (Fig. 9.3.3). Therefore, we can conclude that the main integrin involved in cell attachment onto Matrigel is $\alpha_6\beta_1$, instead of $\alpha_5\beta_1$ and $\alpha_2\beta_1$. By adding $\alpha_6\beta_1$ antibodies into the culture, integrin-dependent cell-matrix adhesion of hPSCs on Matrigel-coated plates could be disrupted.

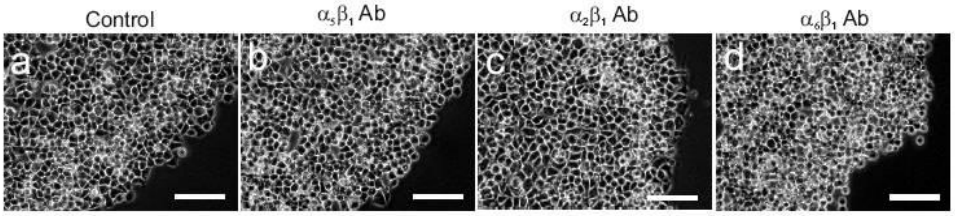

Figure 9.3.1 hPSC attachment to micropatterned Matrigel substrate in the presence of integrin antibodies after 4 hr incubation post cell seeding. (a) Untreated control, (b) 1 μg/ml α5β1, (c) 1 μg/ml α2β1, (d) 0.1 μg/ml α6β1 integrin antibodies. Scale bars = 100 μm.

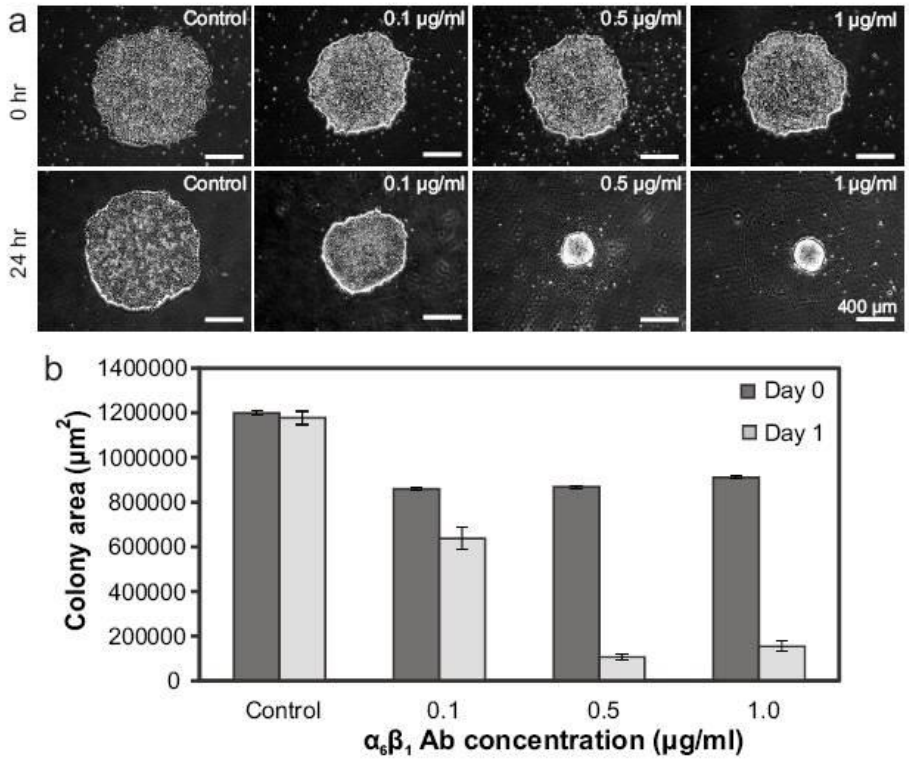

Figure 9.3.2 Blocking of laminin- $\alpha_6\beta_1$ integrin binding by $\alpha_6\beta_1$ antibody caused contraction of differentiating µP-hPSC colonies in a dose-dependent manner. (a) Phase images showing µP-hPSC colonies at the onset (0 hr) and after (24 hr) mesoendoderm differentiation. There was no significant differences in the colony sizes at different antibody concentrations before differentiation was initiated. $\alpha_6\beta_1$ antibody-treated colonies contracted after 24 hr of differentiation. Scale bars = 400 µm. (b) Quantification of colony areas at different concentrations of $\alpha_6\beta_1$ antibody. Data are average ± s.e.m of different sample sizes (n): Control (n=8); 0.1 µg/ml (n=6); 0.5 µg/ml (n=2); 1.0 µg/ml (n=7).

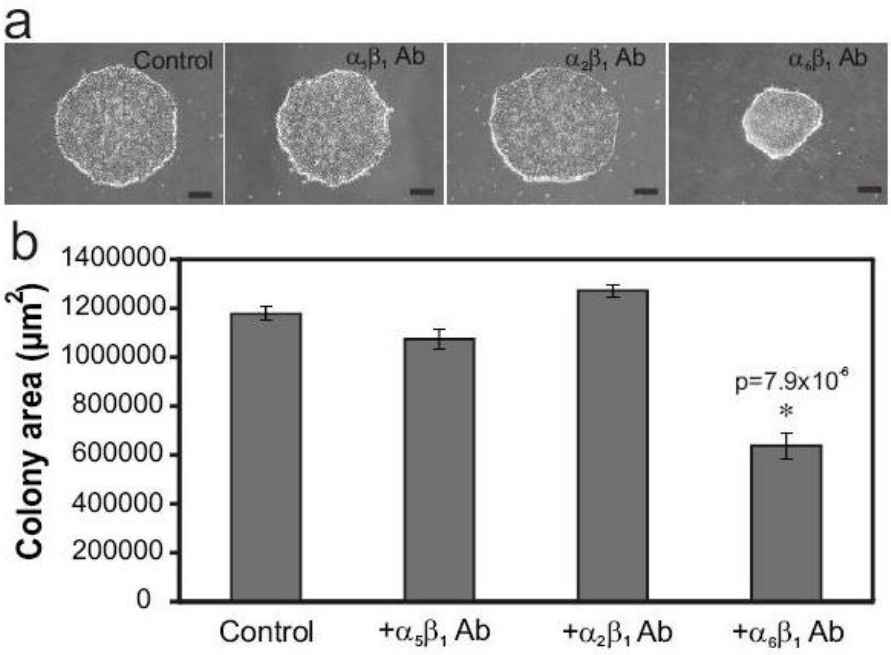

Figure 9.3.3 Specific inhibition of integrin $\alpha_6\beta_1$-laminin binding attenuated cell-ECM interaction and resulted in contraction of μP-hPSC colonies. (a) Phase images of μP-hPSC colonies after 24 hr of mesoendoderm differentiation in the absence (control) or presence of 1 μg/ml $\alpha_5\beta_1$, 1 μg/ml $\alpha_2\beta_1$ and 0.1 μg/ml $\alpha_6\beta_1$ integrin antibodies. Scale bars = 200 μm. (b) Quantification of colony areas after 24 hr of differentiation. Data are average ± s.e.m of different sample sizes (n): Control (n=8); $\alpha_5\beta_1$ Ab (n=5); $\alpha_2\beta_1$ Ab (n=7); $\alpha_6\beta_1$ Ab (n=6). * indicates statistical significance when compared to control colonies (Student's t-test, $p<0.01$).

When adding E-cadherin antibodies into the hPSC culture since cell seeding, cell-cell interactions within the colonies could be disrupted. After 24 hr of differentiation, more scattered morphology of cells could be observed in E-cadherin antibody-treated colonies compared with IgG antibody controls (Fig.9.3.4).

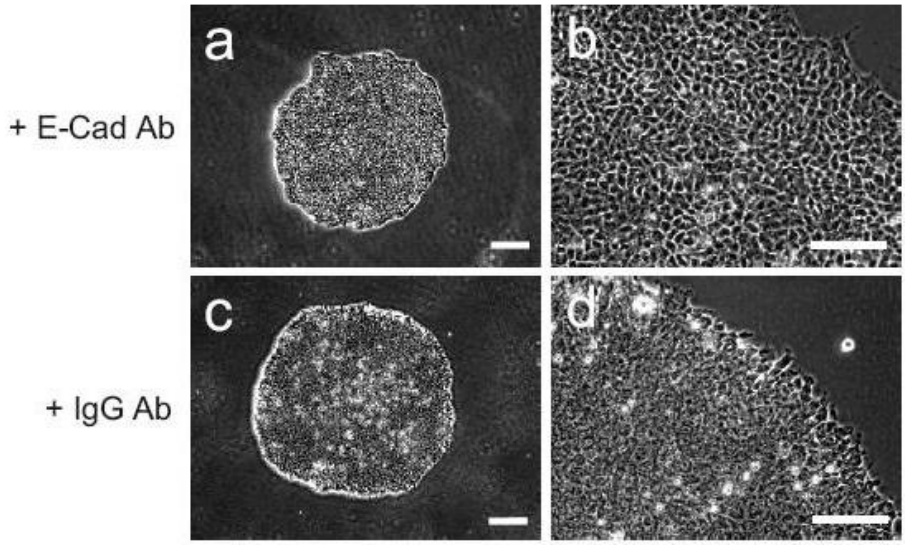

Figure 9.3.4 Specific inhibition of E-cadherin-mediated adhesion in the μP-hPSC colonies resulted in more scattered morphology. (a,b) Phase images of colonies treated with E-cadherin antibody and differentiated for 24 hr. (c,d) Phase images of control colonies treated with unspecific IgG antibody and differentiated for 24 hr. Scale bars in (a,c) = 200 μm, (b, d) = 100 μm.